Supporting Information
for
The effect of locking π-conjugation in organoboron moieties in the structures of luminescent tetracoordinate boron complexes.

Mateusz Urban[a]*, Krzysztof Durka[a]*, Patrycja Górka[a], Gabriela Wiosna-Sałyga[b], Krzysztof Nawara[c] Piotr Jankowski[a], Sergiusz Luliński[a]

[a]*Department of Physical Chemistry, Faculty of Chemistry, Warsaw University of Technology, Noakowskiego 3, 00-664 Warsaw, Poland*

[b]*Department of Molecular Physics, Faculty of Chemistry, Lodz University of Technology, Żeromskiego 116, 90-924 Łódź, Poland*

[c]*Faculty of Mathematics and Science, Cardinal Stefan Wyszyński University, Dewajtis 5, 01-815 Warsaw, Poland*

Corresponding authors:
Krzysztof Durka: kdurka@ch.pw.edu.pl
Mateusz Urban: murban@ch.pw.edu.pl

Table of contents

1. Crystal structures

Table S1. Selected crystal data, data collection and refinement parameters for **1a**-**3a**, **5a**-**8a**, **8b**.

	1a	**2a**	**3a**	**5a**
Formula	$C_{21}H_{14}BNO$	$C_{21}H_6BF_8NO$	$C_{23}H_{16}BNO$	$C_{25}H_{16}BNO_2$
Molecular mass, M_r / a.u.	307.14	451.08	333.18	373.20
Temperature, T / K	100	100	100	100
Crystal system	orthorhombic	triclinic	tetragonal	monoclinic
Space group	$P2_12_12_1$	P-1	$P4_1$	$P2_1/c$
a / Å	12.5739(7)	8.8891(3)	8.7821(1)	12.2286(2)
b / Å	15.6280(9)	9.5342(3)	8.7821(1)	9.9535(2)
c / Å	16.2194(9)	11.7495(4)	21.8367(6)	15.6960(3)
α / °	90	81.488(3)	90	90
β / °	90	68.282(3)	90	104.304(2)
γ / °	90	66.482(3)	90	90
Volume, V / Å^3	3187.2(3)	848.249	1684.2(1)	1851.2(1)
d_{calc} / gcm^{-3}	1.280	1.766	1.314	1.339
F(000)	1280	448	696	776
Absorption coefficient, μ / mm^{-1}	0.078	0.169	0.617	0.666
No. of measured, independent reflections	43050 / 7058	34297 / 5510	8239 / 2889	9116 / 2790
R_{int} / %	8.96	3.92	5.43	2.14
GooF	1.033	1.033	1.069	1.065
$R[F]$ / $wR[F^2]$ ($I > 2\sigma(I)$) / %	7.33 / 13.33	4.57 / 12.36	3.84 / 9.59	3.81 / 9.30
Max. and min. residual density / eÅ^{-3}	-0.259 / 0.273	-0.256 / 0.511	-0.172 / 0.247	-0.222/ 0.244

	6a	**7a**	**8a**	**8b**
Formula	$C_{25}H_{16}BNOS$	$C_{25}H_{18}BN\ O$	$C_{48}H_{32}B_2N_2O_2$	$C_{51}H_{42}B_2N_2O_3$
Molecular mass, M_r / a.u.	389.26	359.21	690.37	752.48
Temperature, T / K	100	100	100	100
Crystal system	monoclinic	tetragonal	monoclinic	triclinic
Space group	$P2_1/c$	$P4_3$	$P2_1/c$	P-1
a / Å	12.3956(1)	10.2453(1)	18.5530(2)	11.7219(4)
b / Å	10.4119(1)	10.2453(1)	10.96080(1)	13.1009(4)
c / Å	15.3378(2)	17.6924(5)	18.0089(2)	14.2731(5)
α / °	90	90	90	70.661(3)
β / °	106.166(1)	90	109.695(1)	85.036(3)
γ / °	90	90	90	82.674(3)
Volume, V / Å^3	1901.3(1)	1857.1(2)	3448.0(1)	2049.0(1)
d_{calc} / gcm^{-3}	1.360	1.285	1.330	1.220
F(000)	808	752	1440	792
Absorption coefficient, μ / mm^{-1}	1.630	0.598	0.623	0.581
No. of measured, independent reflections	13976 / 3796	8036 / 2591	25695 / 5205	19365 / 7292
R_{int} / %	1.94	2.70	2.12	8.42
GooF	1.059	1.047	1.034	1.032
$R[F]$ / $wR[F^2]$ ($I > 2\sigma(I)$) / %	3.25 / 9.46	4.33 / 10.98	5.05 / 19.35	6.90 / 19.63
Max. and min. residual density / eÅ^{-3}	-0.318 / 0.358	-0.152 / 0.455	-0.323 / 1.700	-0.406 / 0.580

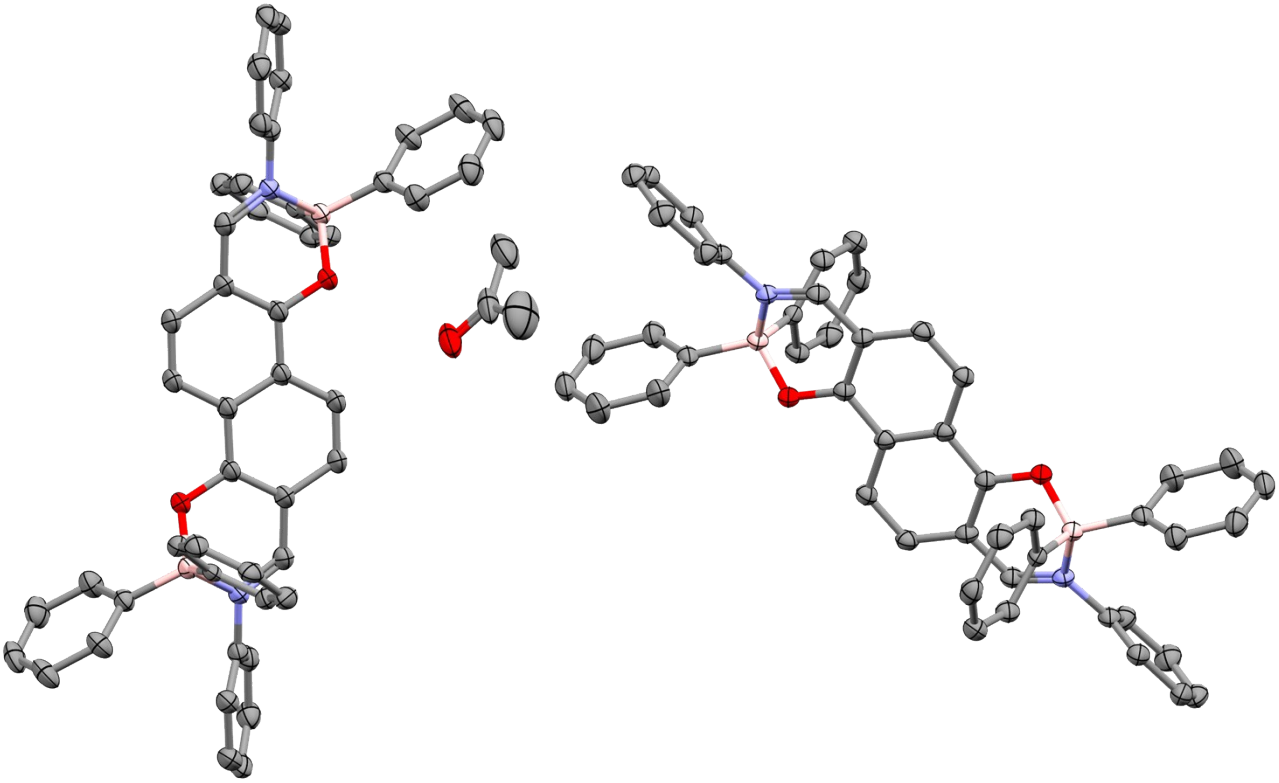

Figure S1. Molecular structure of **8b**. Thermal motions given as ADPs at the 50% probability level. Hydrogens atoms are omitted for clarity. Compound crystallized as a solvate from acetone solution. Two molecules are present in asymmetric unit, symmetry centre is located on the inner C-C naphthalene bond.

Table S2. Comparison of bond length around boron atom in borafluorene complexes (**1a**-**8a**) and their nonannulated analogs (**1b**-**8b**).

	$d_{B\text{-}N}$ / Å	$d_{B\text{-}O}$ / Å	$d_{B\text{-}C1}$ / Å	$d_{B\text{-}C2}$ [b] / Å
1a[a]	1.612(4)	1.514(4)	1.613(4)	1.613(4)
	1.618(4)	1.518(4)	1.627(4)	1.628(4)
1b[1]	1.615	1.561	1.575	1.593
2a	1.620(1)	1.493(1)	1.619(1)	1.615(1)
2b[2]	1.637	1.494	1.629	1.624
3a	1.613(4)	1.465(4)	1.617(4)	1.615(4)
3b[a 3]	1.627	1.48	1.616	1.607
	1.631	1.484	1.607	1.614
4a[4]	1.591	1.480	1.616	1.617
4b[4]	1.595	1.506	1.603	1.608
5a	1.594(2)	1.492(2)	1.611(2)	1.613(2)
5b[5]	1.605	1.505	1.600	1.597
6a	1.603(2)	1.491(2)	1.619(2)	1.617(2)
6b[5]	1.640	1.488	1.614	1.614
7a	1.601(5)	1.488(5)	1.599(5)	1.637(5)
7b[6]	1.635	1.509	1.613	1.614
8a[a]	1.613(3)	1.517(3)	1.618(3)	1.615(3)
	1.601(3)	1.510(3)	1.615(3)	1.620(3)
8b[a 7]	1.630(1)	1.503(1)	1.609(1)	1.620(1)
	1.626(1)	1.517(1)	1.608(1)	1.619(1)

[a]Two non-equivalent boron centre in assymetric unit, [b]negative values are used to distinguish between below and above the plane distortion.

2. Thermal characterisation

Thermal behaviour of all studied compounds was monitored by TGA and DSC techniques (Figure S2-20). All complexes expect **8** show distinct endothermic peak corresponding to sample melting (T_m). The melting temperatures are higher as compared to BPh_2 analogs. In the case of **1**, the difference is rather small (218.1 °C vs 206.6 °C), however it becomes more significant in the case of other studied compounds. Regarding complexes **3a**-**6a**, their melting points are systematically by 50-70 °C higher than **3b**-**6b**. The highest melting difference is observed for fluorinated systems, where **2a** melts at 278 °C and its non-annulated analogue at only 161.1 °C. At this point it is quite interesting to note that melting point of **2b** complex is smaller than **1b**, whereas in the case of borafluorene complexes **1a**, **2a**, the melting relation is reversed indicating that fluorination significantly enhances thermal stability. Furthermore, melting process seems to be reversible for **2a**, as exothermic peak near 221 °C corresponding to sample crystallization during cooling is observed. This behaviour is rather rare for tetracoordinated boron chelate complexes, where typically melting is followed by instant sample decomposition. The gathered TGA data suggest that compounds **1a** and **7a** are also thermally resistant after melting to some extent. Besides, other systems tend to decompose after melting as decomposition temperatures with a 5% weight loss (T_{dec}) cover with T_m. After decomposition, volatile products are produced, which fast evaporate from crucibles. Exceptionally, bis(boranil) complex **8** does not show typical melting behaviour. Instead the sample gradually darkens and slowly decompose above ca. 450 °C indicating its superior thermal stability.

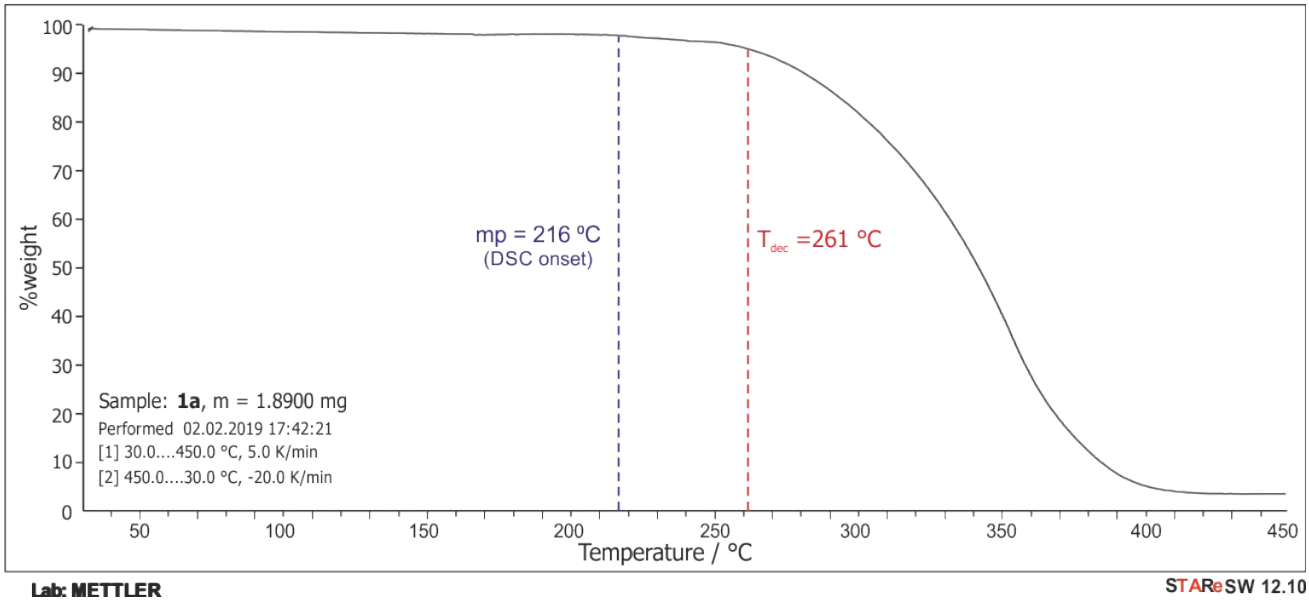

Figure S2. TGA curve of **1a**.

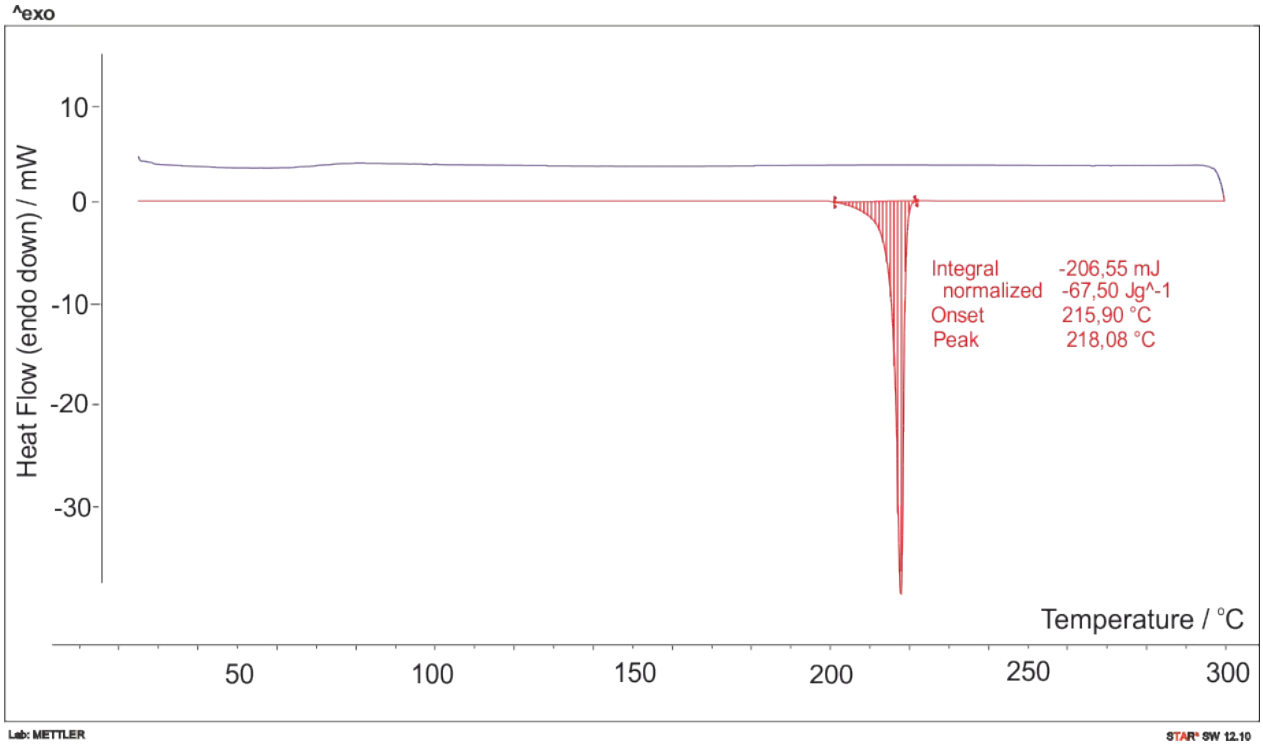

Figure S3. DSC curve of **1a**.

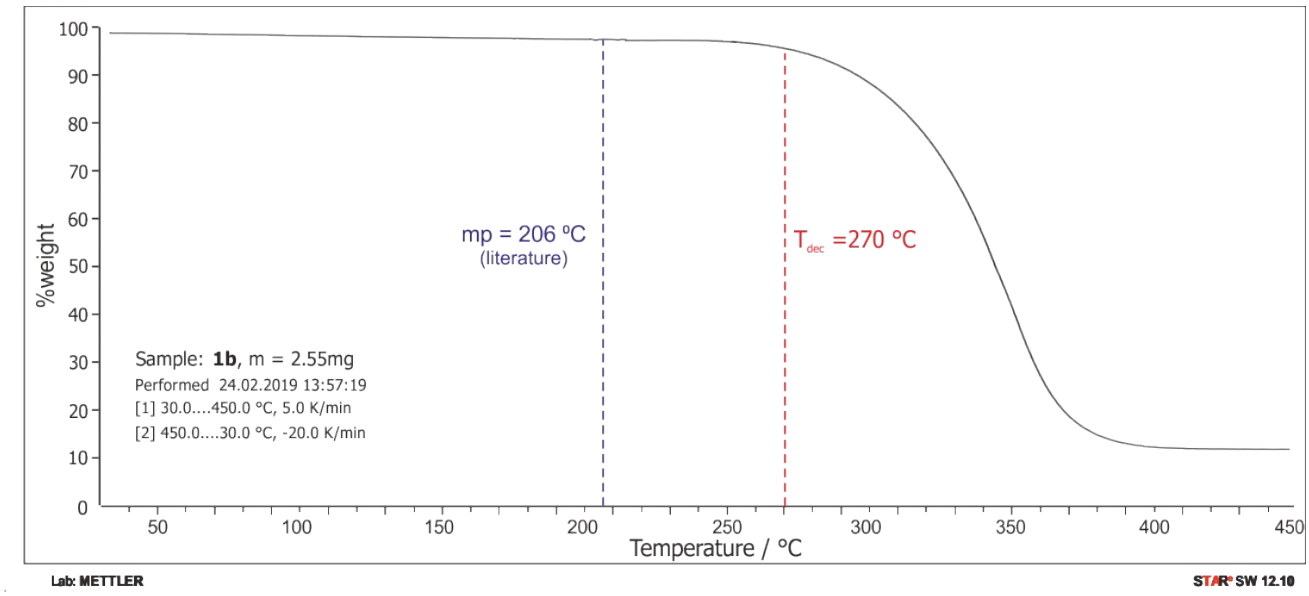

Figure S4. TGA curve of **1b**.

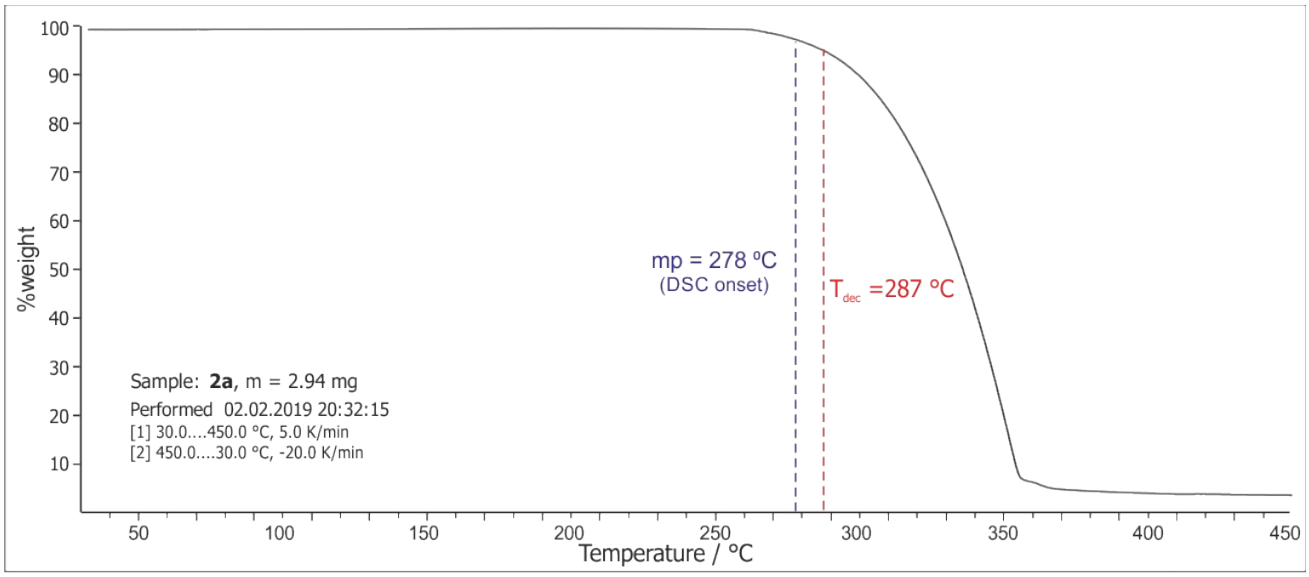

Figure S5. TGA curve of **2a**.

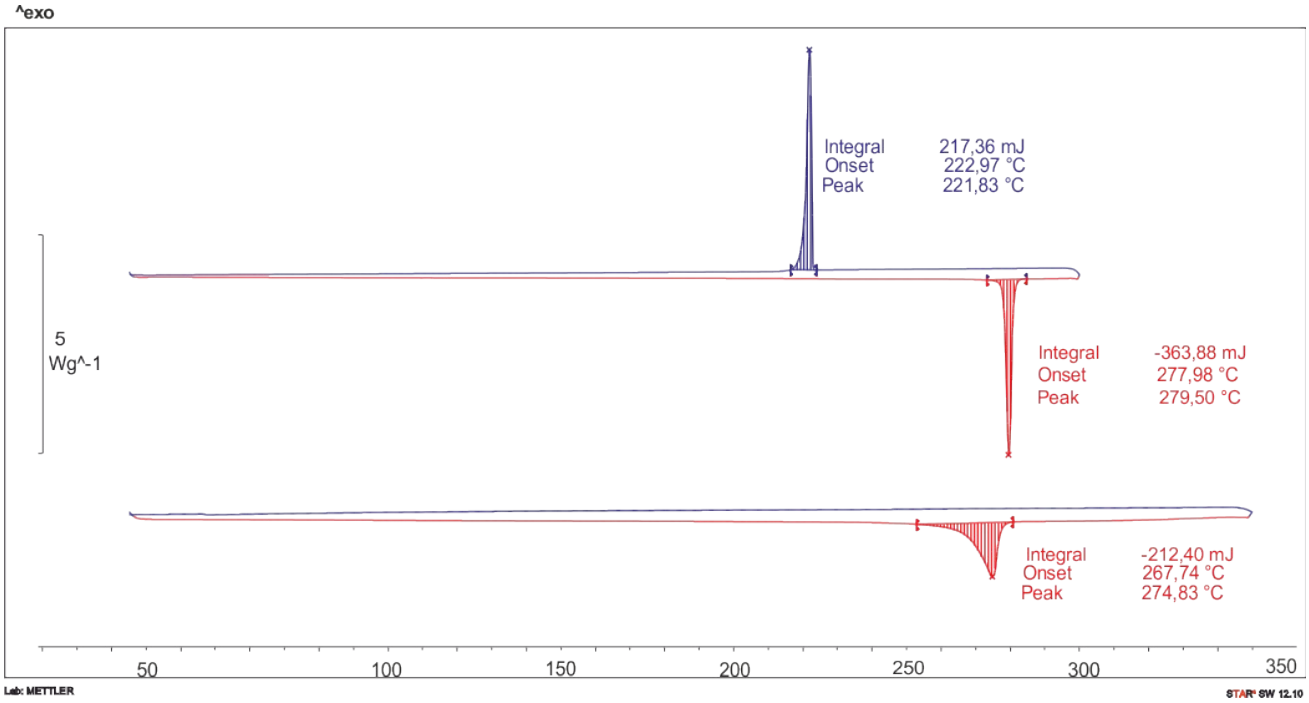

Figure S6. DSC curve of **2a**.

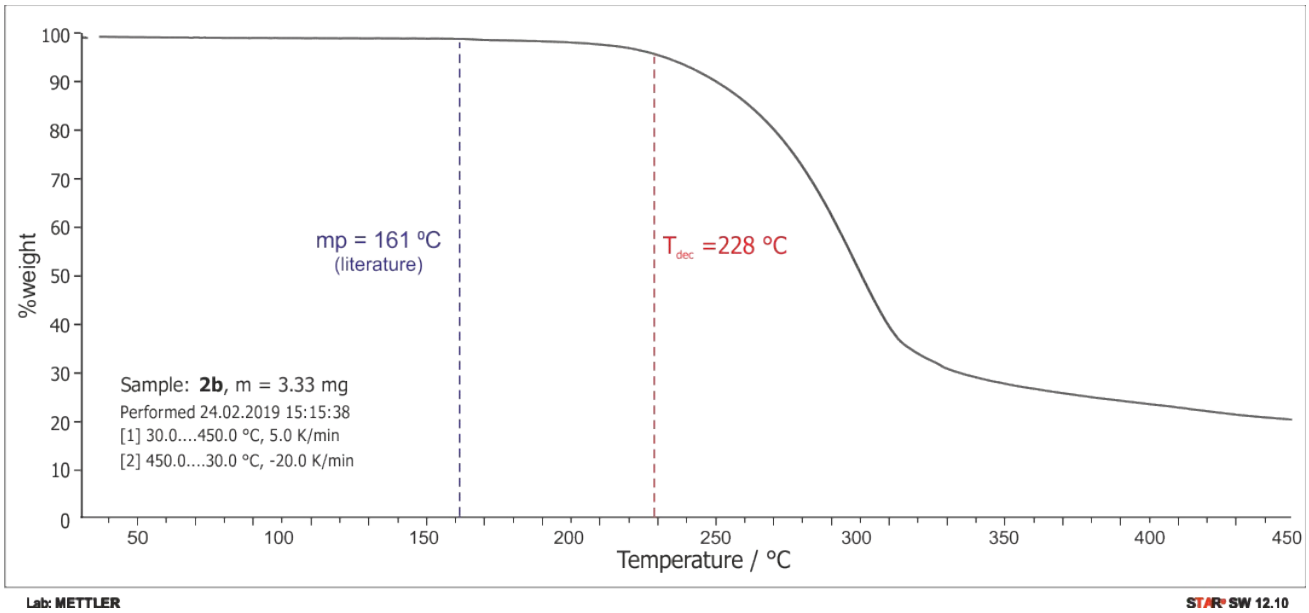

Figure S7. TGA curve of **2b**.

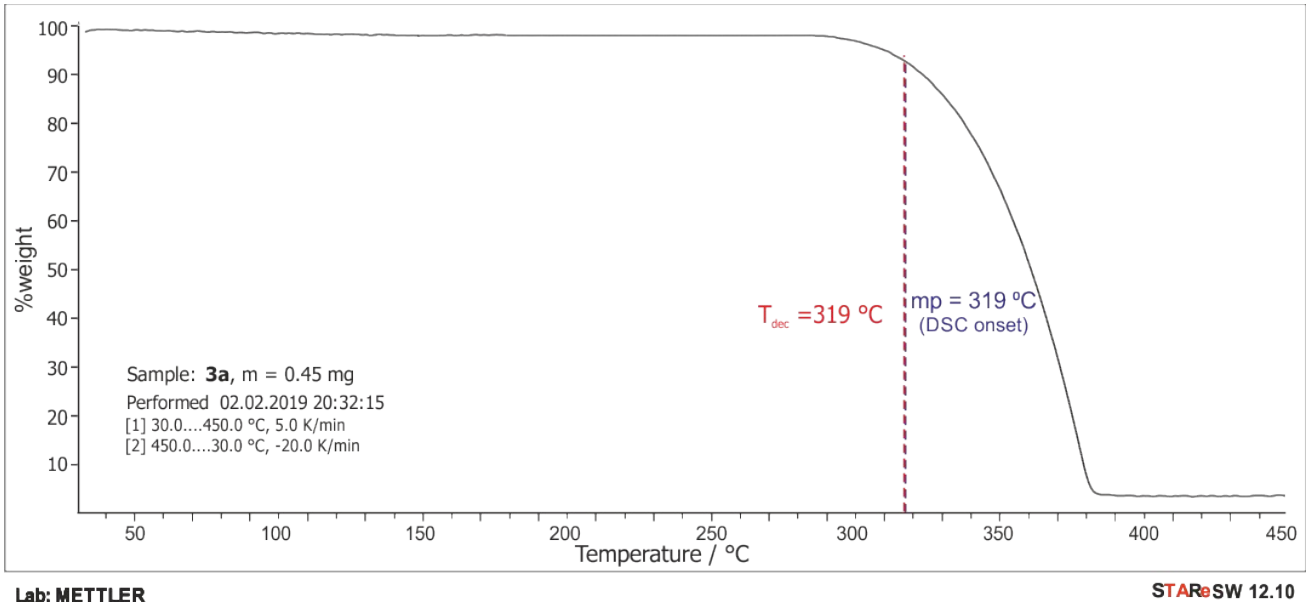

Figure S8. TGA curve of **3a**.

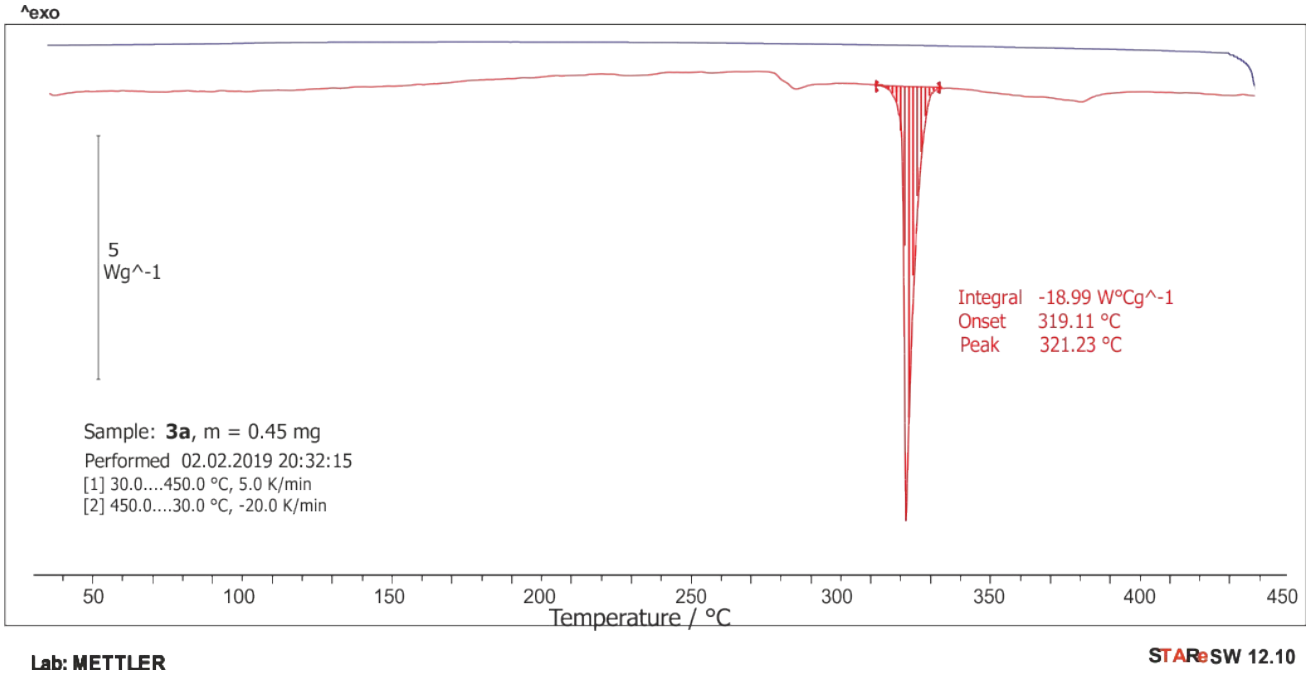

Figure S9. DSC curve of **3a**.

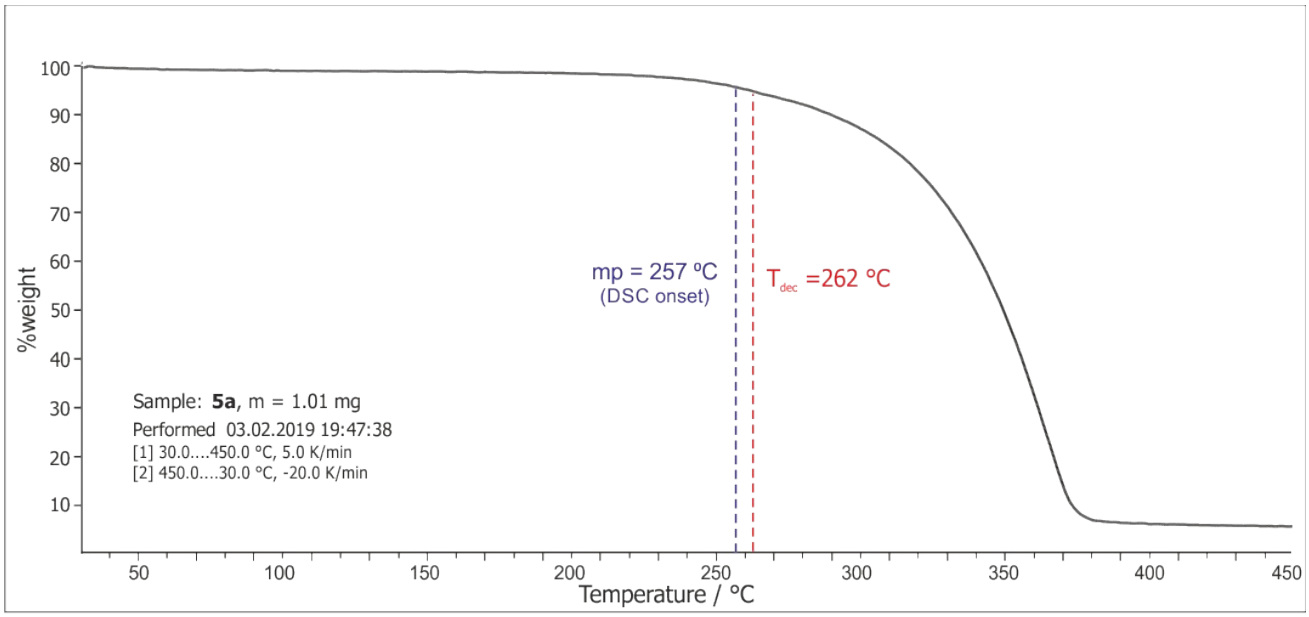

Figure S10. TGA curve of **5a**.

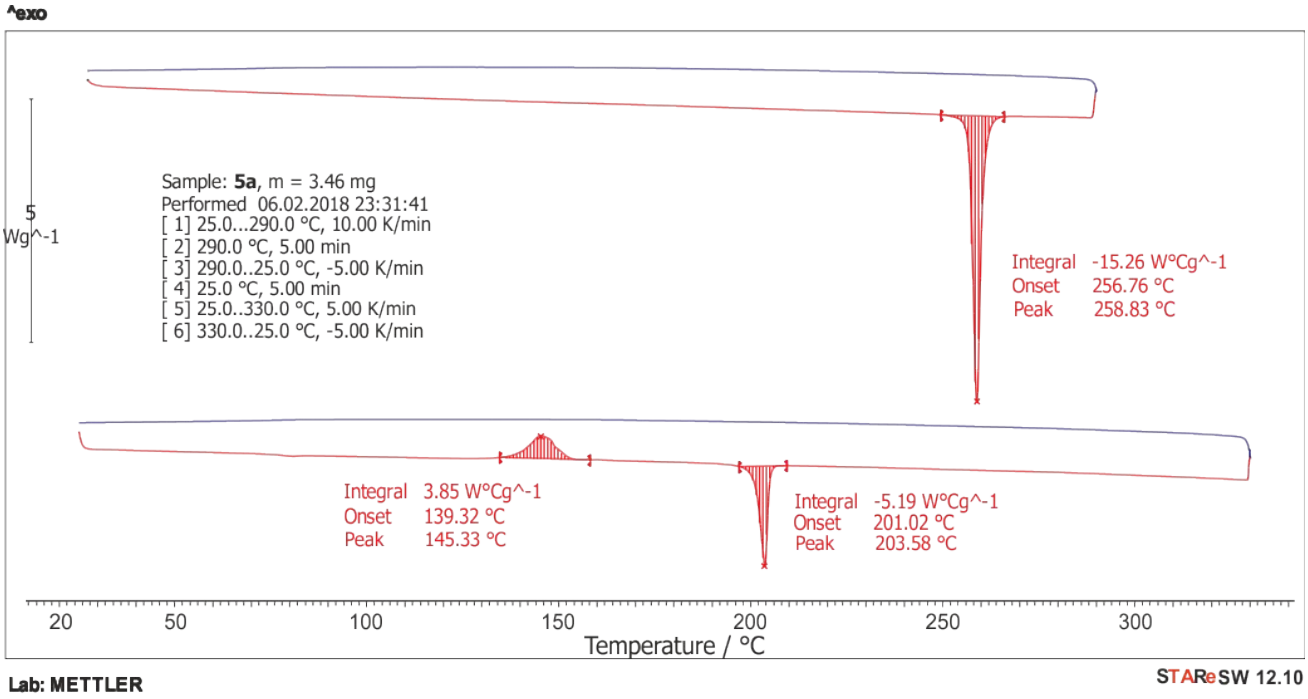

Figure S11. DSC curve of **5a**.

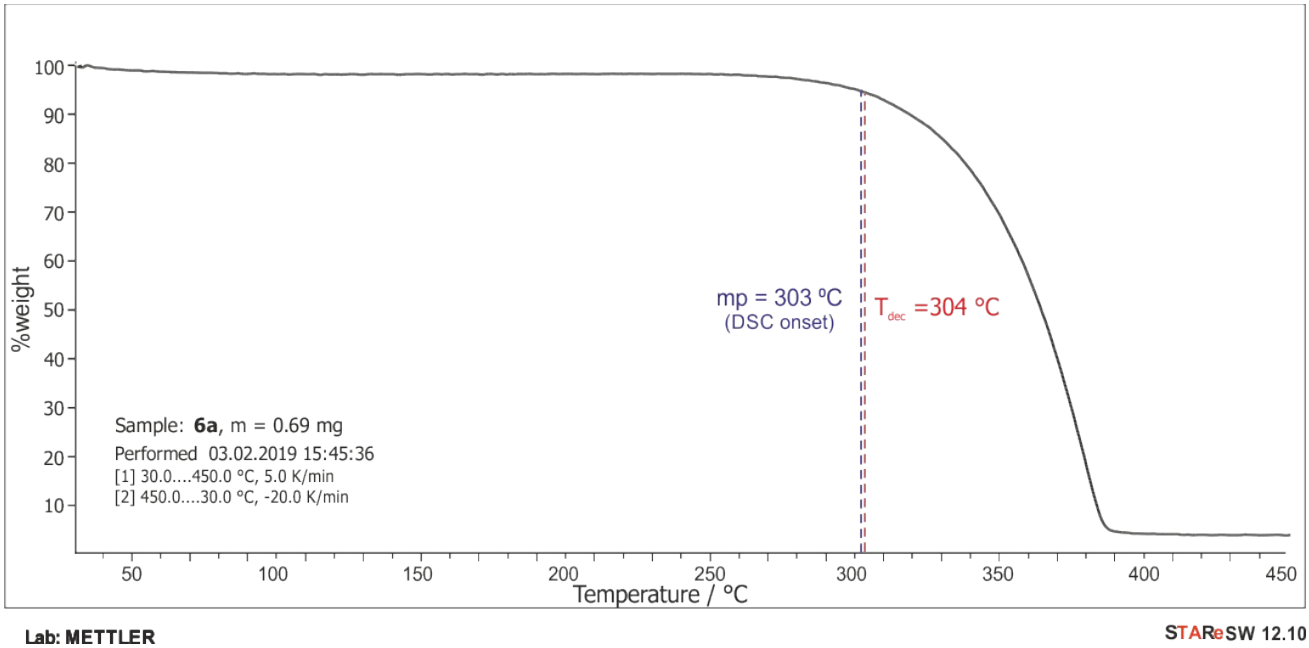

Figure S12. TGA curve of **6a**.

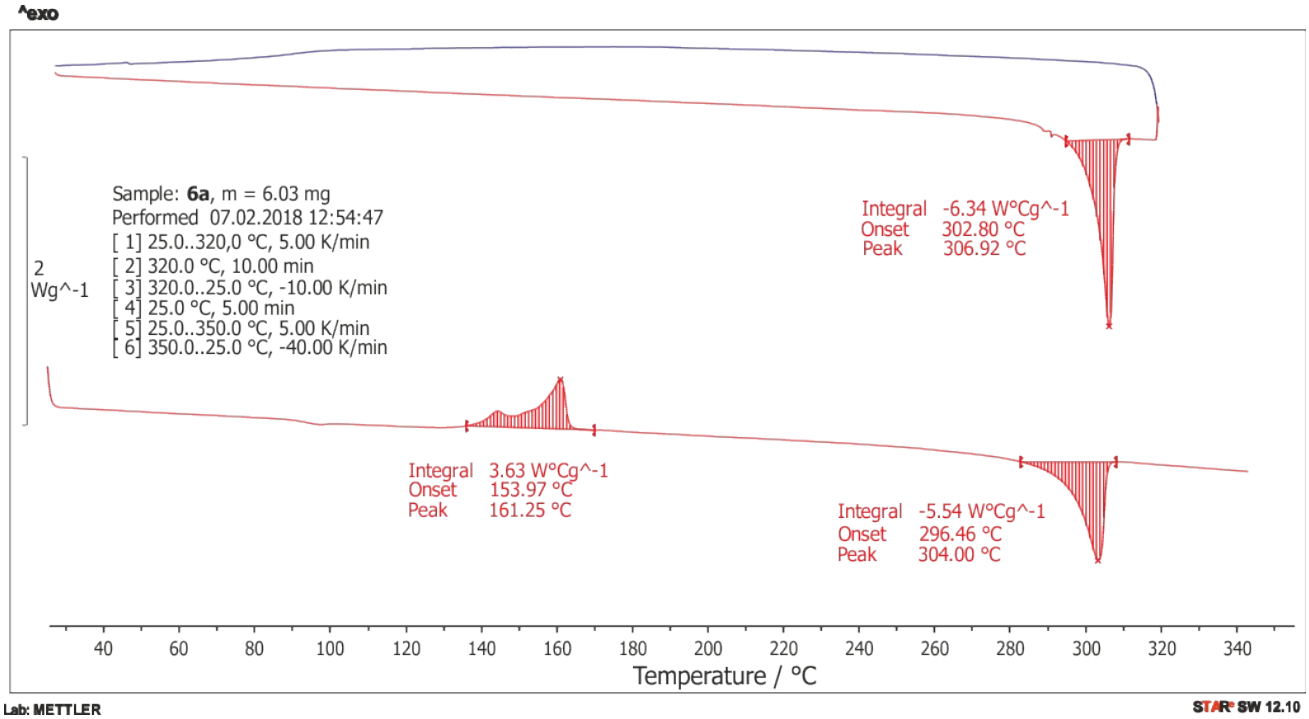

Figure S13. DSC curve of **6a**.

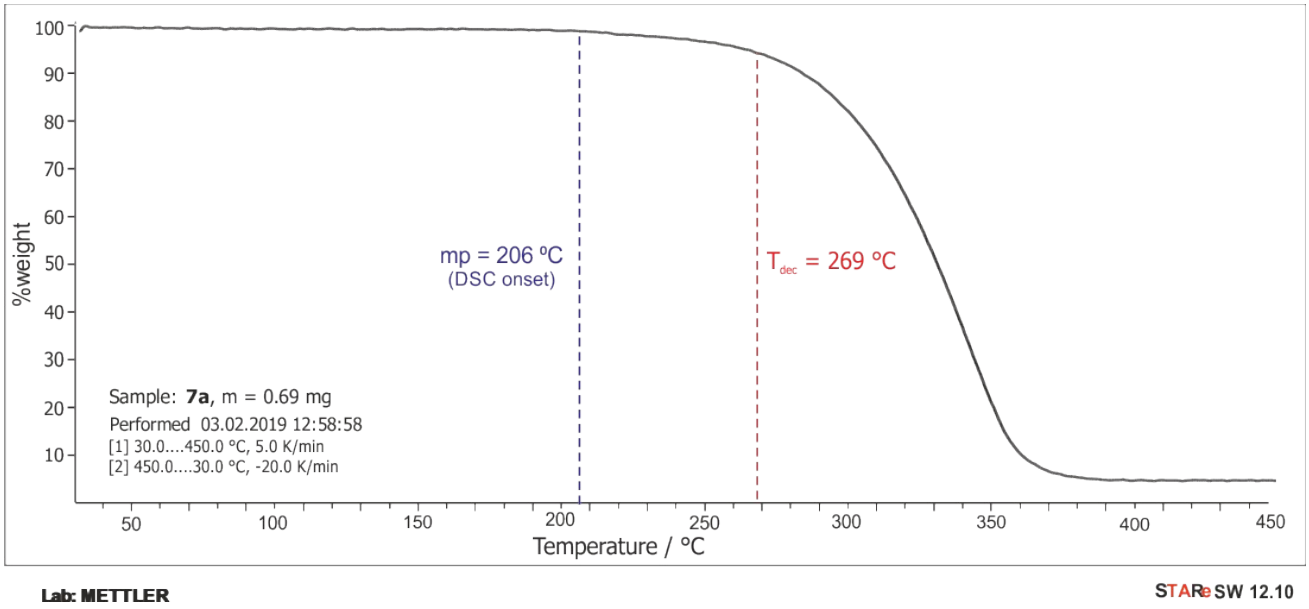

Figure S14. . TGA curve of **7a**.

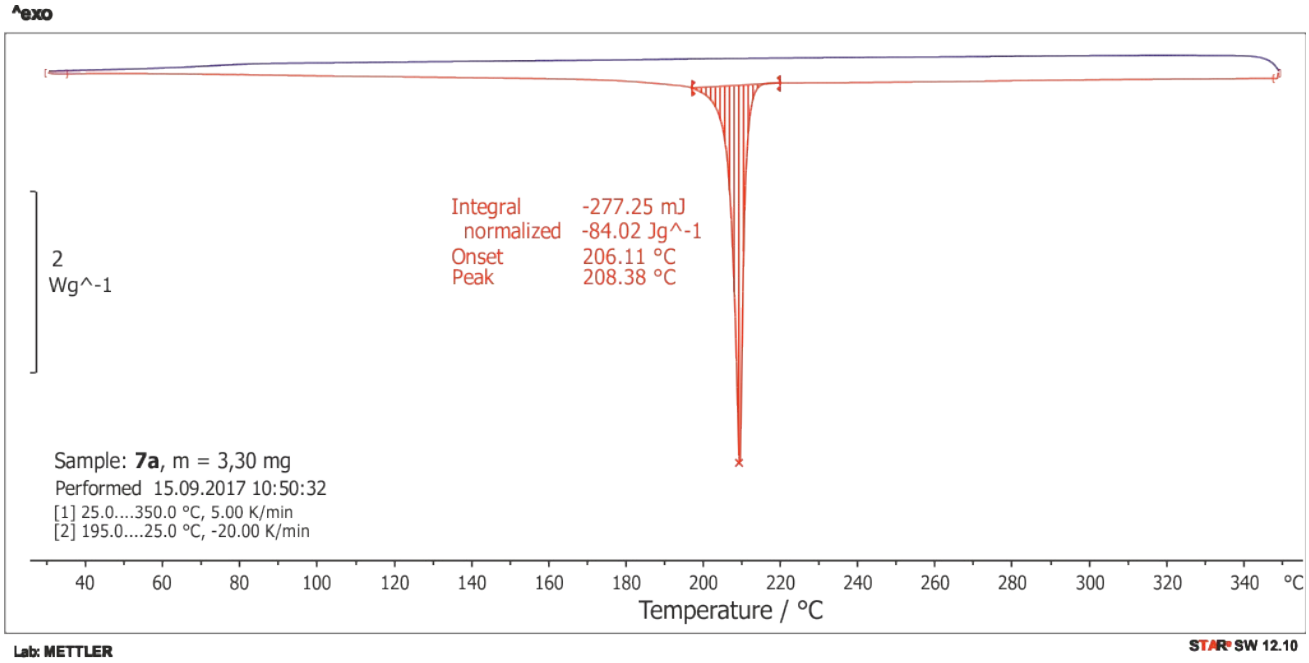

Figure S15. DSC curve of **7a**.

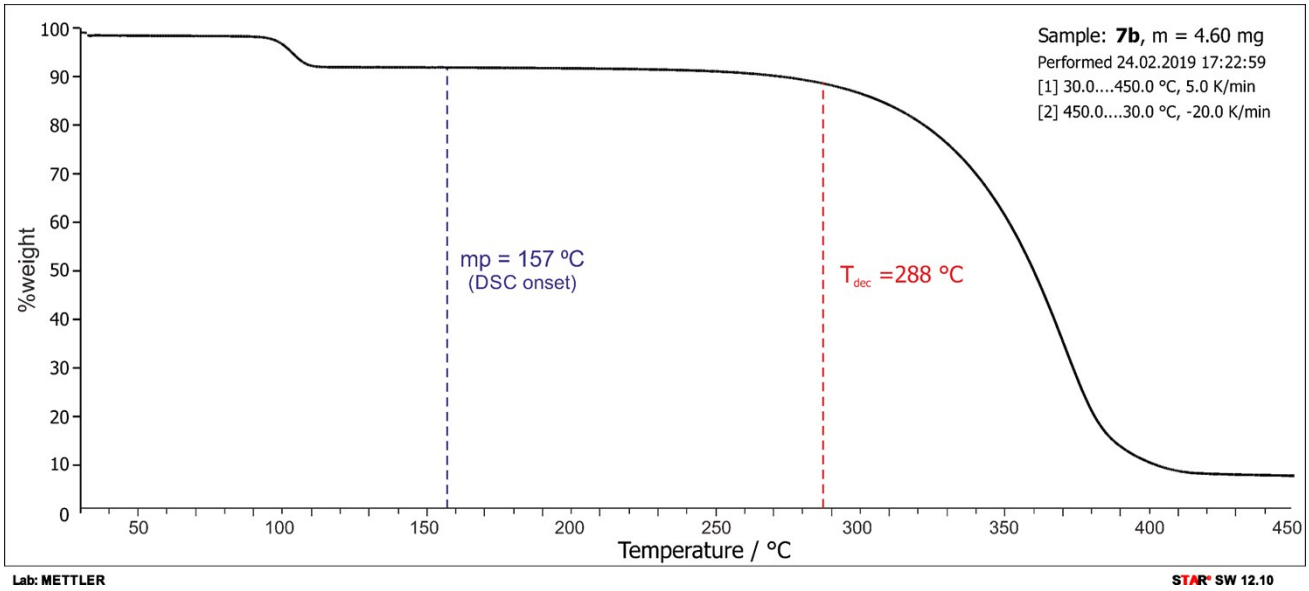

Figure S16. TGA curve of **7b**. Evaporation of acetone molecule is observed at ca. 90 °C.

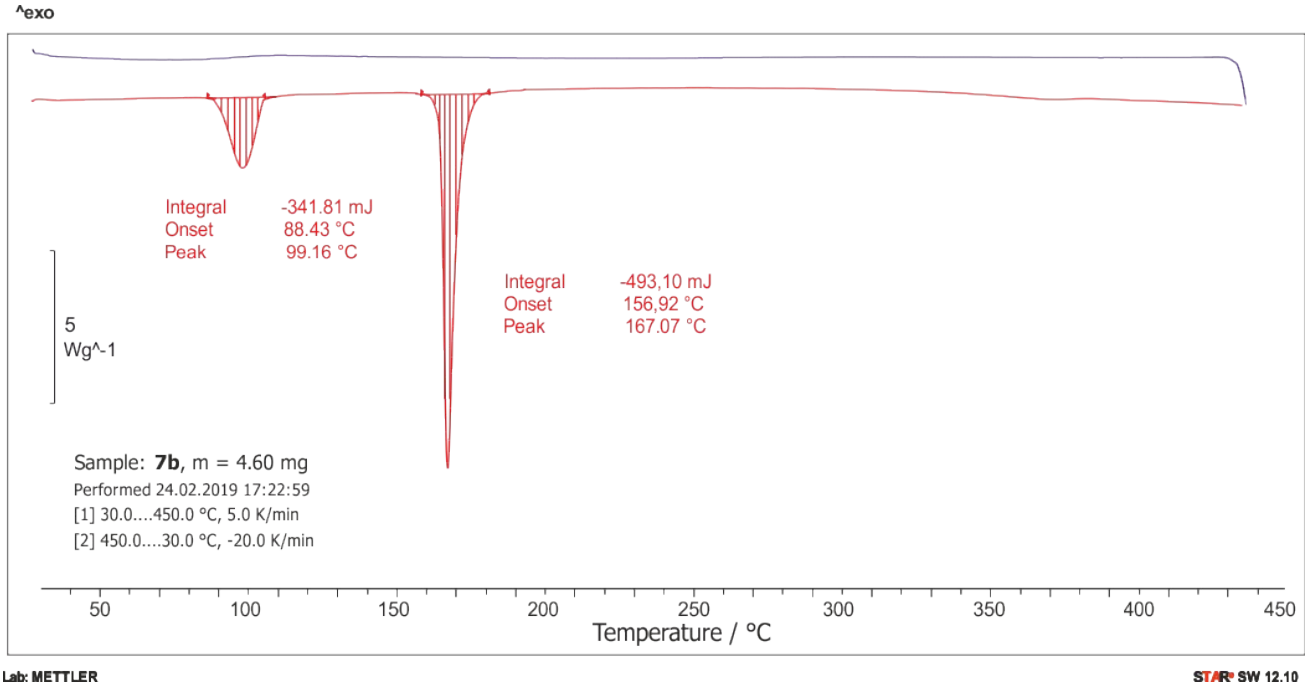

Figure S17. DSC curve of **7b**.

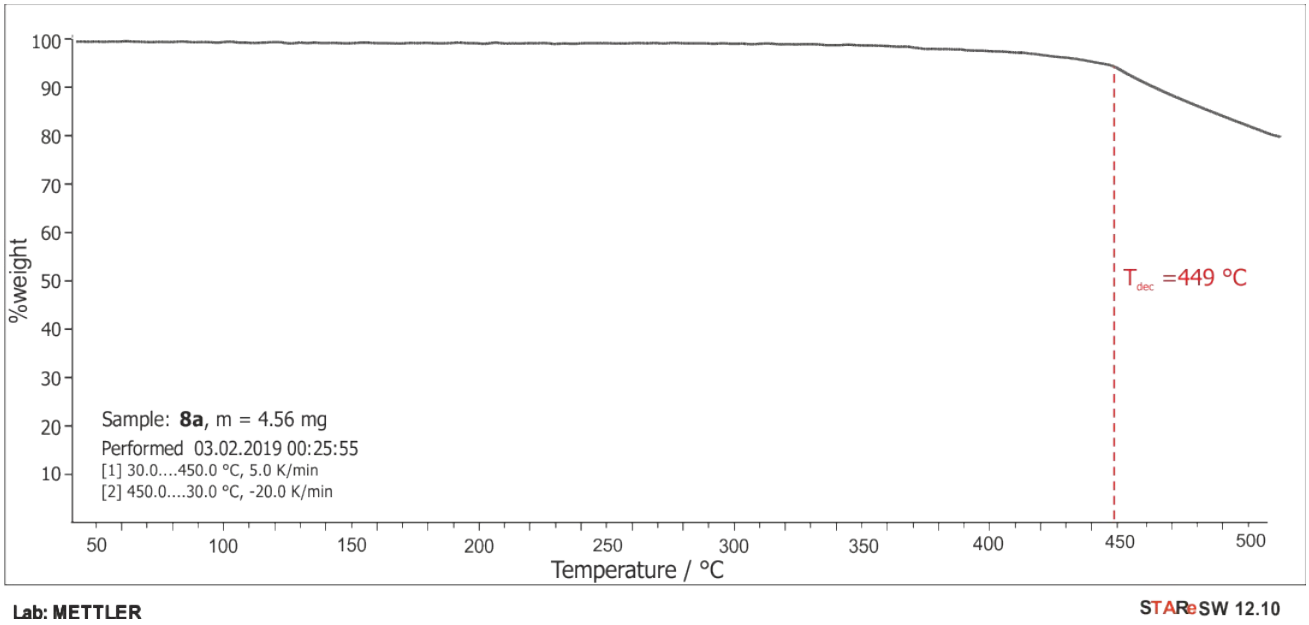

Figure S18. TGA curve of **8a**.

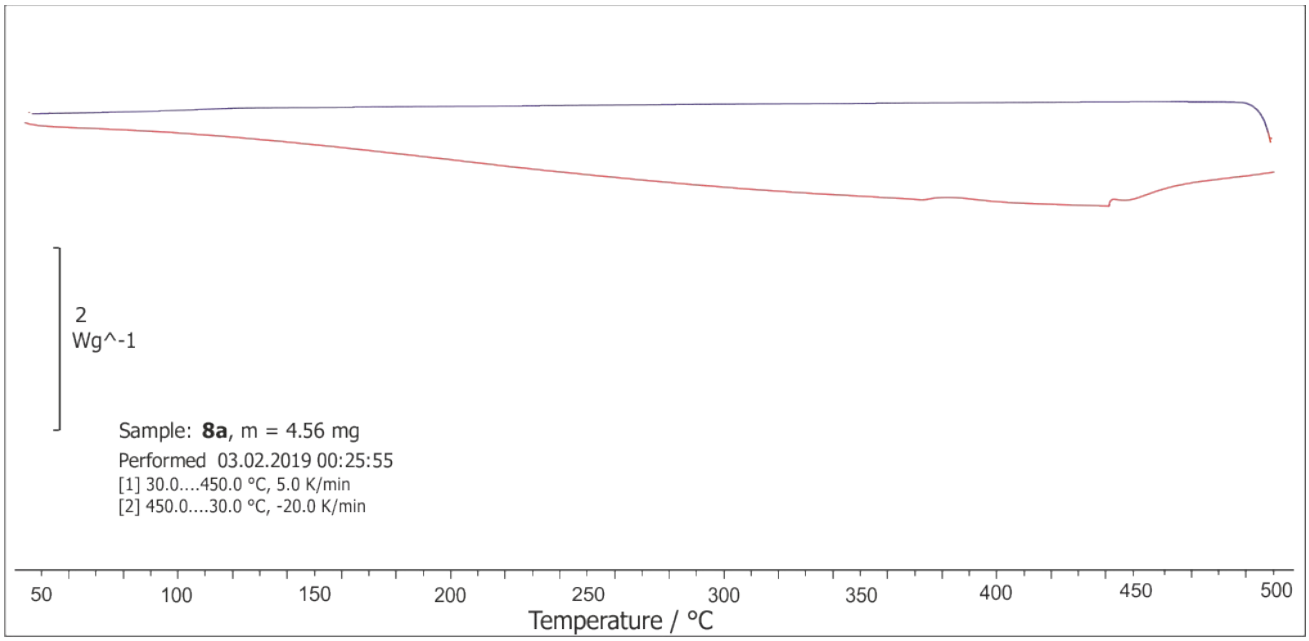

Figure S19. DSC curve of **8a**.

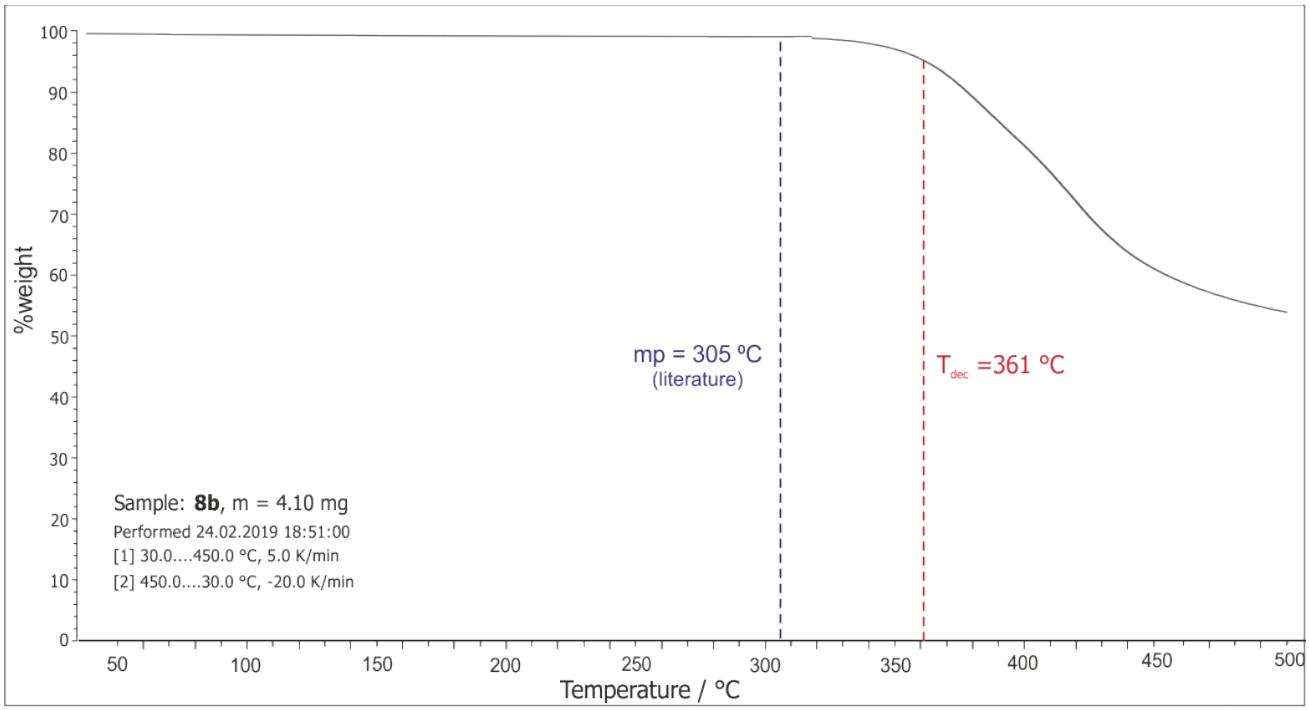

Figure S20. TGA curve of **8b**.

3. Electrochemical data

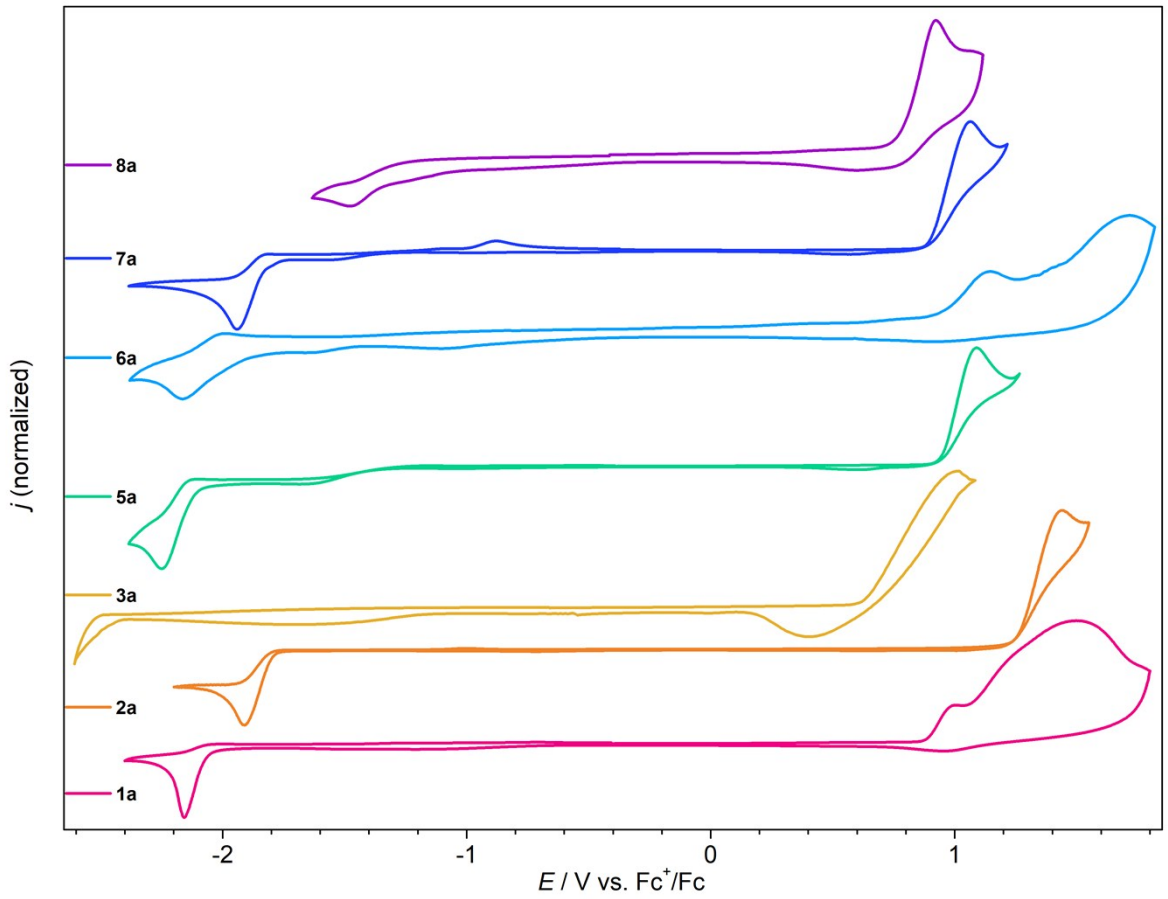

Figure S21. Overlay of CV for **1a** – **8a** in DCM.

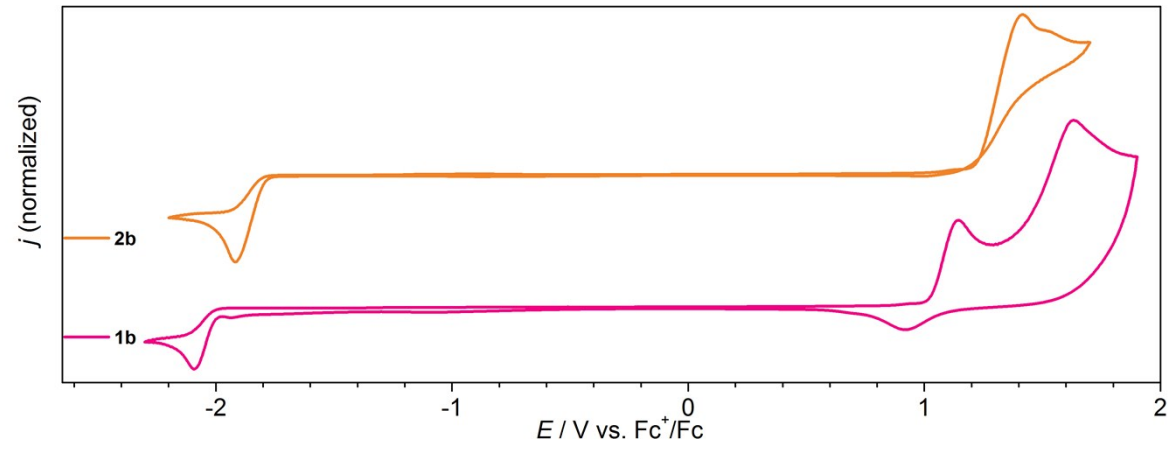

Figure S22. Overlay of CV for **1b** and **2b** in DCM.

4. UV-Vis spectra

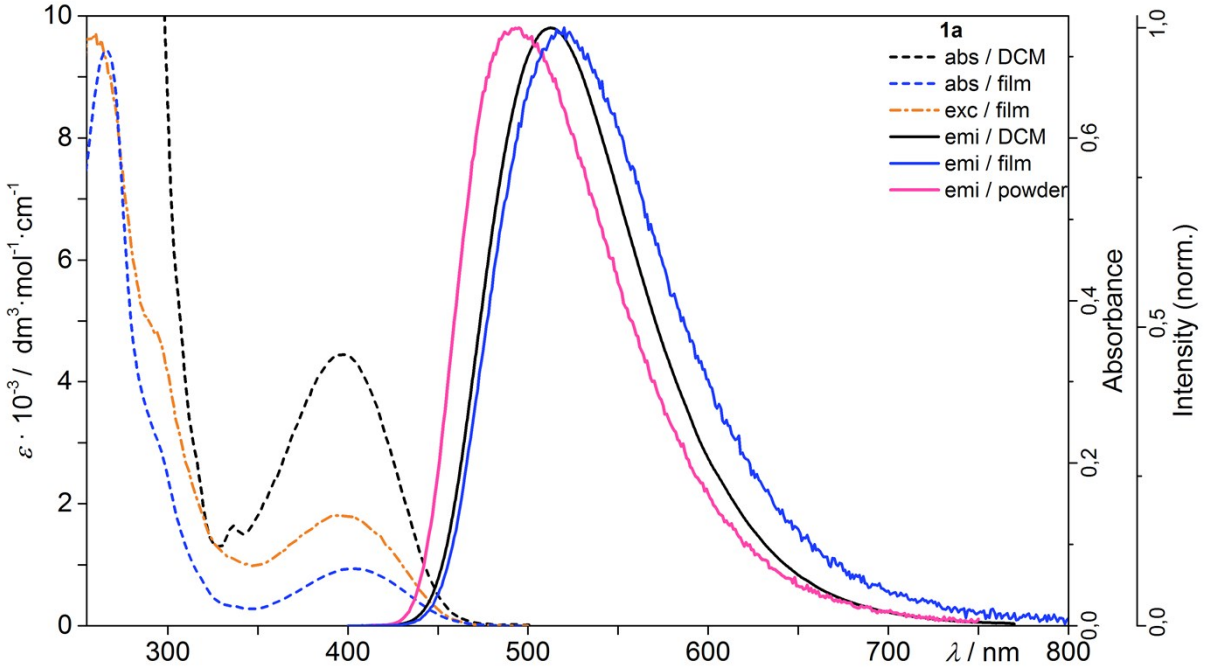

Figure S23. Overlay of UV-Vis absorption, excitation and emission spectra of **1a** in DCM solution and solid state. Absorption spectra of solution is depicted in ε scale (left), and absorption of film sample is in absorbance scale (right); remaining spectra are normalized.

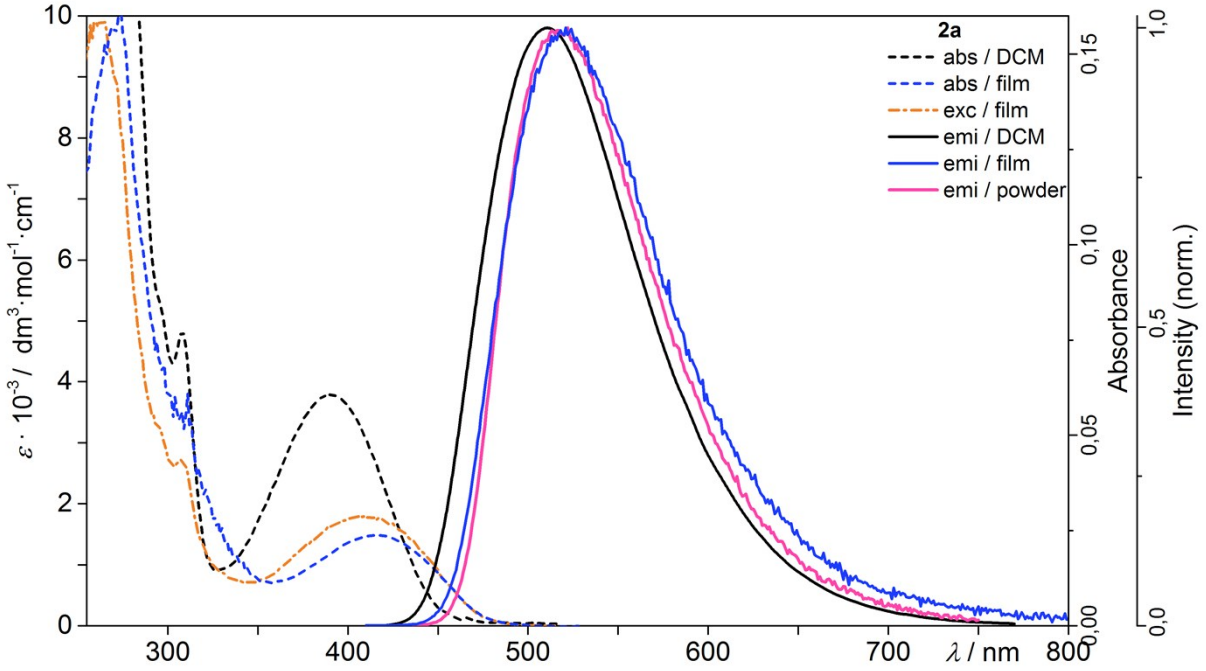

Figure S24. Overlay of UV-Vis absorption, excitation and emission spectra of **2a** in DCM solution and solid state. Absorption spectra of solution is depicted in ε scale (left), and absorption of film sample is in absorbance scale (right); remaining spectra are normalized.

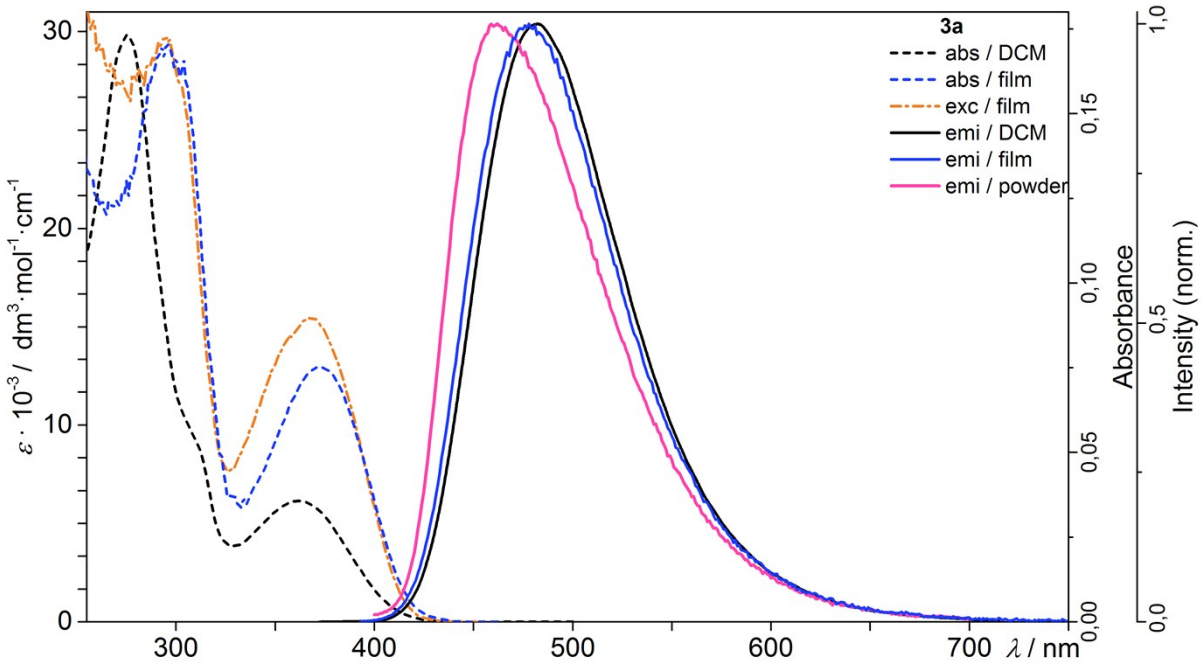

Figure S25. Overlay of UV-Vis absorption, excitation and emission spectra of **3a** in DCM solution and solid state. Absorption spectra of solution is depicted in ε scale (left), and absorption of film sample is in absorbance scale (right); remaining spectra are normalized.

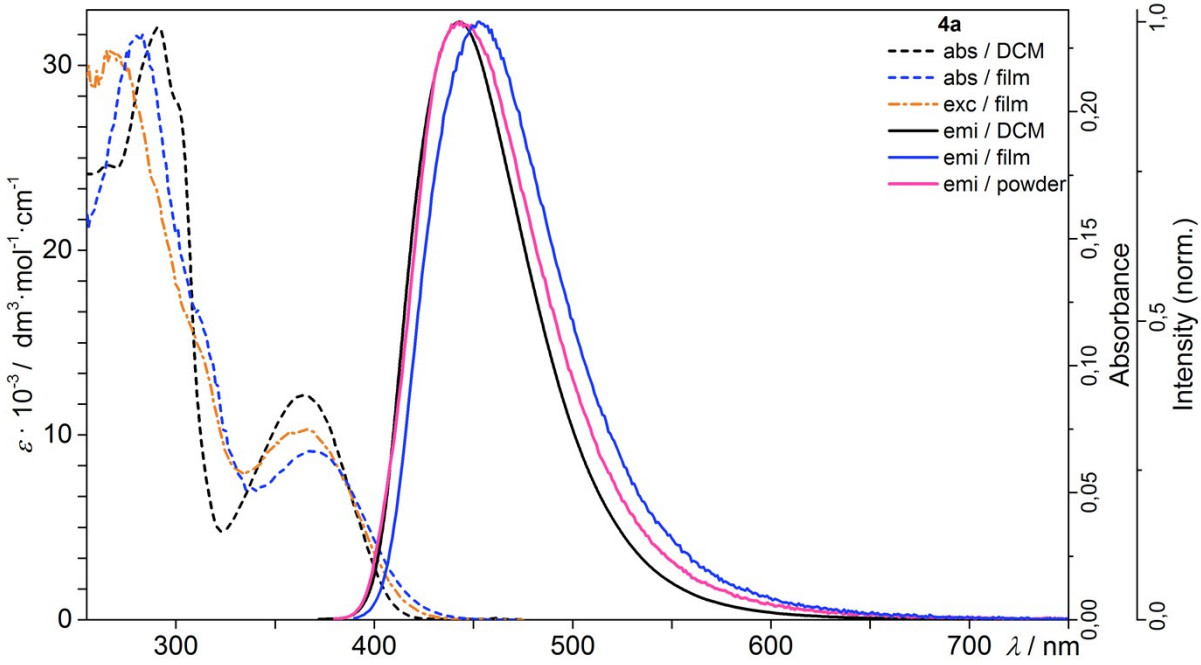

Figure S26. Overlay of UV-Vis absorption, excitation and emission spectra of **4a** in DCM solution and solid state. Absorption spectra of solution is depicted in ε scale (left), and absorption of film sample is in absorbance scale (right); remaining spectra are normalized.

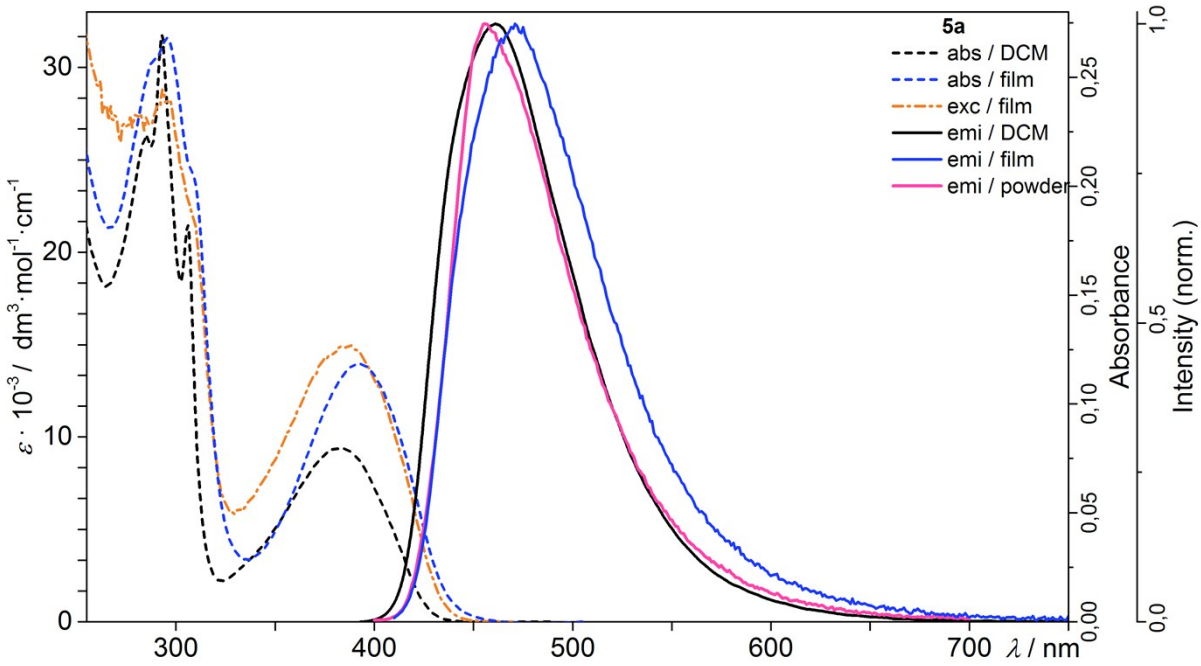

Figure S27. Overlay of UV-Vis absorption, excitation and emission spectra of **5a** in DCM solution and solid state. Absorption spectra of solution is depicted in ε scale (left), and absorption of film sample is in absorbance scale (right); remaining spectra are normalized.

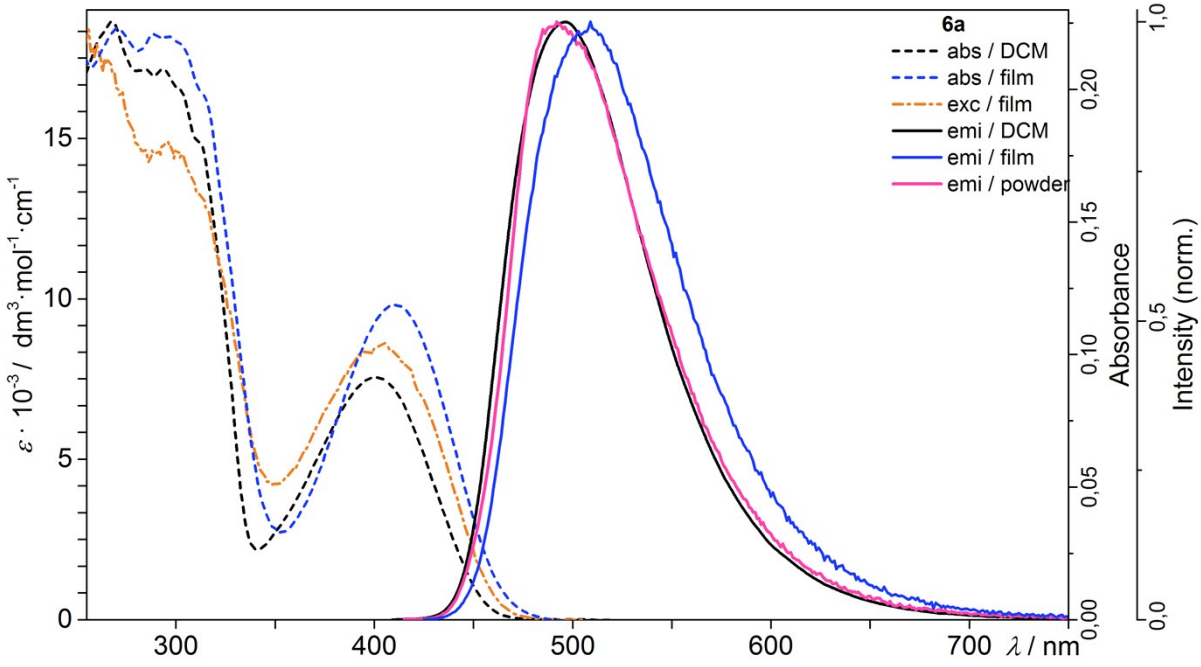

Figure S28. Overlay of UV-Vis absorption, excitation and emission spectra of **6a** in DCM solution and solid state. Absorption spectra of solution is depicted in ε scale (left), and absorption of film sample is in absorbance scale (right); remaining spectra are normalized.

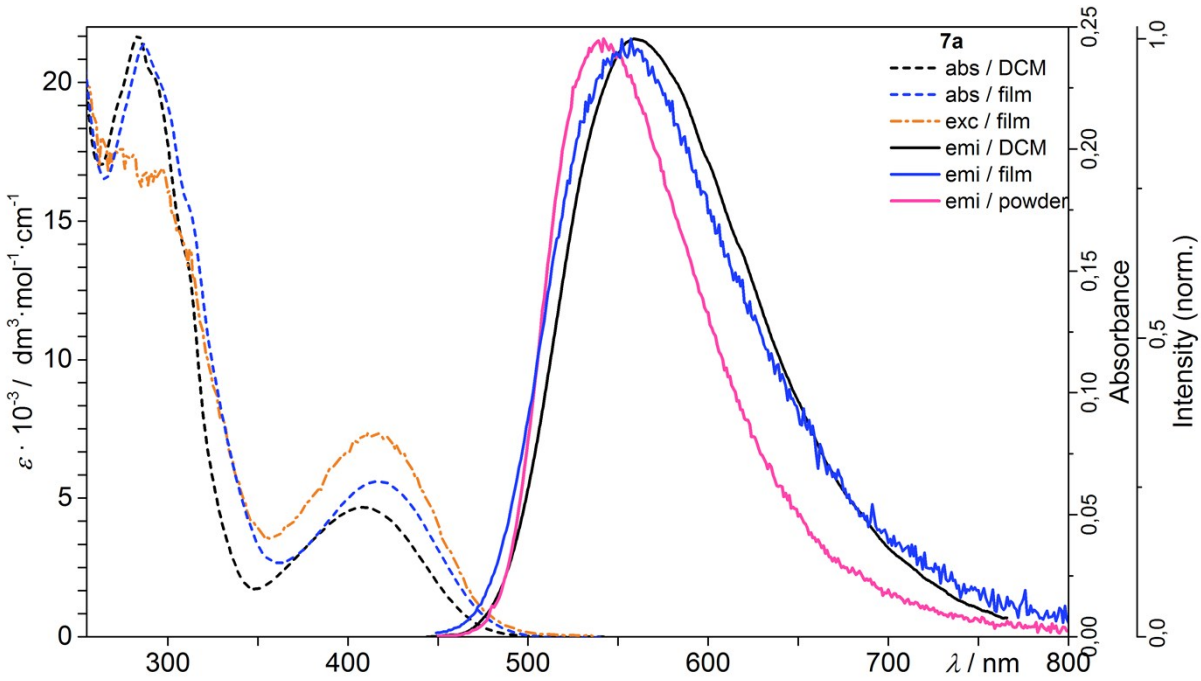

Figure S29. Overlay of UV-Vis absorption, excitation and emission spectra of **7a** in DCM solution and solid state. Absorption spectra of solution is depicted in ε scale (left), and absorption of film sample is in absorbance scale (right); remaining spectra are normalized.

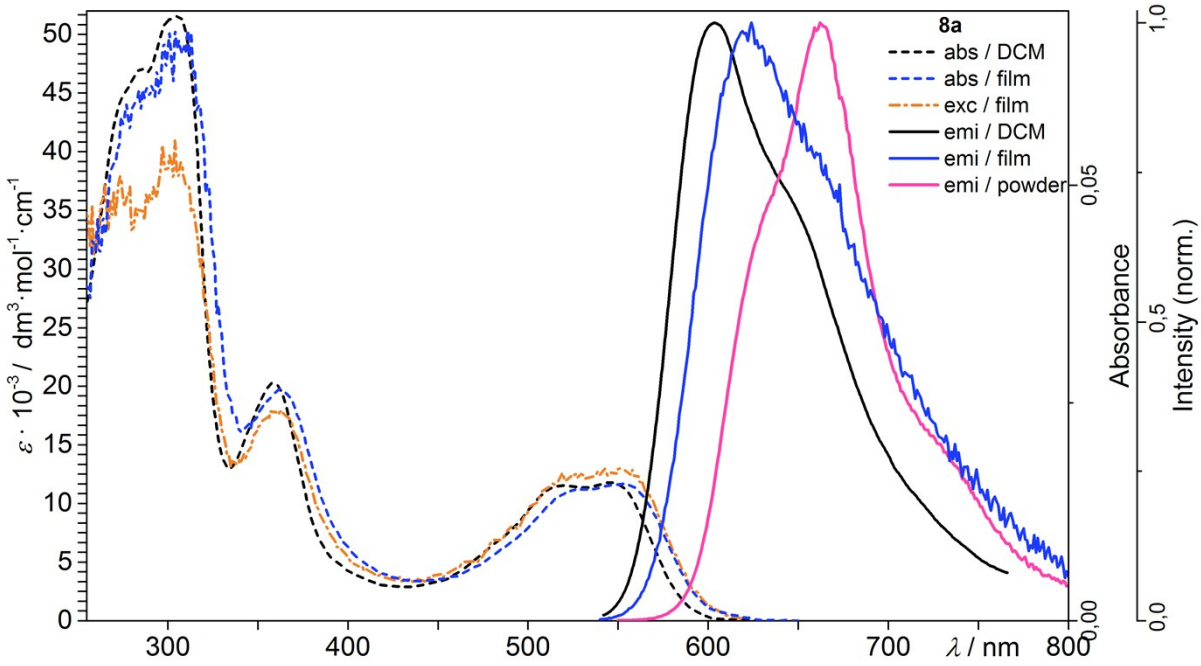

Figure S30. Overlay of UV-Vis absorption, excitation and emission spectra of **8a** in DCM solution and solid state. Absorption spectra of solution is depicted in ε scale (left), and absorption of film sample is in absorbance scale (right); remaining spectra are normalized

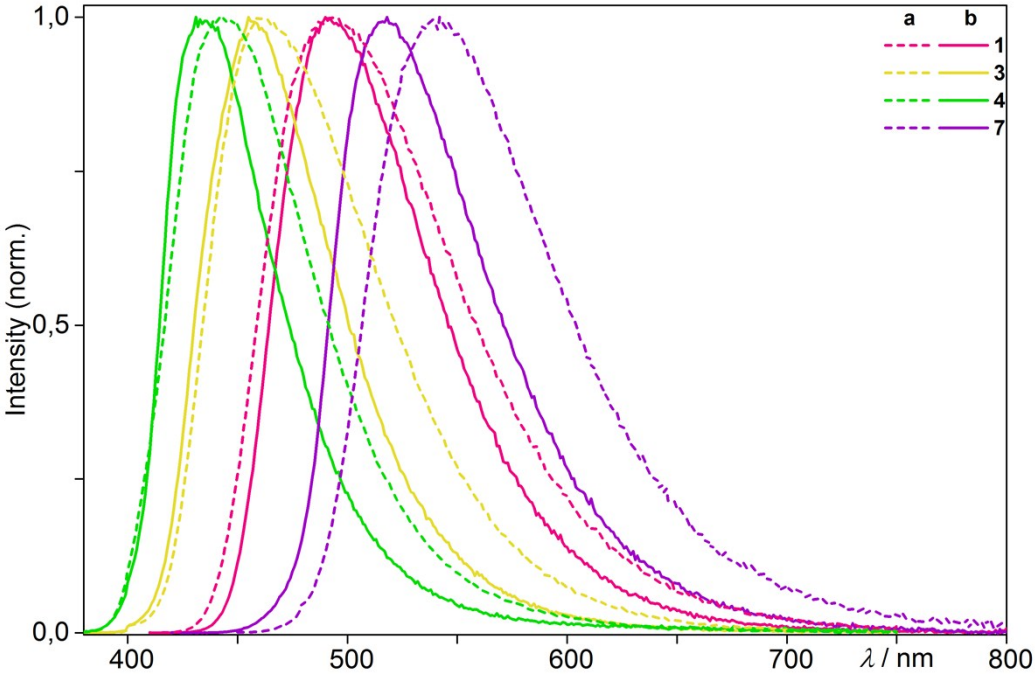

Figure S31. Overlay of emission spectra of **1a,b**, **3a**,**b**, **4a**,**b** and **7a**,**b** in solid state (powder).

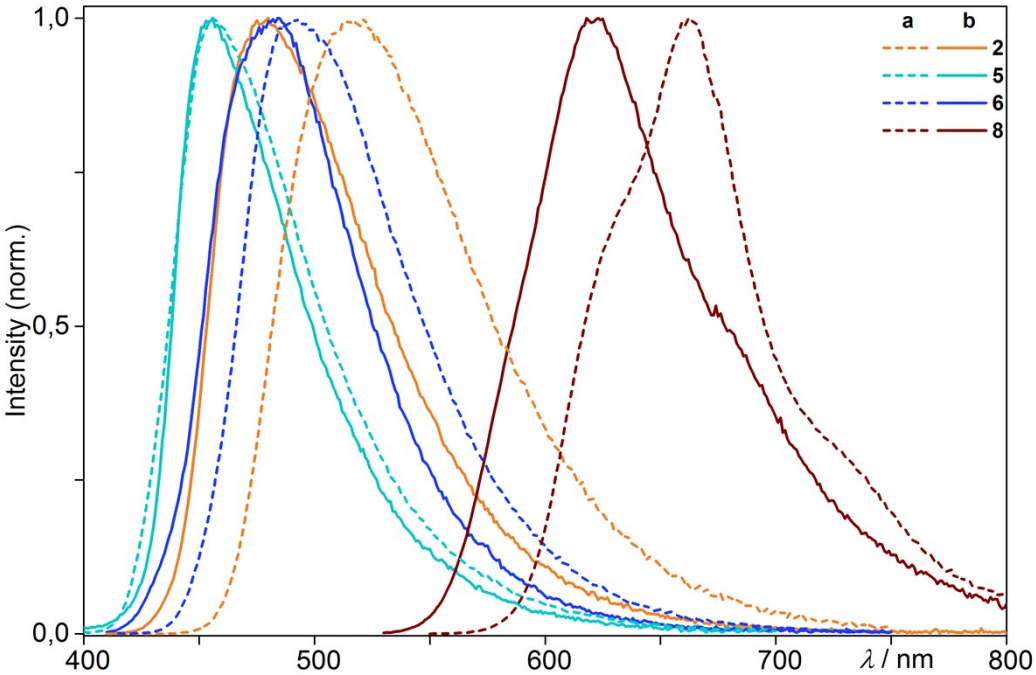

Figure S32. Overlay of emission spectra of **2a**,**b**, **5a**,**b**, **6a**,**b** and **8a**,**b** in solid state (powder).

5. Fluorescence decay data

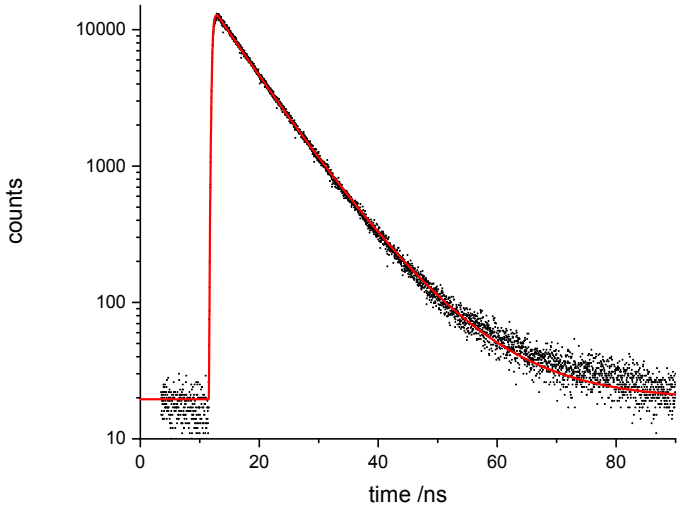

Figure S33. TCSPC data for compound **5b** – double exponential decay, fluorescence lifetime 6.4 ns and 11.1 ns in dichloromethane; black - experimental fluorescence decay; red - modelled curve.

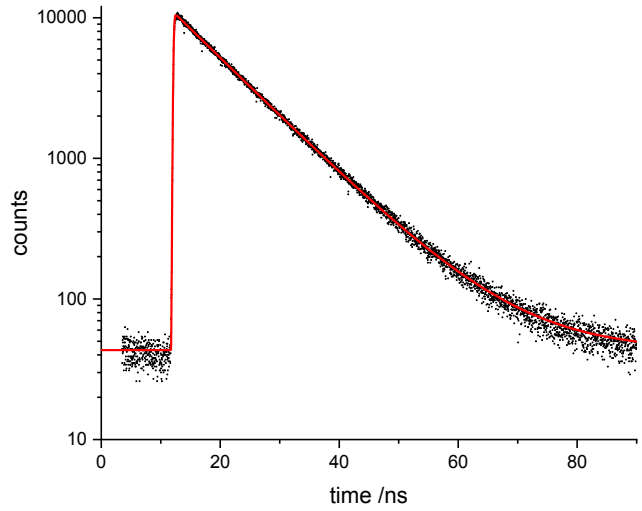

Figure S34. TCSPC data for compound **8b** in dichloromethane – single exponential decay, fluorescence lifetime of 10.5 ns; black - experimental fluorescence decay; red - modelled curve.

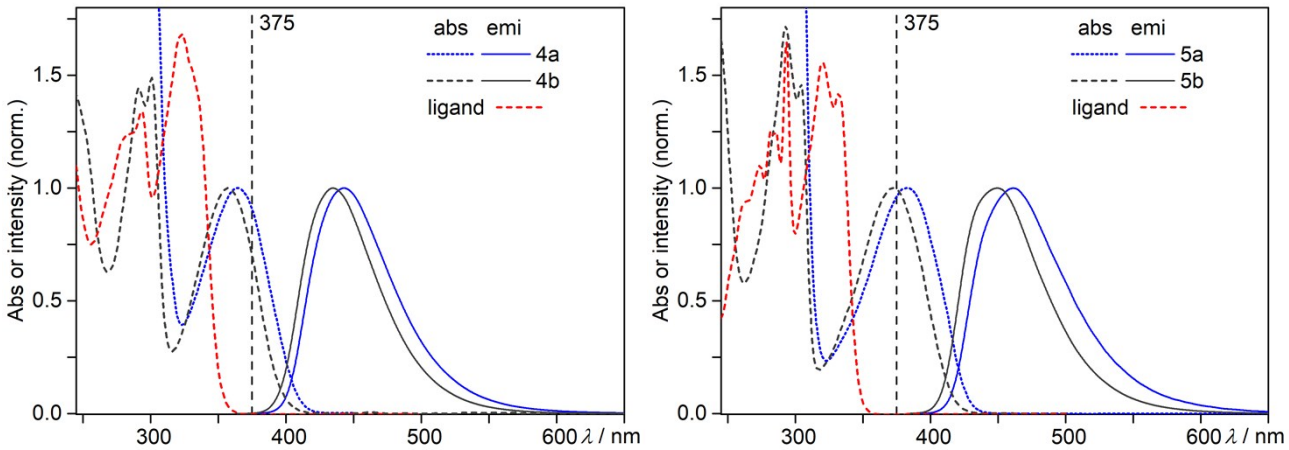

Figure S35. Overlay of absorption and fluorescence spectra of **4a**,b (left) and **5a**,**b** (right) with their corresponding ligands. Excitation wavelength used for lifetime measurements is marked with vertical dashed line.

6. Hydrolytic stability

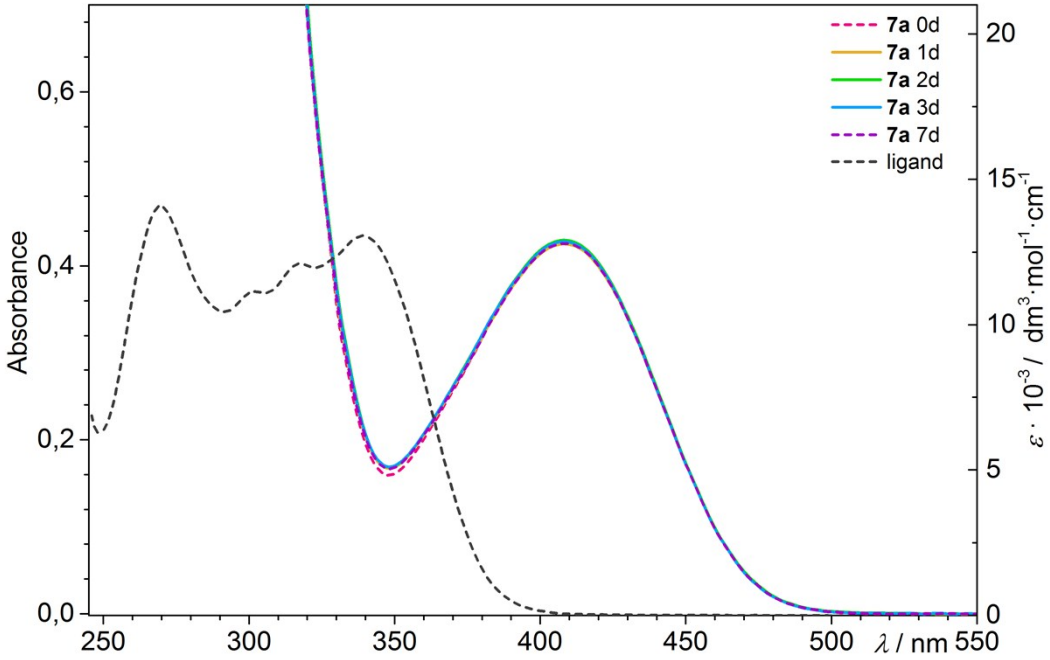

Figure S36. Overlay of UV-Vis spectra of compound **7a** in CH_2Cl_2 measured over 7 days along and free ligand - salicylideneaniline (in ε scale).

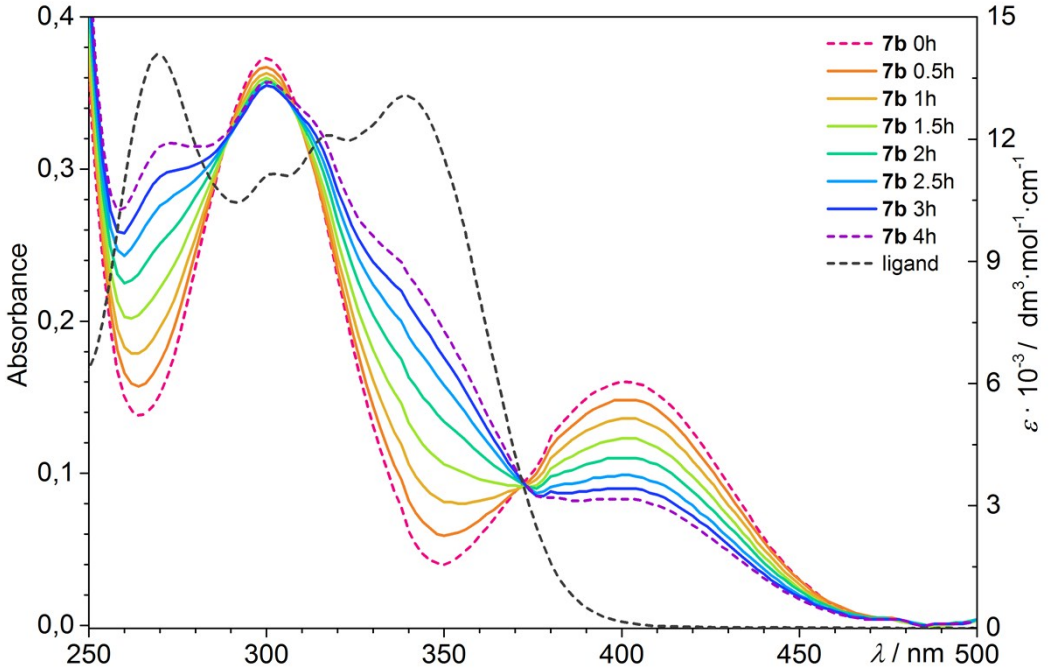

Figure S37. Overlay of UV-Vis spectra of compound **7b** in CH_2Cl_2 measured over 4 hours and free ligand - salicylideneaniline (in ε scale). Data were taken for comparison from our previous work.[6]

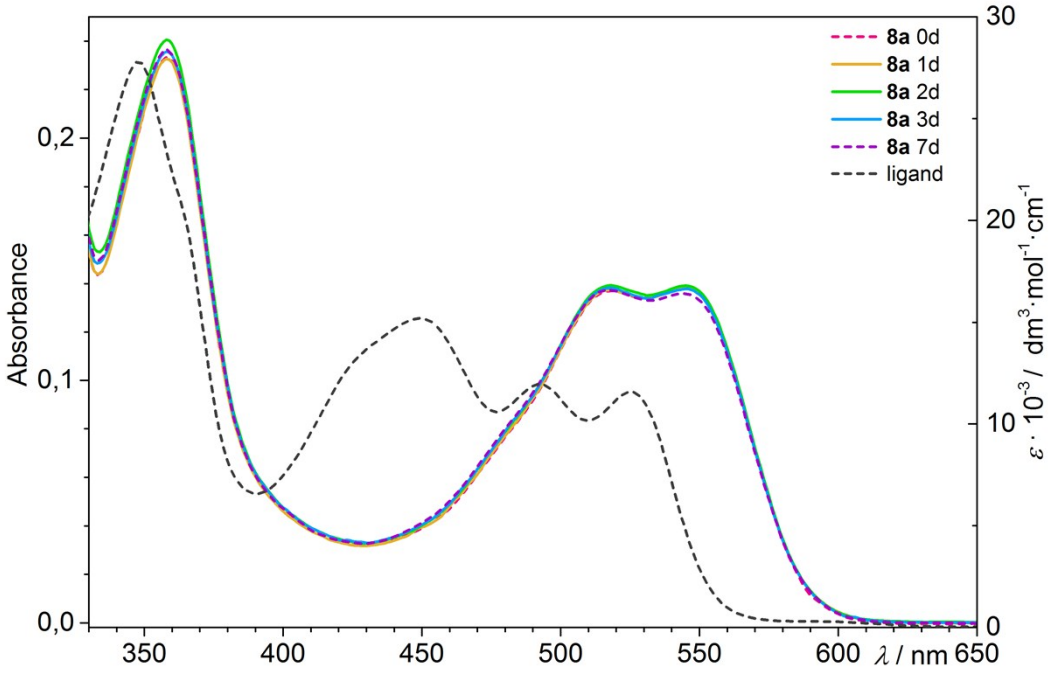

Figure S38. Overlay of UV-Vis spectra of compound **8a** in CH_2Cl_2 measured over 7 days and free ligand (in ε scale).

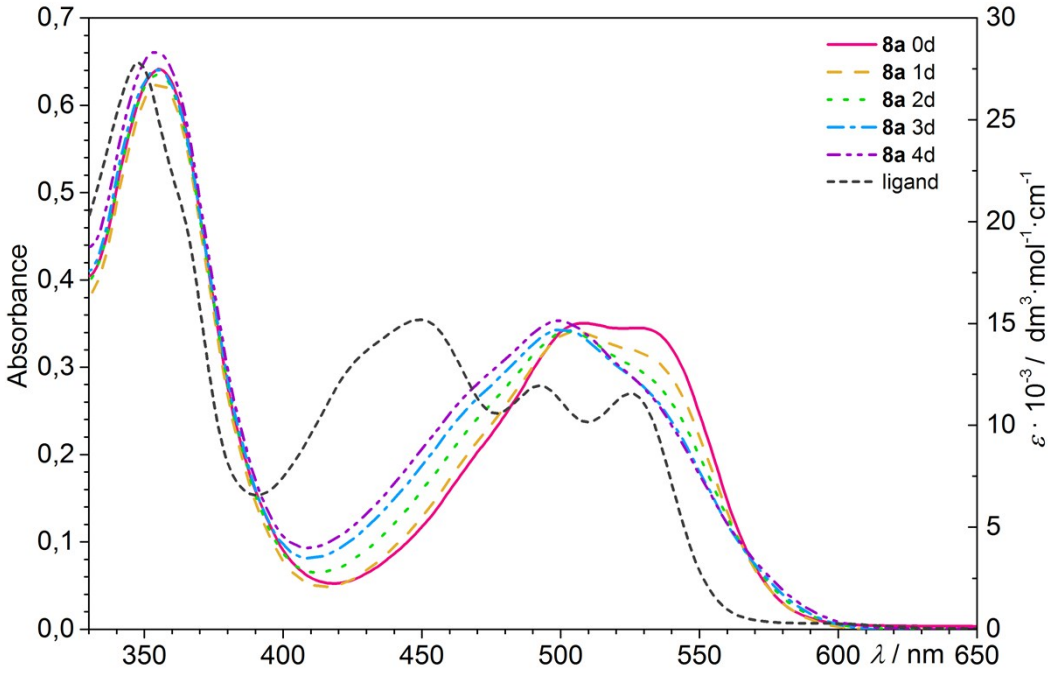

Figure S39. Overlay of UV-Vis spectra of compound **8a** in CH_2Cl_2 measured over 4 days and free ligand (in ε scale). Data were taken for comparison from our previous work.[7]

7. Quantum chemical calculations

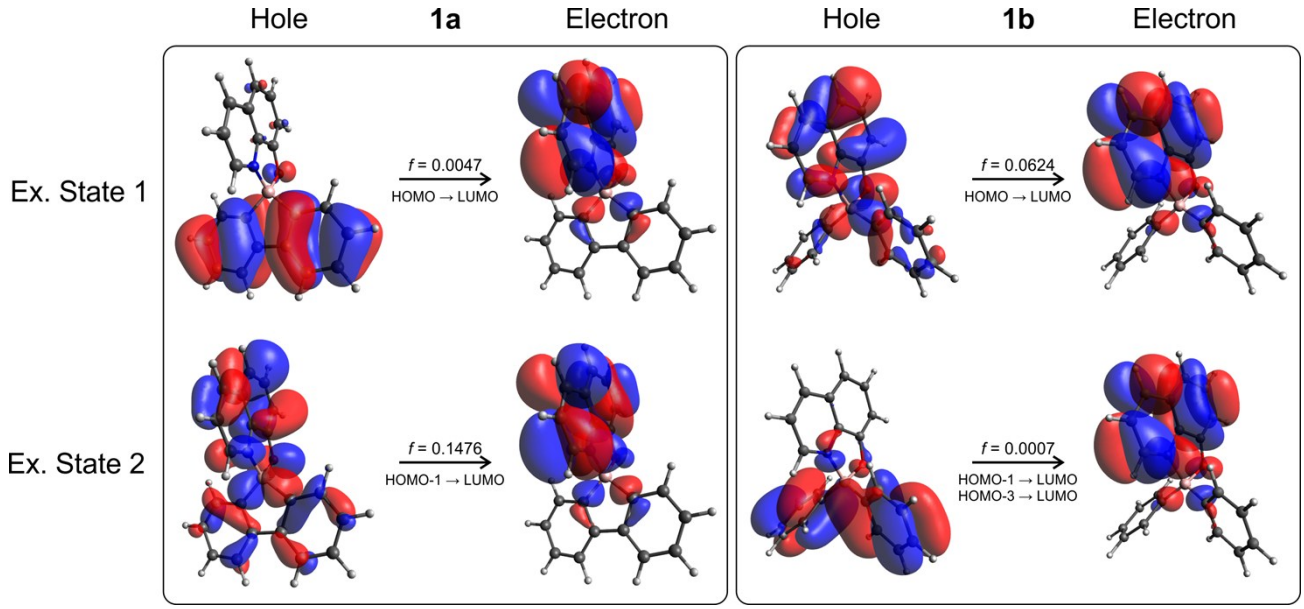

Figure S40. NTO orbitals for **1a** and **1b**

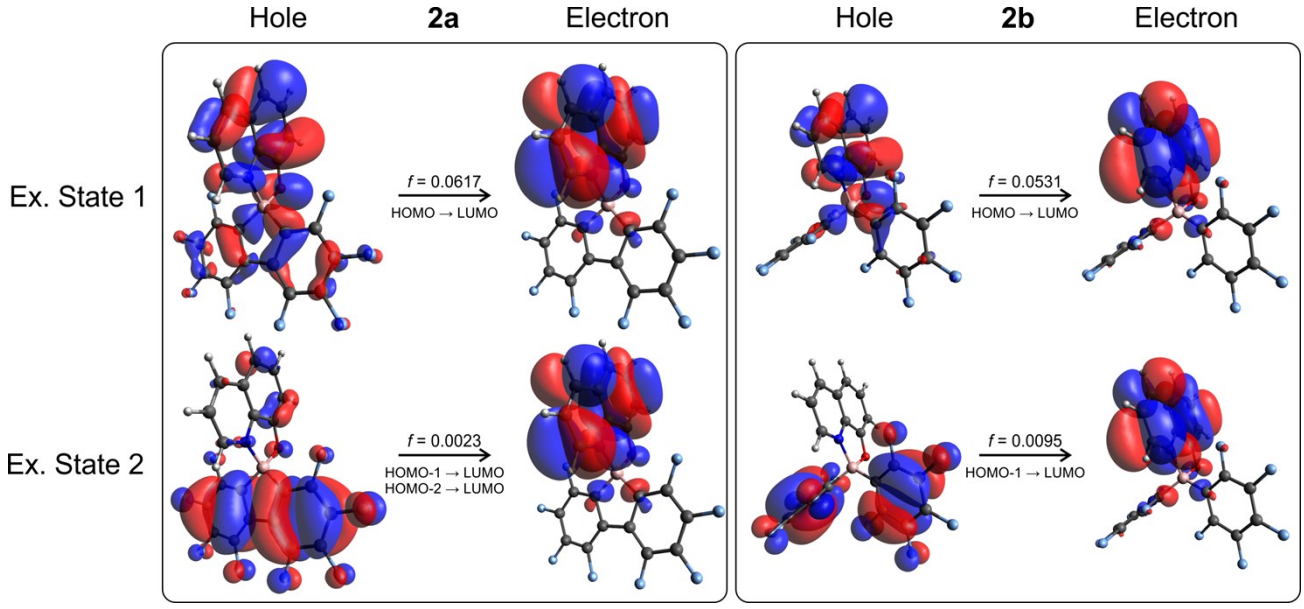

Figure S41. NTO orbitals for **2a** and **2b**

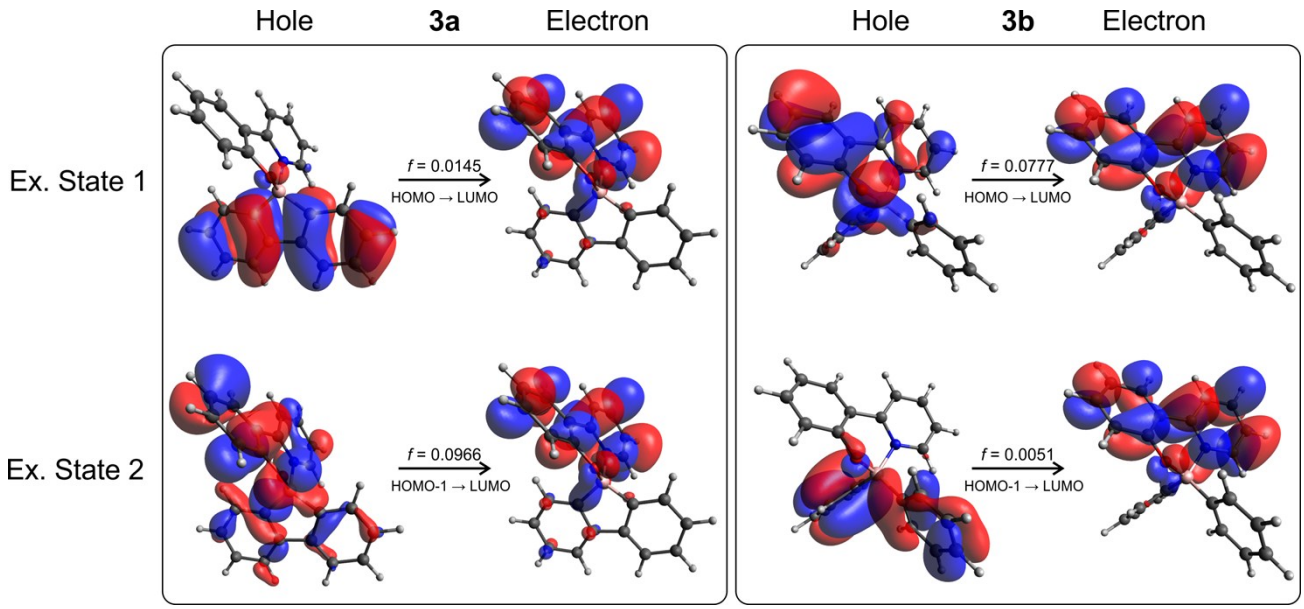

Figure S42. NTO orbitals for **3a** and **3b**.

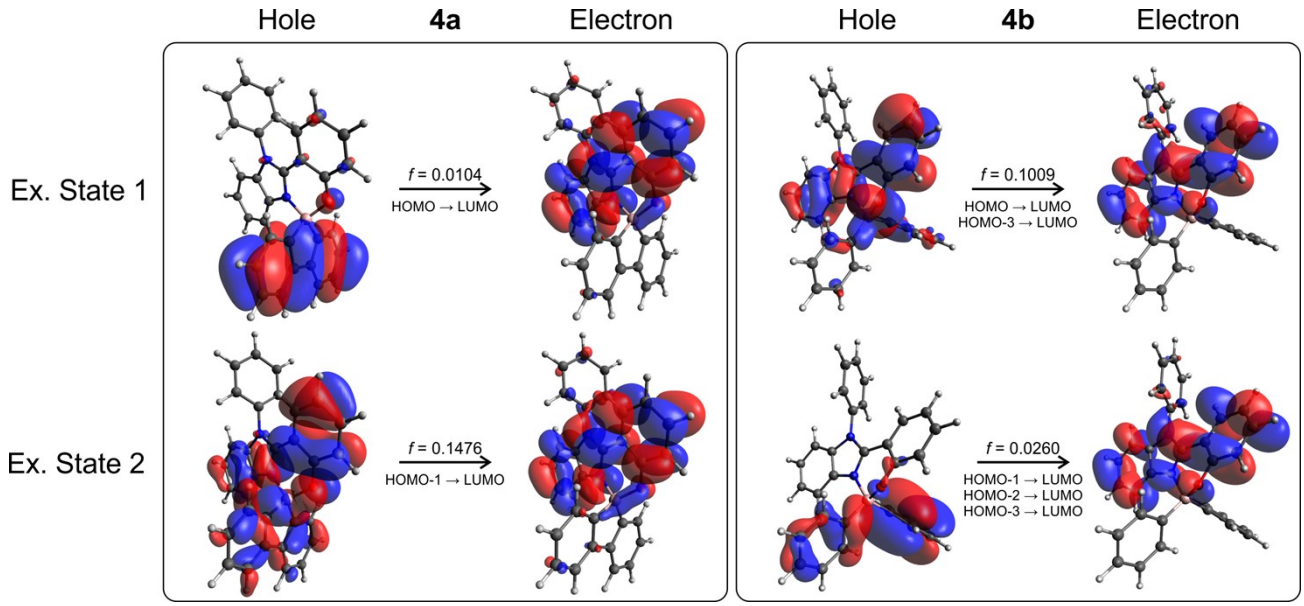

Figure S43. NTO orbitals for **4a** and **4b**.

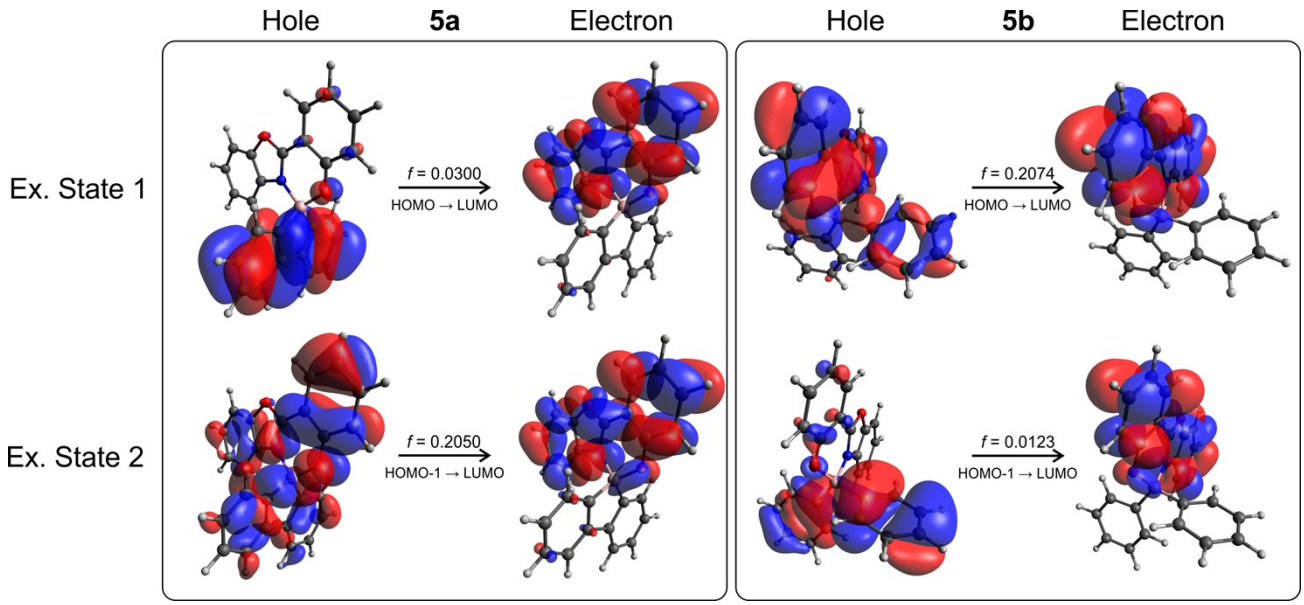

Figure S44. NTO orbitals for **5a** and **5b**.

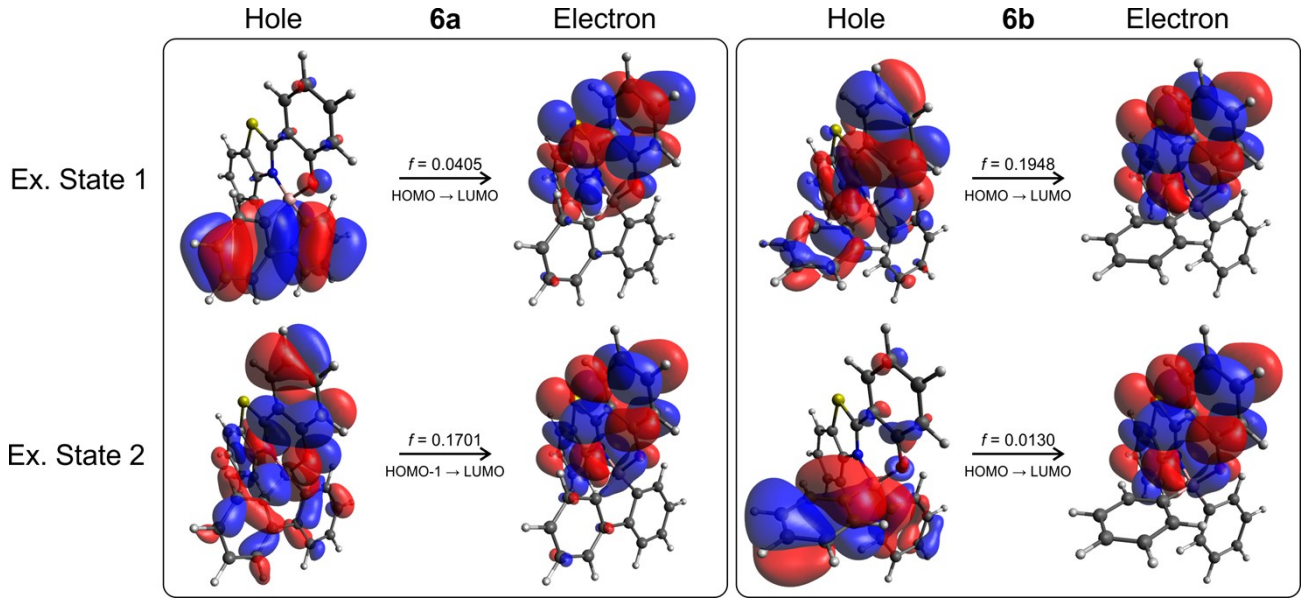

Figure S45. NTO orbitals for **6a** and **6b**.

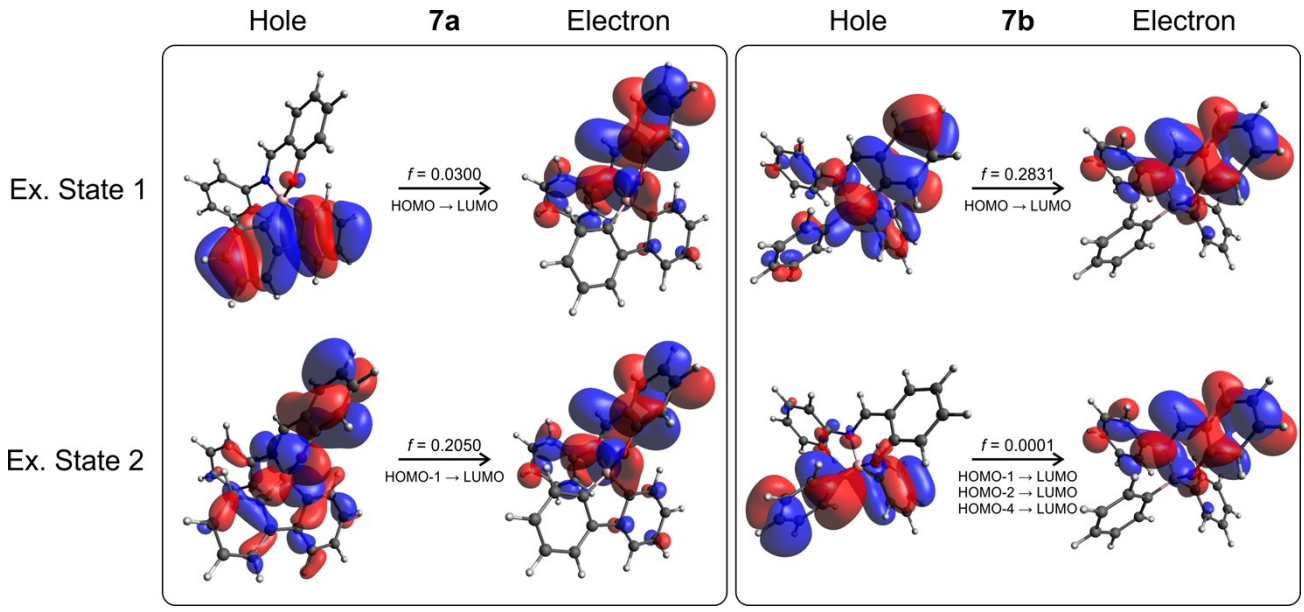

Figure S46. NTO orbitals for **7a** and **7b**.

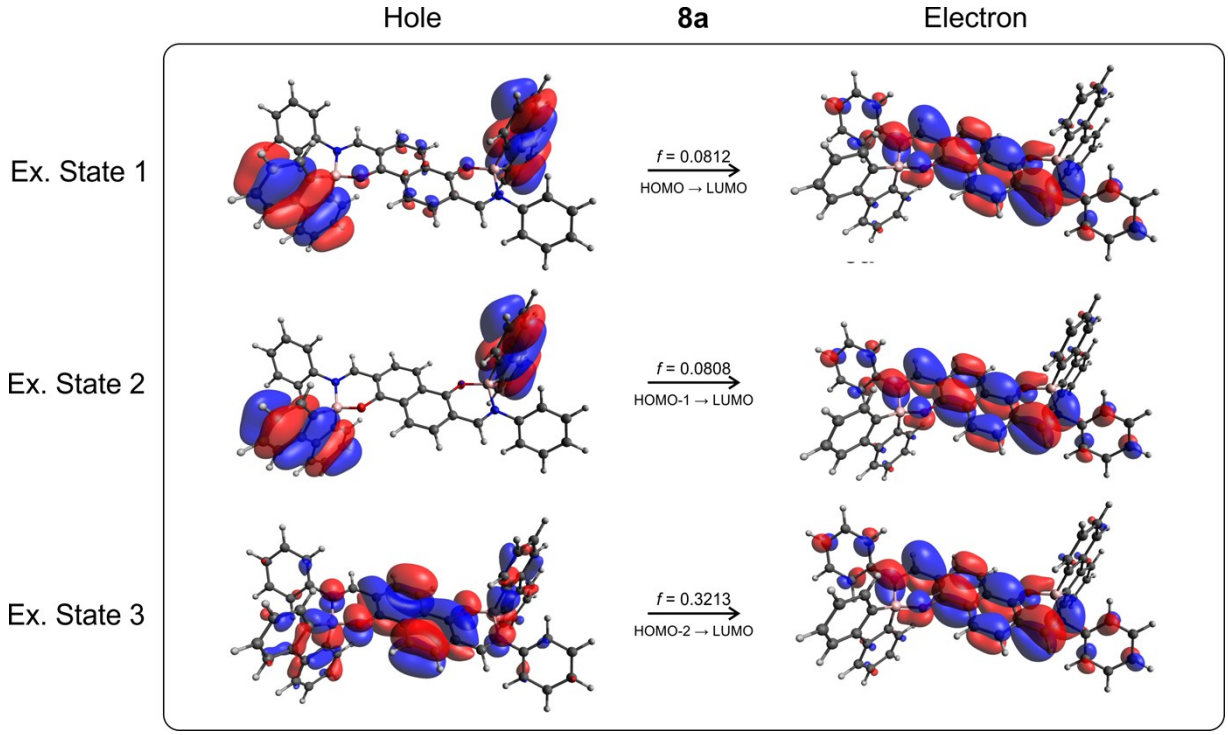

Figure S47. NTO orbitals for **8a**.

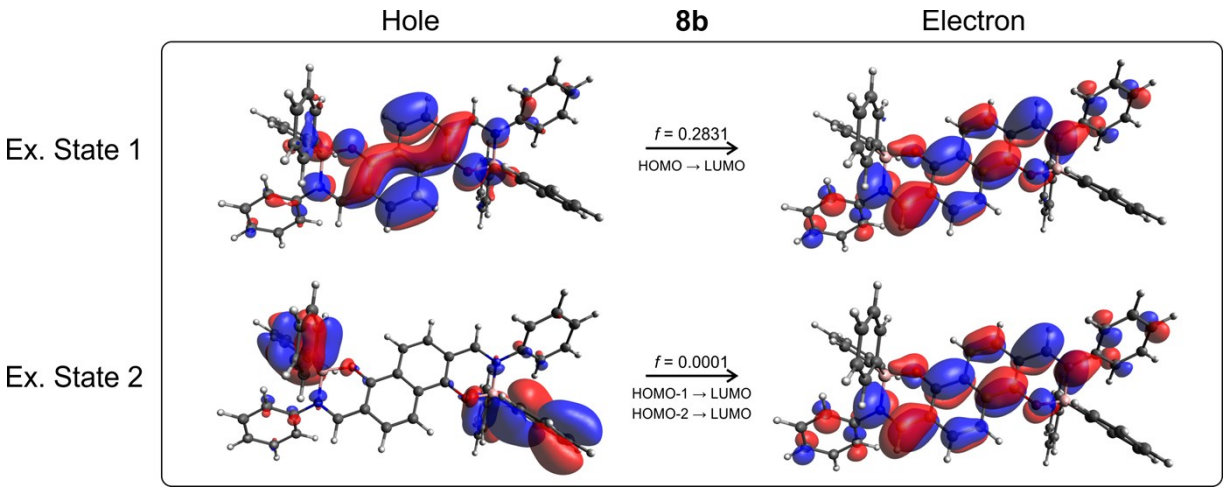

Figure S48. NTO orbitals for **8b**.

Table S3. Comparison of experimental and calculates TD-DFT photophysical results.

	Experimental	Theoretical		
	λ_{em} / nm	λ_{em} / nm	f	Transition
1a	513	549.9	0.0047	HOMO (80)→LUMO (81)
		474.6	0.1476	HOMO-1 (79)→LUMO (81)
1b	511	479.2	0.0624	HOMO (81)→LUMO (82)
		304.3	0.0007	HOMO-1 (80)→LUMO (82) HOMO-3 (78)→LUMO (82)
2a	510	485.1	0.0617	HOMO (112)→LUMO (113)
		316.7	0.0023	HOMO-1 (111)→LUMO (113) HOMO-2 (110)→LUMO (113)
2b	514	482.1	0.0531	HOMO (121)→LUMO (122)
		296.5	0.0095	HOMO-1 (121)→LUMO (122)
3a	482	520.0	0.0145	HOMO (87)→LUMO (88)
		477.1	0.0966	HOMO-1 (86)→LUMO (88)
3b	471	486.5	0.0777	HOMO (88)→LUMO (89)
		358.5	0.0051	HOMO-1 (87)→LUMO (89)
4a	443	500.3	0.0104	HOMO (117)→LUMO (118)
		437.8	0.1476	HOMO-1 (116)→LUMO (118)
4b	435	455.0	0.1009	HOMO (118)→LUMO (119) HOMO (115)→LUMO (119)
		342.4	0.0260	HOMO-1 (117)→LUMO (119) HOMO-2 (116)→LUMO (119) HOMO-3 (115)→LUMO (119)
5a	461	543.8	0.0300	HOMO (97)→LUMO (98)
		458.0	0.2050	HOMO-1 (96)→LUMO (98)
5b	449	472.7	0.2074	HOMO (98)→LUMO (99)
		372.2	0.0123	HOMO-1 (97)→LUMO (99)
6a	496	579.6	0.0405	HOMO (101)→LUMO (102)
		478.0	0.1701	HOMO-1 (100)→LUMO (102)
6b	482	508.0	0.1948	HOMO (102)→LUMO (103)

		486.6	0.0130	HOMO-1 (101)→LUMO (103)
7a	559	656.7	0.0300	HOMO (94)→LUMO (95)
		500.1	0.2050	HOMO-1 (93)→LUMO (95)
7b	534	480.9	0.2831	HOMO (95)→LUMO (96)
				HOMO-1 (94)→LUMO (96)
		336.2	0.0001	HOMO-2 (93)→LUMO (96)
				HOMO-3 (92)→LUMO (96)
8a	604	704.7	0.0812	HOMO (181)→LUMO (182)
		698.7	0.0808	HOMO-1 (180)→LUMO (182)
		639.7	0.3213	HOMO-2 (179)→LUMO (182)
8b	594	583.3	0.2831	HOMO (182)→LUMO (183)
		483.9	0.0001	HOMO-1 (181)→LUMO (183)
				HOMO-2 (180)→LUMO (183)

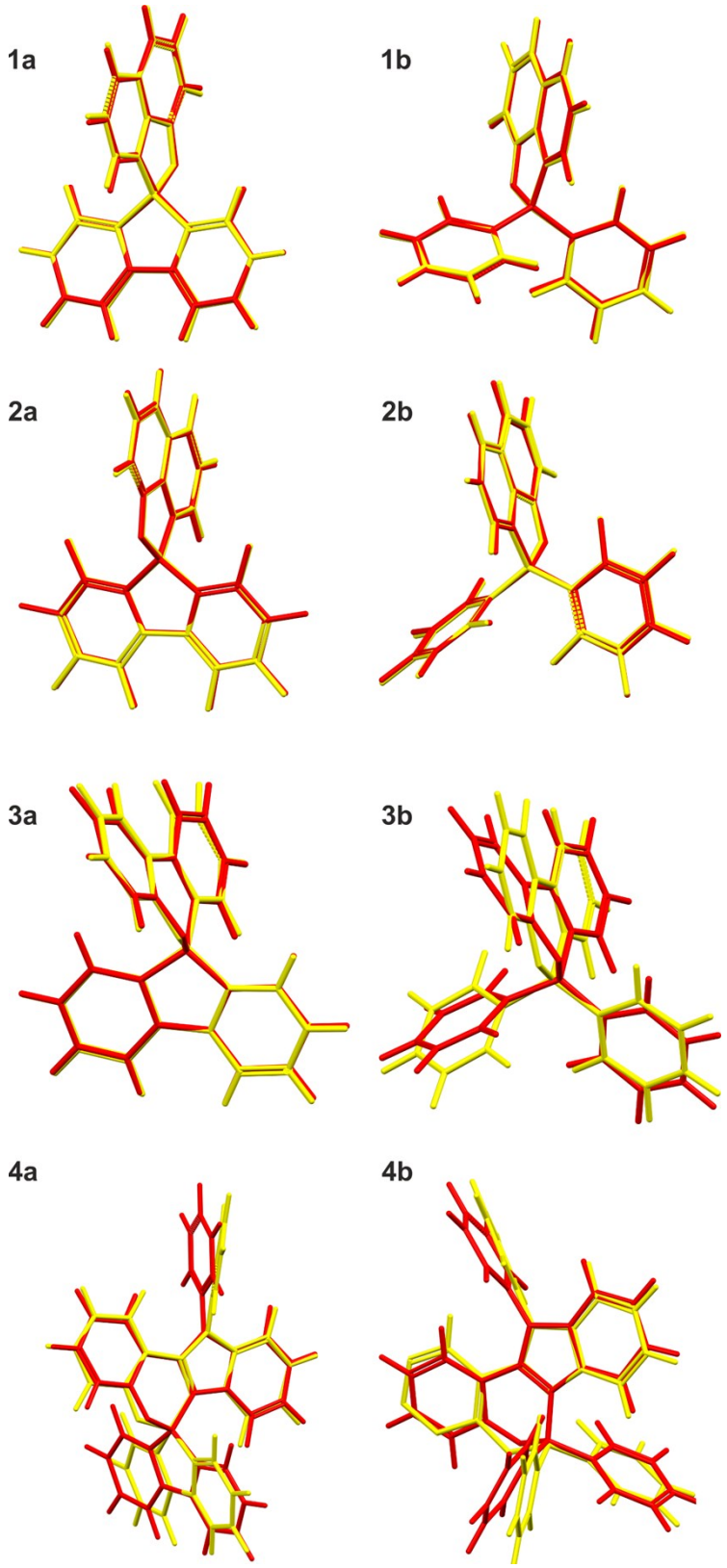

Figure S49. The overlay of optimal ground (red) and excited (yellow) states geometries derived from TD-DFT calculations for **1**-**4**.

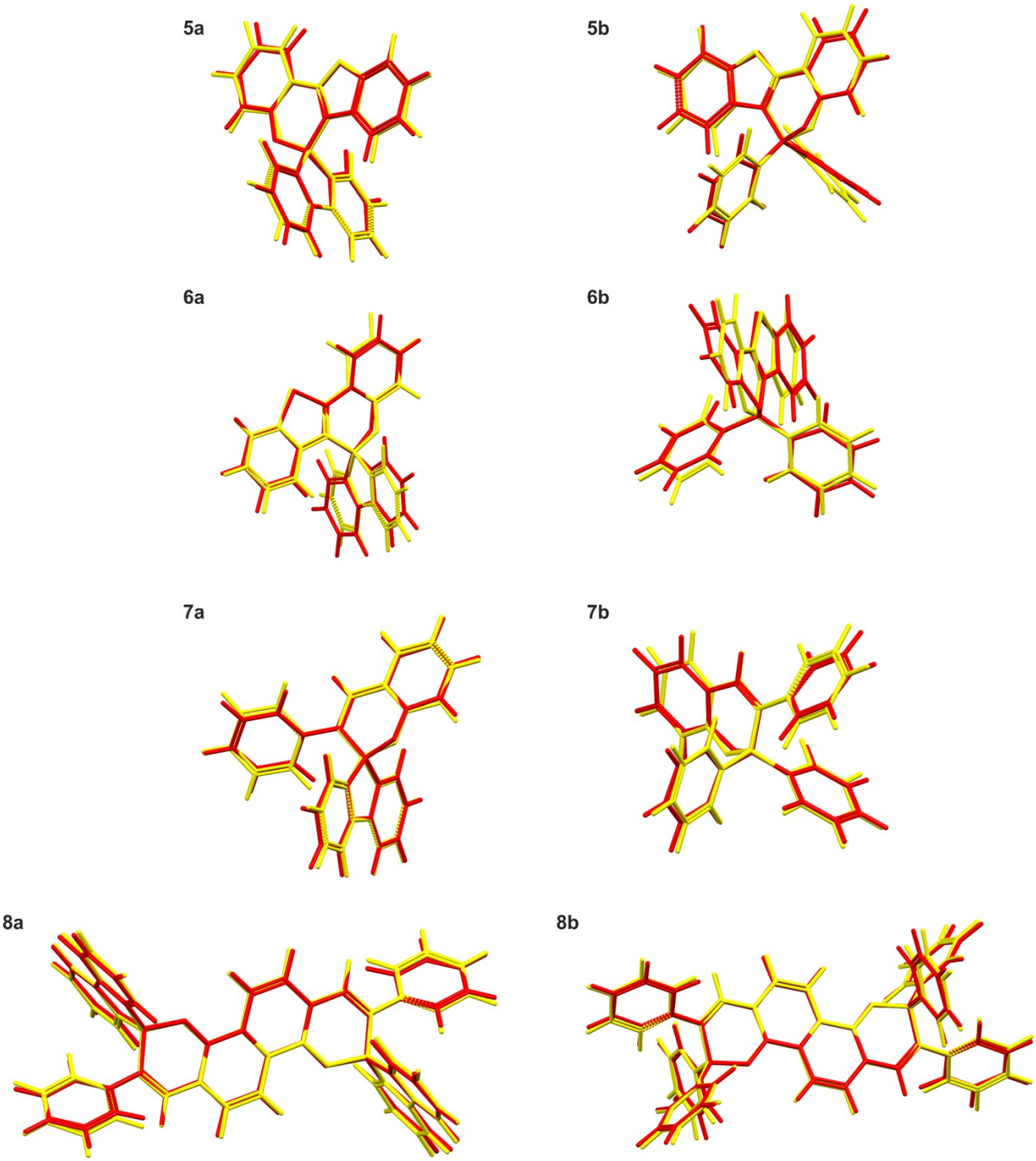

Figure S50. The overlay of optimal ground (red) and excited (yellow) states geometries derived from TD-DFT calculations for **5**-**8**.

The $\tau_{P1\text{-}P4}$-constrained optimisation energy scan for 7a.

The $\tau_{P1\text{-}P4}$-constrained optimisation energy scan (the $\tau_{P1\text{-}P4}$ angle varies from 0° to 90° in steps of 10°, all other parameters were fully optimised), performed at the CAM-B3LYP/6-311++G(d,p) level of theory for isolated molecule of **6a**, revealed that in the ground state the most stable is the conformation with $\tau_{P1\text{-}P4}$ close to 50°. However, the $\Delta E = f(\tau_{P1\text{-}P4})$ curve is flat for $\tau_{P1\text{-}P4} > 30°$ angles (Figure S48a) pointing to some molecular flexibility

in solution (below 5 kJmol^{-1}). In turn, flattening of ligand structure leads to significant steric repulsion between ligand and borafluorene moiety, which decreases system stability. In excited state (TD-DFT - CAM-B3LYP/6-311++g(d,p)) the $\Delta E = f(\tau_{P1\text{-}P4})$ minimum is shifted toward a lower $\tau_{P1\text{-}P4}$ angle (30°). Furthermore, the stability of a flat conformation increases, and destabilization of the twisted conformation is observed. According to our previous assumptions, the absorption wavelength decreases with twisting of ligand structure (Figure S48b). Similar effect is observed for emission, however, the function reaches the minimum at 60°, and then emission wavelength increases for the highest $\tau_{P1\text{-}P4}$ angle, which is somewhat confusing. On the basis of computations, we suppose that borafluorene ring plays more important role in the electron transition process when it is aligned parallel to the ligand plane. In such a case, charge transfer from the orbital located at the borafluorene moiety to the ligand may be promoted.

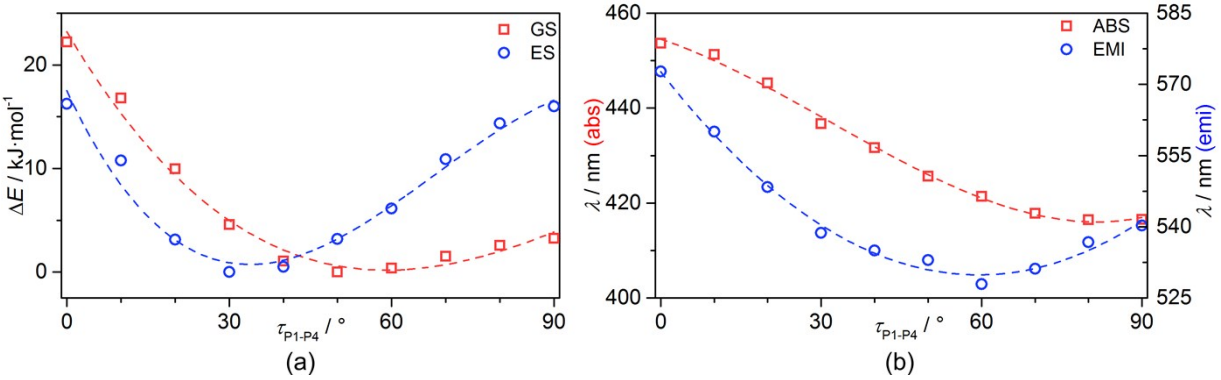

Figure S51. τ-Constrained optimization scan performed for **7a**. (a) Relative energy ΔE as a function of $\tau_{P1\text{-}P4}$ angle for ground and excited states. (b) Absorption and emission wavelength as a function of $\tau_{P1\text{-}P4}$ angle. The regression equations are given as follows: (GS) $\Delta E = 23.20962 - 0.88678 \cdot \tau_{P1\text{-}P4} + 0.01022 \cdot \tau_{P1\text{-}P4}^2 - 3.06106 \cdot 10^{-5} \cdot \tau_{P1\text{-}P4}^3$ ($R^2 = 0.9813$); (ES) $\Delta E = 17.50096 - 1.11622 \cdot \tau_{P1\text{-}P4} + 0.02199 \cdot \tau_{P1\text{-}P4}^2 - 1.078 \cdot 10^{-4} \cdot \tau_{P1\text{-}P4}^3$ ($R^2 = 0.9733$); $\lambda_{abs} = 454.55041 - 0.38102 \cdot \tau_{P1\text{-}P4} - 0.00806 \cdot \tau_{P1\text{-}P4}^2 + 8.50777 \cdot 10^{-5} \cdot \tau_{P1\text{-}P4}^3$ ($R^2 = 0.9968$); $\lambda_{emi} = 572.63055 - 1.44053 \cdot \tau_{P1\text{-}P4} + 0.01213 \cdot \tau_{P1\text{-}P4}^2$ ($R^2 = 0{,}9917$).

Table S4. Result of τ-Constrained optimization scan performed for **7a**.

$\tau_{P1\text{-}P4}$ /°	ΔE (GS) / kJmol^{-1}	ΔE (ES) / kJmol^{-1}	λ_{abs} / nm	λ_{em} / nm
0	22.2	16.2	453.7	572.7
10	16.8	10.8	451.3	560.0
20	10.0	3.1	445.3	548.4
30	4.6	0.0	436.7	538.7
40	1.1	0.5	431.6	535.0
50	0.0	3.2	425.6	533.0
60	0.4	6.1	421.4	527.9
70	1.5	10.9	417.8	531.1
80	2.6	14.4	416.5	536.8
90	3.3	16.0	416.6	540.3

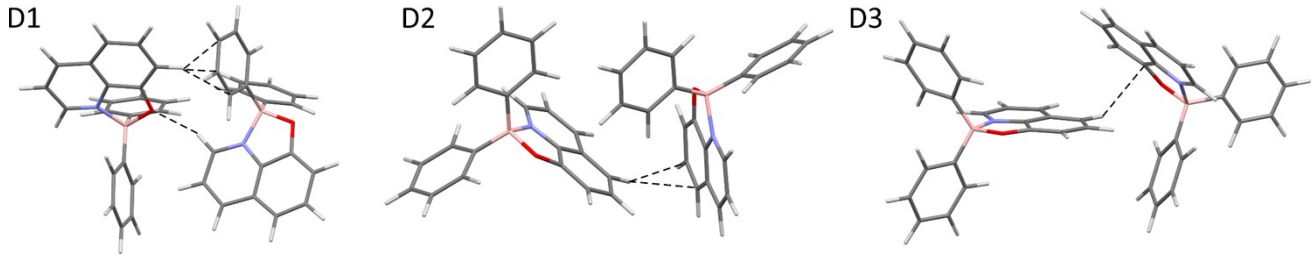

Figure S52. Dimeric motifs contributing the most in charge hopping processes in **1b**.

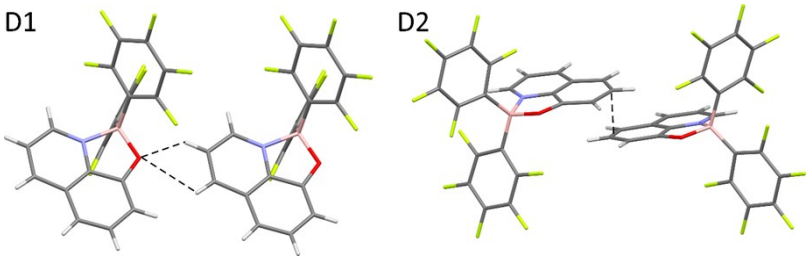

Figure S53. Dimeric motifs contributing the most in charge hopping processes in **2b**.

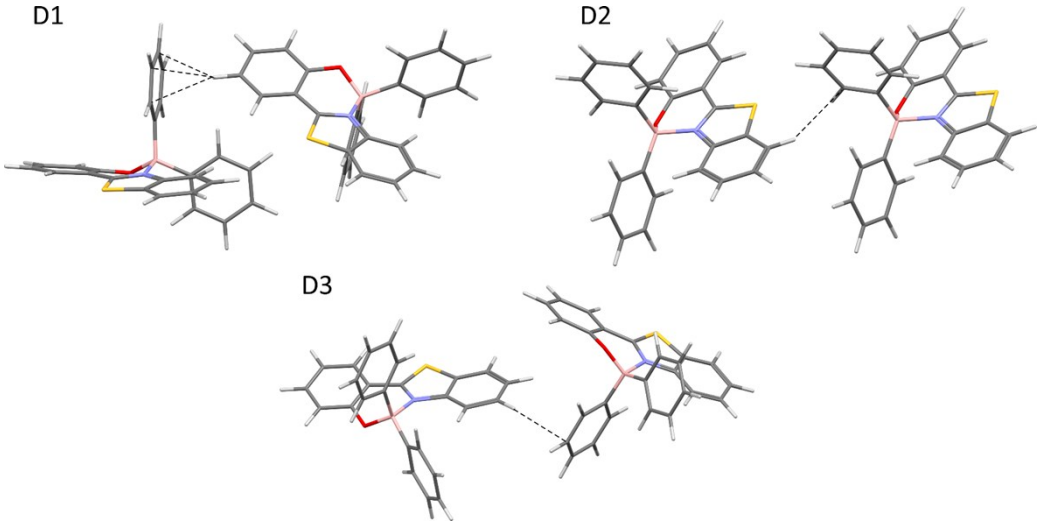

Figure S54. Dimeric motifs contributing the most in charge hopping processes in **6b**.

Table S5. The energies of the neutral ($E_0^{GS(0)}$), cationic ($E_+^{GS(0)}$) and anionic ($E_-^{GS(0)}$) states of all studied systems with the optimized geometry of neutral species, energies of neutral ($E_0^{GS(+)}$), cationic ($E_+^{GS(+)}$) states with the optimized geometry of the cationic species, and energies of neutral ($E_0^{GS(-)}$), anionic ($E_-^{GS(-)}$) states with the optimized geometry of the anionic species. All energy values values are given in a.u.

	$E_0^{GS(0)}$	$E_0^{GS(-)}$	$E_0^{GS(+)}$	$E_-^{GS(-)}$	$E_+^{GS(+)}$	$E_-^{GS(0)}$	$E_+^{GS(0)}$
1a	-963.820916	-963.560096	-963.860152	-963.867067	-963.564564	-963.815891	-963.814227
1b	-965.022022	-965.017785	-965.015194	-965.068025	-964.749026	-964.746049	-965.060910
2a	-1757.927297	-1757.922913	-1757.919720	-1757.992058	-1757.639680	-1757.635451	-1757.984409
2b	-1957.648467	-1957.641592	-1957.640355	-1957.714994	-1957.353782	-1957.348061	-1957.705709
3a	-1041.259491	-1041.253648	-1041.252865	-1041.300107	-1041.006454	-1041.001080	-1041.293459
3b	-1042.461524	-1042.447268	-1042.454563	-1042.500733	-1042.191319	-1042.185440	-1042.493588
4a	-1403.979248	-1403.973900	-1403.968580	-1404.017823	-1403.736133	-1403.729947	-1404.007069

4b	-1405.180500	-1405.173926	-1405.169938	-1405.217434	-1404.923678	-1404.914977	-1405.206467
5a	-1192.738215	-1192.733010	-1192.730391	-1192.783915	-1192.485544	-1192.480377	-1192.775957
5b	-1193.939223	-1193.933741	-1193.931156	-1193.983903	-1193.670447	-1193.662614	-1193.975872
6a	-1515.713908	-1515.708783	-1515.707198	-1515.765623	-1515.462634	-1515.456806	-1515.758835
6b	-1516.914669	-1516.908789	-1516.907571	-1516.965209	-1516.648270	-1516.639409	-1516.957985
7a	-1118.684203	-1118.678492	-1118.674358	-1118.740799	-1118.432318	-1118.426701	-1118.729437
7b	-1119.883925	-1119.878026	-1119.873936	-1119.939954	-1119.613833	-1119.606459	-1119.928930
8a	-2158.740847	-2158.740819	-2158.733759	-2158.824959	-2158.498371	-2158.487771	-2158.816259
8b	-2161.139932	-2161.133908	-2161.131382	-2161.223276	-2160.890975	-2160.885080	-2161.214404

Table S6. Calculated electronic coupling energies for electrons (V_e) and holes (V_h), hopping rates (W_e/W_h), and drift mobilities contributions (%μ_e/ %μ_h) given relative to the total value for all dimers in complexes **1a**, **1b**, **2a**, **2b**, **6a** and **6b**. *r* corresponds to the distance between centres of mass, *N* is the number of the same neighbour pairs found in the corresponding crystal structures.

	Dimer	*r* / Å	*N*	V_h / eV	V_e / eV	W_h ×10^{-12} / s^{-1}	W_e ×10^{-12} / s^{-1}	%μ_h	%μ_e
1a	D1	6.138	2	0.2161	0.2112	32.49	207.54	61.28%	58.44%
	D2	7.499	2	0.1093	0.1714	8.31	136.79	5.98%	37.90%
	D3	8.590	1	0.2208	0.1112	33.94	57.51	32.74%	2.20%
	D4	9.892	2	0.0064	0.0616	0.03	17.68	0.00%	1.10%
	D5	7.803	1	0.0116	0.0744	0.09	25.78	0.00%	0.36%
1b	D1	8.411	1	0.1079	0.4173	8.97	472.98	7.88%	69.82%
	D2	9.049	1	0.1833	0.0747	25.87	15.16	75.89%	0.08%
	D3	8.506	1	0.1263	0.3335	12.28	302.07	15.11%	29.12%
	D4	5.612	1	0.0580	0.0422	2.59	4.83	0.29%	0.00%
	D5	6.600	1	0.0684	0.1605	3.61	70.01	0.79%	0.94%
	D6	9.044	1	0.0137	0.0154	0.15	0.64	0.00%	0.00%
	D7	9.392	1	0.0261	0.0574	0.53	8.95	0.03%	0.03%
	D8	9.541	1	0.0199	0.0166	0.30	0.75	0.01%	0.00%
2a	D1	11.882	2	0.0969	0.2820	4.46	285.92	69.11%	91.60%
	D2	8.889	2	0.0453	0.1795	0.98	115.75	1.85%	8.40%
	D3	8.613	1	0.1295	0.0197	7.97	1.40	29.02%	0.00%
	D4	8.513	1	0.0222	0.0015	0.23	0.01	0.02%	0.00%
	D5	7.708	1	0.0027	0.0024	0.00	0.02	0.00%	0.00%
	D6	6.412	1	0.0116	0.0018	0.06	0.01	0.00%	0.00%
2b	D1	7.805	2	0.2954	0.3154	21.94	103.75	85.40%	95.79%
	D2	9.440	2	0.1721	0.1293	7.45	17.43	14.40%	3.95%
	D3	9.981	1	0.0001	0.0004	0.00	0.00	0.00%	0.00%
	D4	9.965	2	0.0463	0.0586	0.54	3.59	0.08%	0.19%
	D5	10.606	2	0.0010	0.0001	0.00	0.00	0.00%	0.00%
	D6	7.757	2	0.0542	0.0453	0.74	2.14	0.10%	0.04%
	D7	8.517	1	0.0524	0.0554	0.69	3.20	0.03%	0.03%
6a	D1	8.553	2	0.1321	0.1076	10.85	6.36	32.83%	5.79%
	D2	9.767	2	0.1188	0.1778	8.77	17.36	27.98%	56.33%
	D3	10.133	2	0.1264	0.1580	9.93	13.70	38.62%	37.75%
	D4	7.555	2	0.0471	0.0419	1.38	0.96	0.41%	0.10%
	D5	10.955	2	0.0306	0.0220	0.58	0.27	0.16%	0.02%
	D6	8.221	1	0.0170	0.0294	0.18	0.47	0.00%	0.01%
	D7	8.061	1	0.0182	0.0001	0.21	0.00	0.00%	0.00%
6b	D1	8.036	2	0.1793	0.3757	25.57	243.08	86.71%	99.44%
	D2	10.412	2	0.0755	0.0801	4.53	11.06	4.58%	0.35%

D3	9.984	1	0.0044	0.0479	0.02	3.95	0.00%	0.01%
D4	8.489	1	0.0007	0.0140	0.00	0.34	0.00%	0.00%
D5	11.091	2	0.0852	0.0668	5.77	7.69	8.41%	0.19%
D6	8.067	2	0.0435	0.0376	1.51	2.43	0.30%	0.01%
D7	7.051	1	0.0008	0.0011	0.00	0.00	0.00%	0.00%

8. Synthesis

2-(2'-hydroxyphenyl)-*N*-phenyl-benzoimidazole

Mixture of salicylaldehyde (1.6 mL, 15 mmol), *N*-Phenyl-o-phenylenediamine (2.26 g, 15 mmol) and $Na_2S_2O_5$ (2.85 g, 15 mmol) in DMF (20 mL) was stirred at 150 °C for 3 hours. After cooling, water (100 mL) was added and precipitated solid was filtered off, washed with water and dried. Crude product was recrystallised from EtOH with activated carbon and dried under vacuum. Beige crystalline solid was obtained with yield 3.02 g (70%). ^{1}H NMR (400 MHz, $CDCl_3$) δ = 13.54 (s, 1H), 7.82 (ddd, *J* = 8.0, 1.1, 0.7 Hz, 1H), 7.66 – 7.58 (m, 3H), 7.46 – 7.39 (m, 2H), 7.36 (ddd, *J* = 8.2, 7.2, 1.2 Hz, 1H), 7.27 (ddd, *J* = 8.3, 7.2, 1.2 Hz, 1H), 7.26 – 7.21 (m, 1H), 7.11 (dddd, *J* = 8.1, 6.3, 1.2, 0.6 Hz, 2H), 6.86 (ddd, *J* = 8.1, 1.6, 0.4 Hz, 1H), 6.54 (ddd, *J* = 8.1, 7.2, 1.3 Hz, 1H).

2-(2'-hydroxyphenyl)-1,3-benzothiazole

Mixture of salicylaldehyde (2.0 ml, 19 mmol), 2-aminotiophenol (2.0 mL, 19 mmol) and $Na_2S_2O_5$ (3.61 g, 19 mmol) in DMF (20 mL) was stirred at 150 °C for 3 hours. After cooling water (100 mL) was added and precipitated solid was filtered off, washed with water and dried. Crude product was recrystallised from MeOH/$CHCl_3$ mixture with activated carbon and dried under vacuum. Beige crystalline solid was obtained with yield 3.09 g (72%). ^{1}H NMR (300 MHz, $CDCl_3$) δ = 12.52 (s, 1H), 7.99 (ddd, *J* = 8.2, 1.2, 0.6 Hz, 1H), 7.90 (ddd, *J* = 7.9, 1.4, 0.6 Hz, 1H), 7.70 (dd, *J* = 7.8, 1.6 Hz, 1H), 7.51 (ddd, *J* = 8.0, 7.2, 1.3 Hz, 1H), 7.45 – 7.35 (m, 2H), 7.11 (dd, *J* = 8.3, 1.2 Hz, 1H), 6.96 (ddd, *J* = 7.7, 7.2, 1.2 Hz, 1H) ppm.

Complex 2b

Bromopentafluorobenzene (0.50 g, 2.0 mmol) was added dropwise to solution of *n*-BuLi (1.25 ml, 2.0 mmol, 1.6 M) in anhydrous Et_2O (10 ml) at −78 °C and stirred at this temperature for 30 min. $C_6F_5B(OEt)_2$ (0.53 g, 2.0 mmol) was added dropwise at -78°C. White precipitate was formed. After 30 min. HCl/Et_2O (1.0 ml, 2.0 mmol, 2M) was added; mixture clarified. After warming up to rt white precipitate was formed. 1 hour later 8-hydroxyquinoline (0.29 g, 2.0 mmol) was added and stirred for 4 hours. Mixture was extracted with water; organic phase was dried with Na_2SO_4 and volatiles were removed under reduced pressure. To obtained crude solid EtOH (5 ml) was added and after cooling in the freezer crystalline product was collected by filtration. Solid was washed with cold EtOH/pentane mixture and dried under vacuum. Yield 0.60 g (66%)
^{1}H NMR (300 MHz, $CDCl_3$) δ = 8.87 (dd, *J* = 5.3, 1.1 Hz, 1H), 8.59 (dd, *J* = 8.3, 1.1 Hz, 1H), 7.77 (dd, *J* = 8.3, 5.3 Hz, 1H), 7.71 (dd, *J* = 8.4, 7.7 Hz, 1H), 7.40 (dd, *J* = 8.4, 0.8 Hz, 1H), 7.23 (dd, *J* = 7.6, 0.7 Hz, 1H) ppm.
^{19}F NMR (282 MHz, $CDCl_3$) δ = -134.75 (dd, *J* = 23.9, 9.2 Hz), -155.79 (tt, *J* = 20.3, 2.4 Hz), -162.92 (ddd, *J* = 23.9, 20.3, 9.4 Hz) ppm.

Complex 3b

To a solution of Ph_2BOEt (123 mg, 0.58 mmol) in anhydrous EtOH (3 ml) 2-(pyridine-2-yl)phenol (86 mg, 0.50 mmol) was added in one portion. Mixture was stirred at 50 °C for 3 h and left overnight in freezer. Crystalline precipitate was filtered off, washed with cold EtOH, hexane and dried. Pale yellowish crystalline solid waso obtained with yield 140 mg (84%). The product was further purified by recrystallization from acetone and dried under vacuum. ^{1}H NMR (400 MHz, $CDCl_3$) δ = 8.14 (ddd, *J* = 6.0, 1.7, 0.8 Hz, 1H), 8.00 (ddd, *J* = 8.3, 7.2, 1.6 Hz, 1H), 7.97 – 7.93 (m, 1H), 7.61 (ddt, *J* = 8.0, 1.7, 0.5 Hz, 1H), 7.37 (ddd, *J* = 8.3, 7.2, 1.6 Hz, 1H), 7.32 (ddd, *J* = 7.2, 5.9, 1.6 Hz, 1H), 7.28 – 7.24 (m, 4H), 7.24 – 7.15 (m, 7H), 6.83 (ddd, *J* = 8.0, 7.2, 1.3 Hz, 1H) ppm.

Complex 4b

Compound **4b** was synthesized as described for **3a** using Ph_2BOEt (165 mg, 0.78 mmol), EtOH (5 ml) and 2-(2'-hydroxyphenyl)-1-phenyl-benzoimidazole (200 mg, 0.70 mmol). Whitish crystalline solid was obtained, yield 253mg (80%). ^{1}H NMR (400 MHz, $CDCl_3$) δ = 7.73 – 7.66 (m, 3H), 7.53 – 7.48 (m, 2H), 7.48 – 7.44 (m, 4H), 7.33 – 7.20 (m, 9H), 7.16 (ddd, *J* = 8.4, 7.2, 1.2 Hz, 1H), 7.07 (ddd, *J* = 8.2, 1.2, 0.8 Hz, 1H), 6.99 (dt, *J* = 8.3, 1.0 Hz, 1H), 6.62 (ddd, *J* = 8.1, 1.6, 0.5 Hz, 1H), 6.43 (ddd, *J* = 8.2, 7.0, 1.4 Hz, 1H) ppm.

Complex 5b

Compound **5b** was synthesized as described for **3a** using Ph_2BOEt (127 mg, 0.61 mmol), EtOH (5 ml) and 2-(2'-hydroxyphenyl)-1,3-benzooxazole (106 mg, 0.55 mmol). Pale yellow crystalline solid was obtained , yield 182 mg (80%).^{1}H NMR (400 MHz, $CDCl_3$) δ = 7.80 (ddd, *J* = 7.9, 1.8, 0.6 Hz, 1H), 7.66 (ddd, *J* = 8.3, 1.1, 0.7 Hz, 1H), 7.53 (ddd, *J* = 8.4, 7.2, 1.8 Hz, 1H), 7.48 – 7.38 (m, 5H), 7.30 – 7.19 (m, 8H), 6.99 (ddd, *J* = 8.2, 1.3, 0.7 Hz, 1H), 6.90 (ddd, *J* = 8.1, 7.2, 1.0 Hz, 1H) ppm.

Complex 6b

Compound **6b** was synthesized as described for **3a** using Ph_2BOEt (211 mg, 1.0 mmol), EtOH (5 ml) and 2-(2'-hydroxyphenyl)-1,3-benzothiazole (205 mg, 0.90 mmol). Yellow crystalline solid with yield 320 mg (91%) was obtained. ^{1}H NMR (400 MHz, $CDCl_3$) δ = 7.86 (dt, *J* = 8.1, 0.9 Hz, 1H), 7.52 (dd, *J* = 7.9, 1.6 Hz, 1H), 7.45 (ddd, *J* = 8.7, 7.2, 1.6 Hz, 1H), 7.43 – 7.39 (m, 1H), 7.39 – 7.35 (m, 4H), 7.30 – 7.24 (m, 2H), 7.24 – 7.20 (m, 6H), 7.17 (dd, *J* = 8.4, 1.1 Hz, 1H), 6.84 (ddd, *J* = 8.1, 7.2, 1.1 Hz, 1H) ppm.

9. Copies of NMR spectra

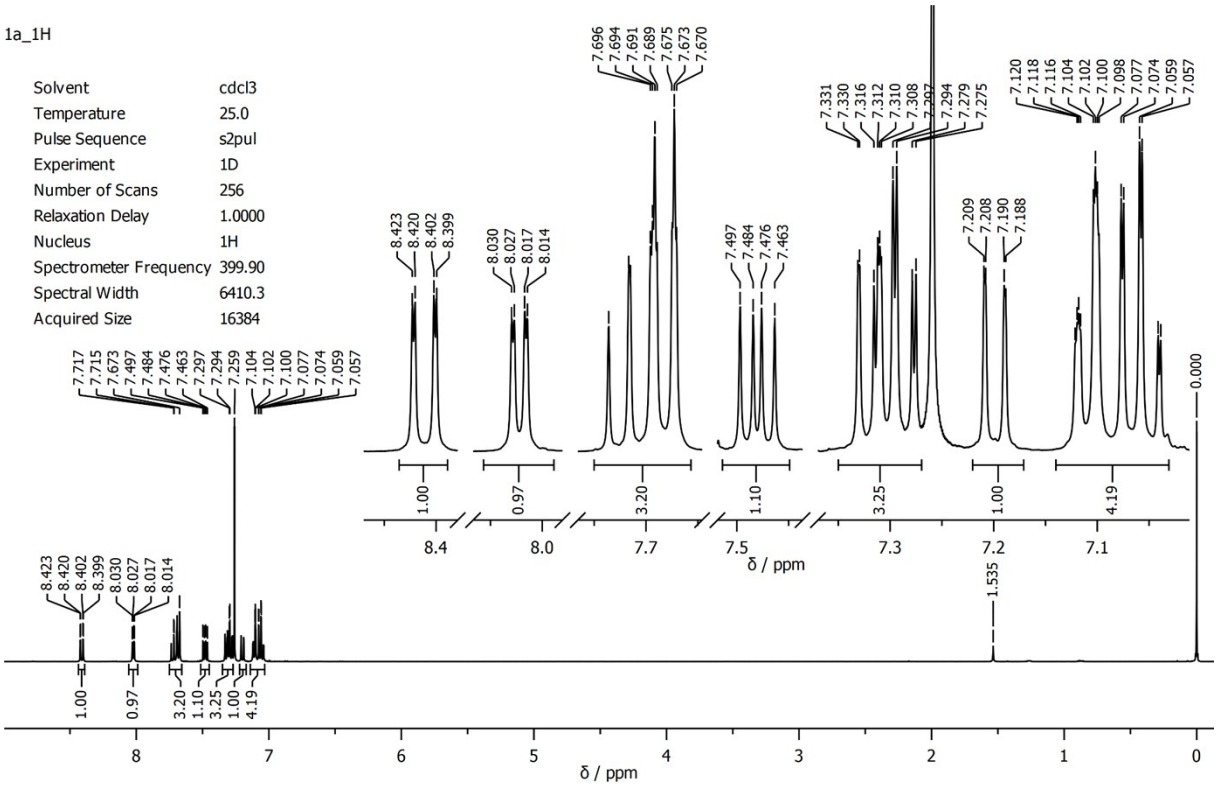

Figure S55. ^{1}H NMR spectrum of **1a** in $CDCl_3$

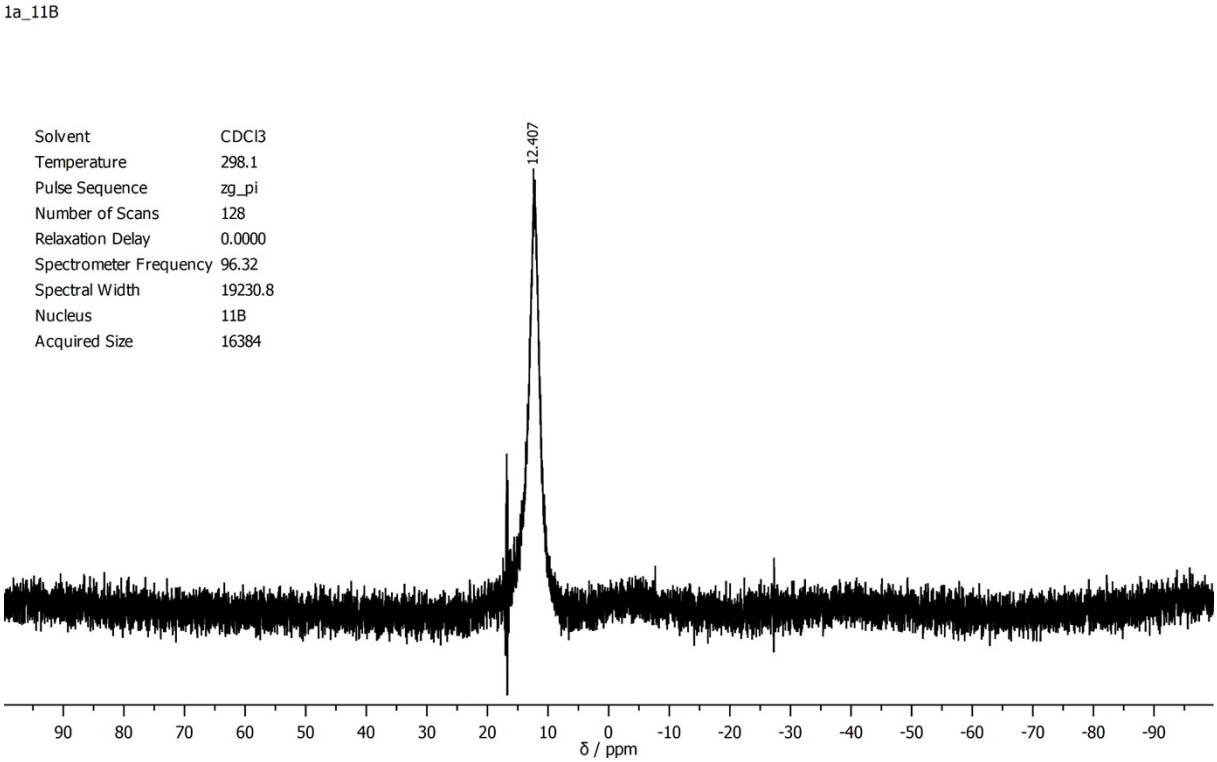

Figure S56. ^{11}B NMR spectrum of **1a** in $CDCl_3$

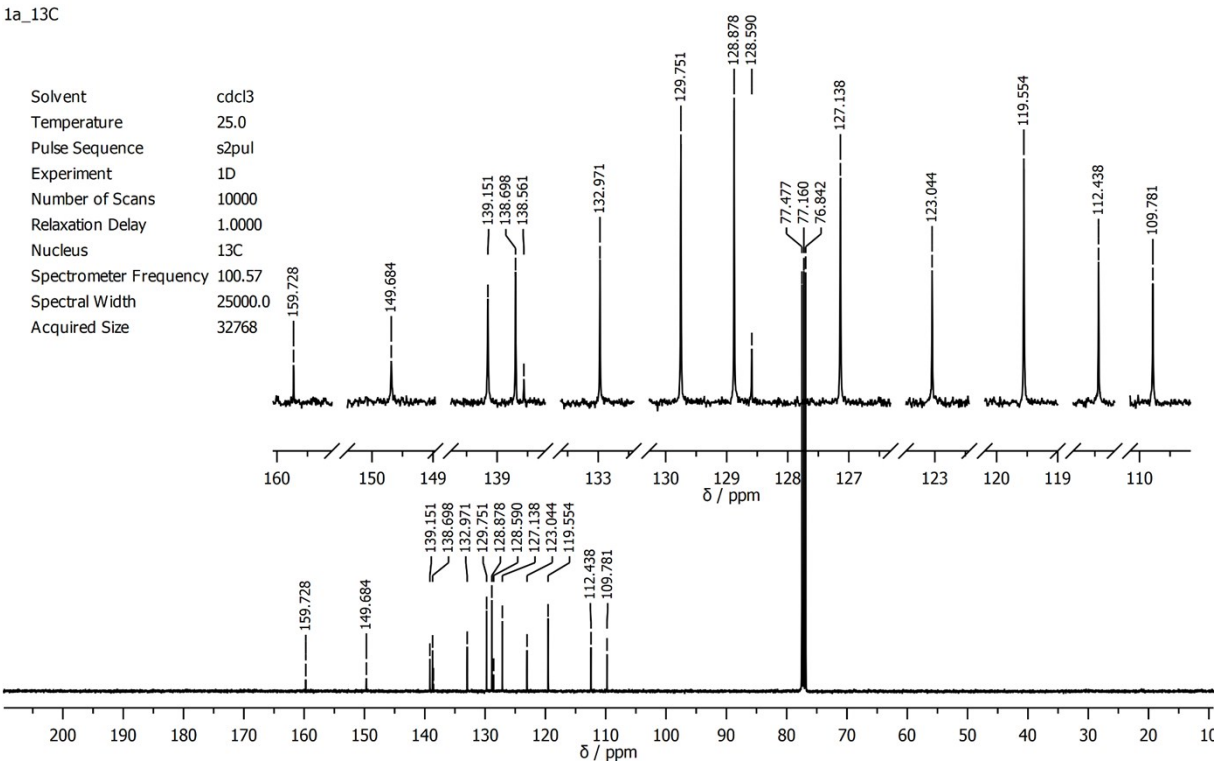

Figure S57. ^{13}C NMR spectrum of **1a** in $CDCl_3$

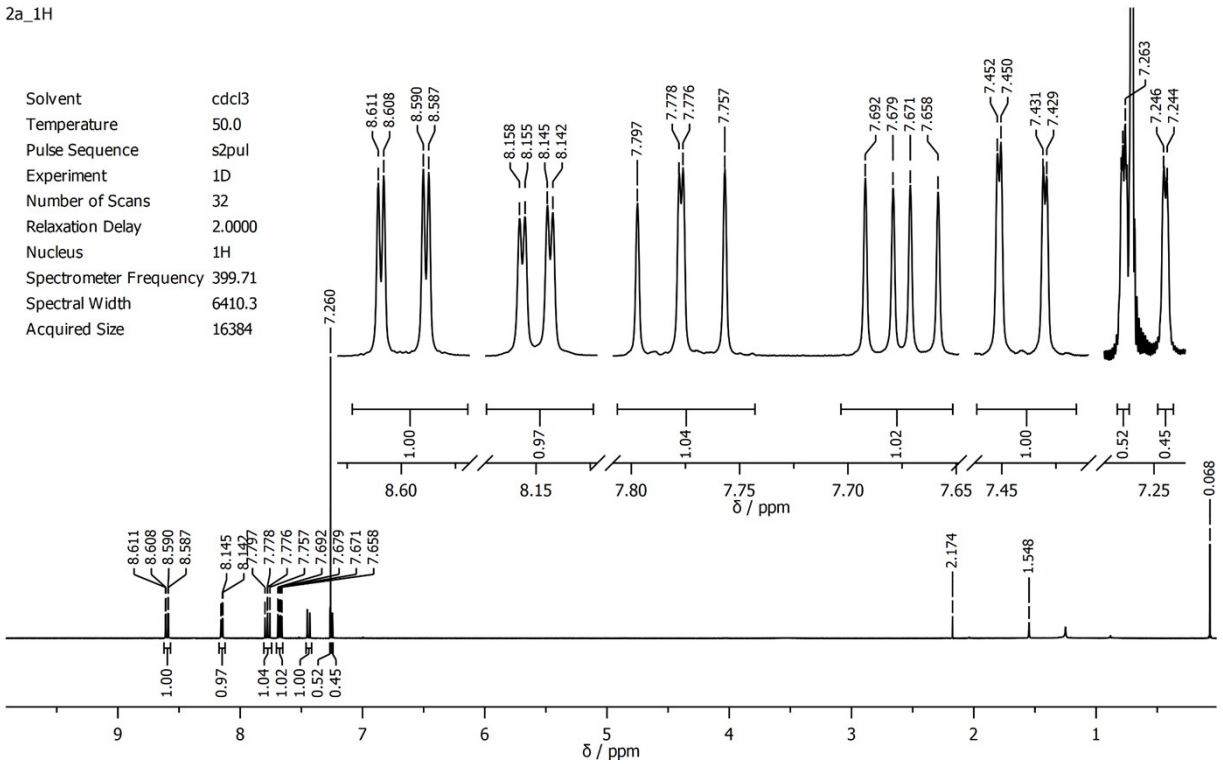

Figure S58. ^{1}H NMR spectrum of **2a** in $CDCl_3$

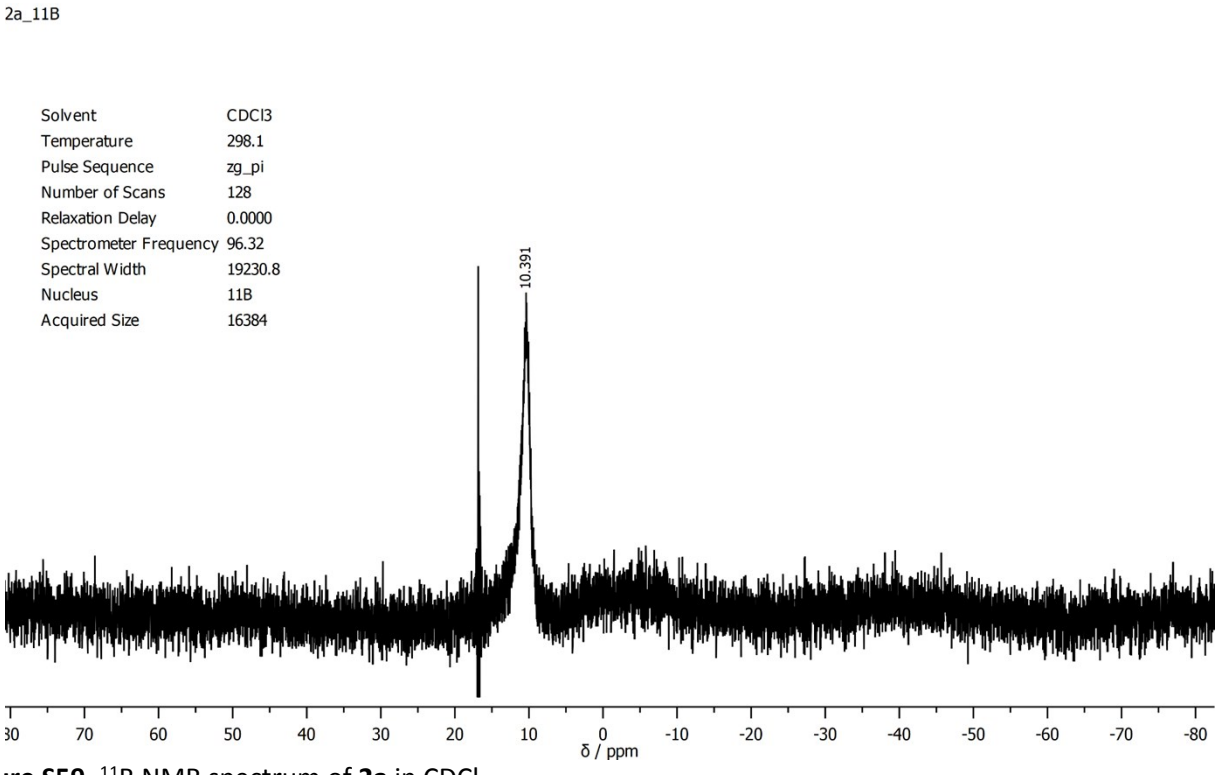

Figure S59. ^{11}B NMR spectrum of **2a** in $CDCl_3$

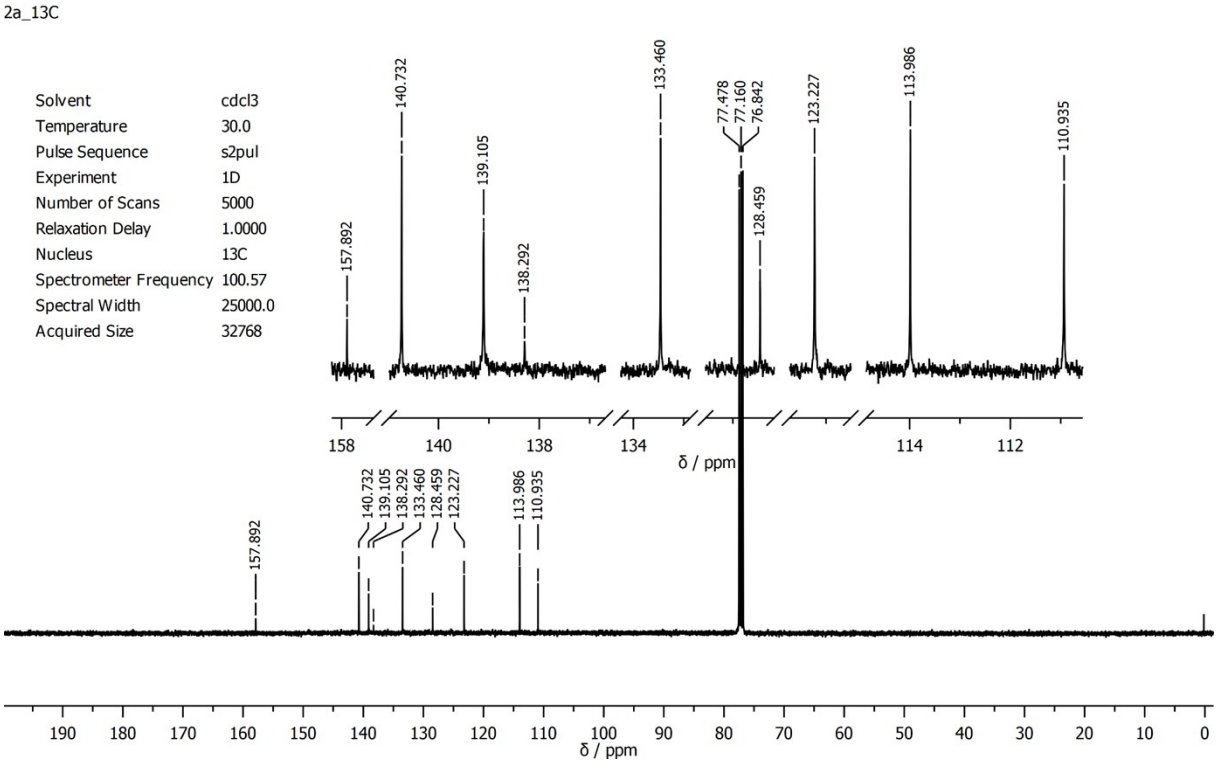

Figure S60. ^{13}C NMR spectrum of **2a** in $CDCl_3$

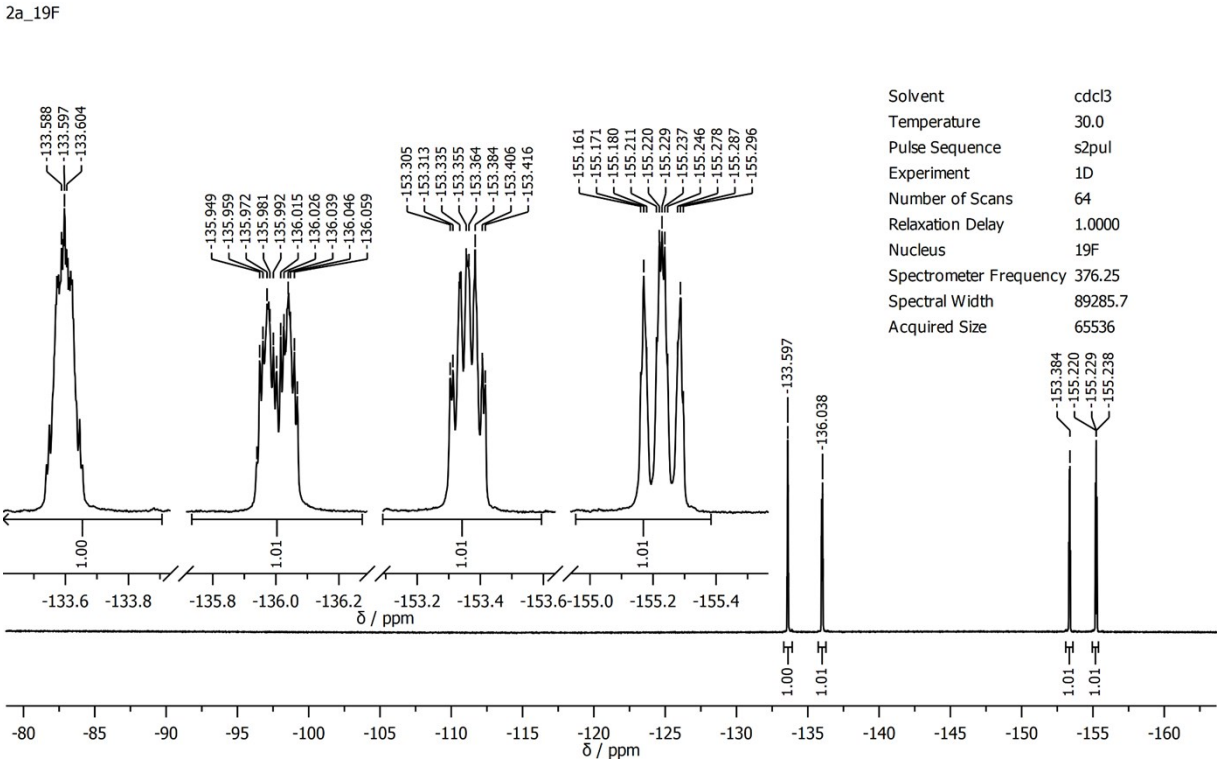

Figure S61. ^{19}F NMR spectrum of **2a** in $CDCl_3$

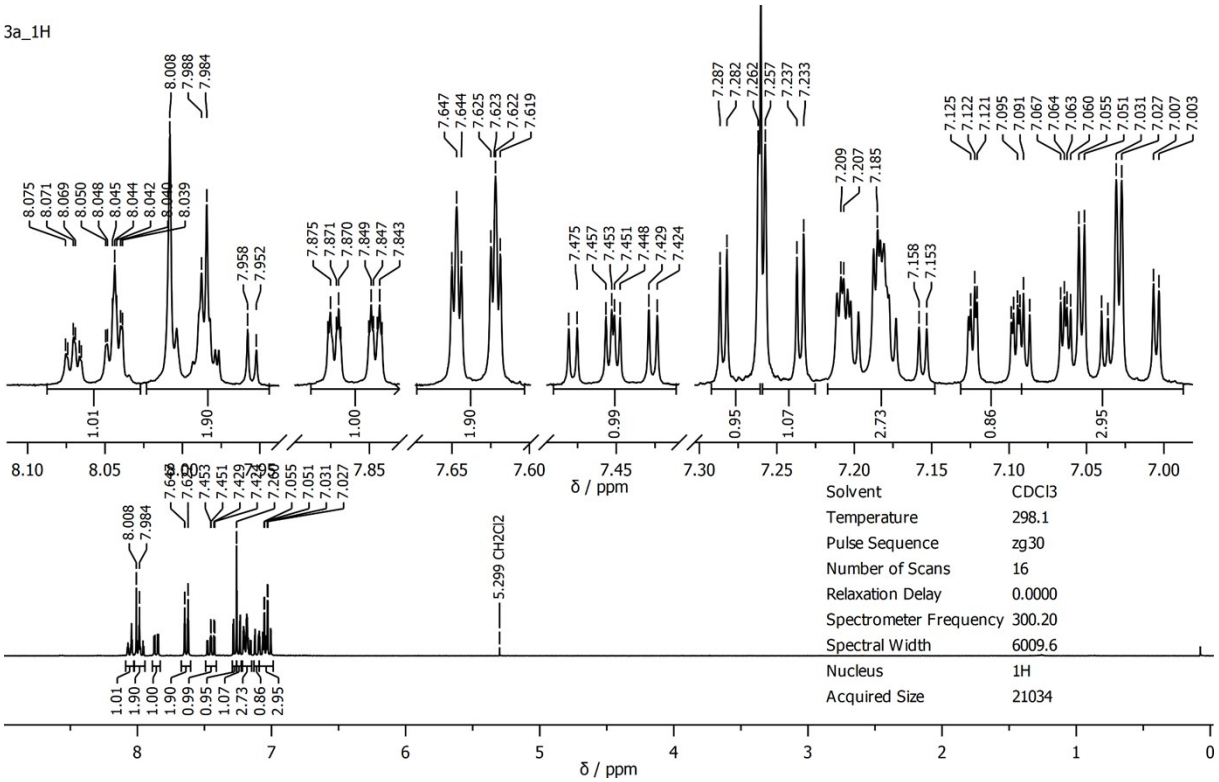

Figure S62. ^{1}H NMR spectrum of **3a** in $CDCl_3$

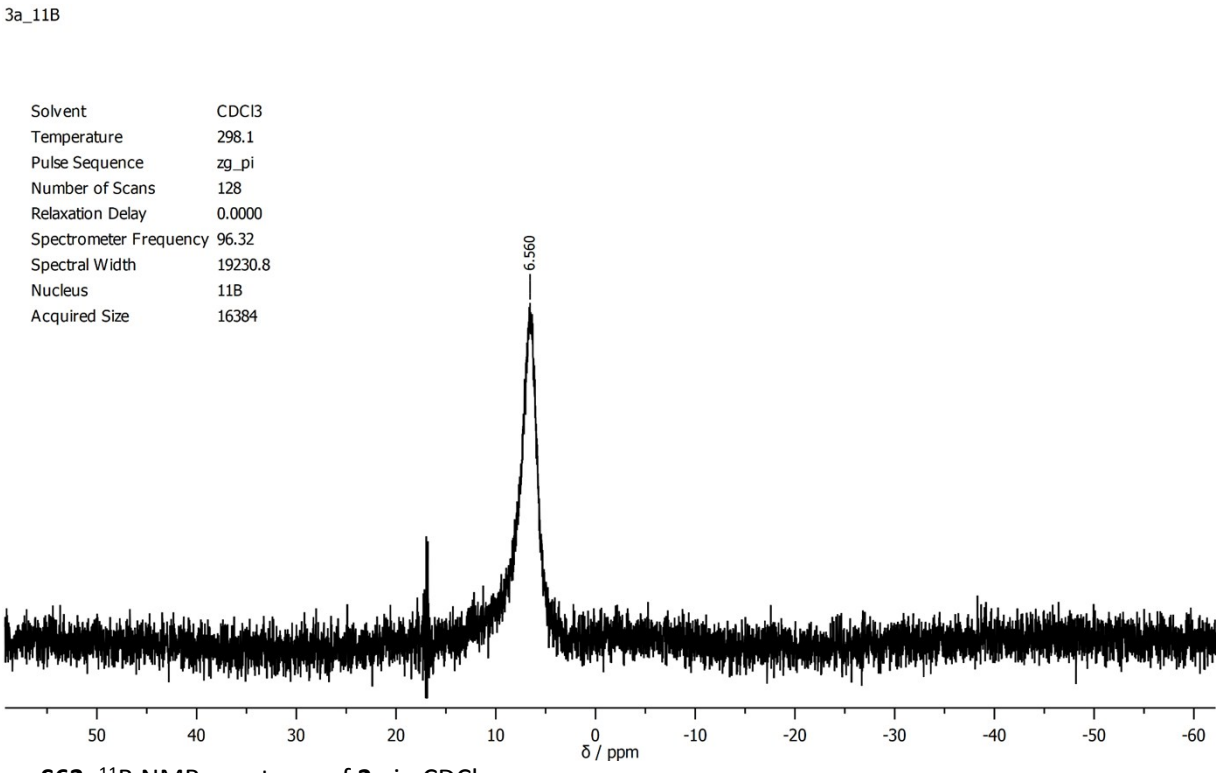

Figure S63. ^{11}B NMR spectrum of **3a** in $CDCl_3$

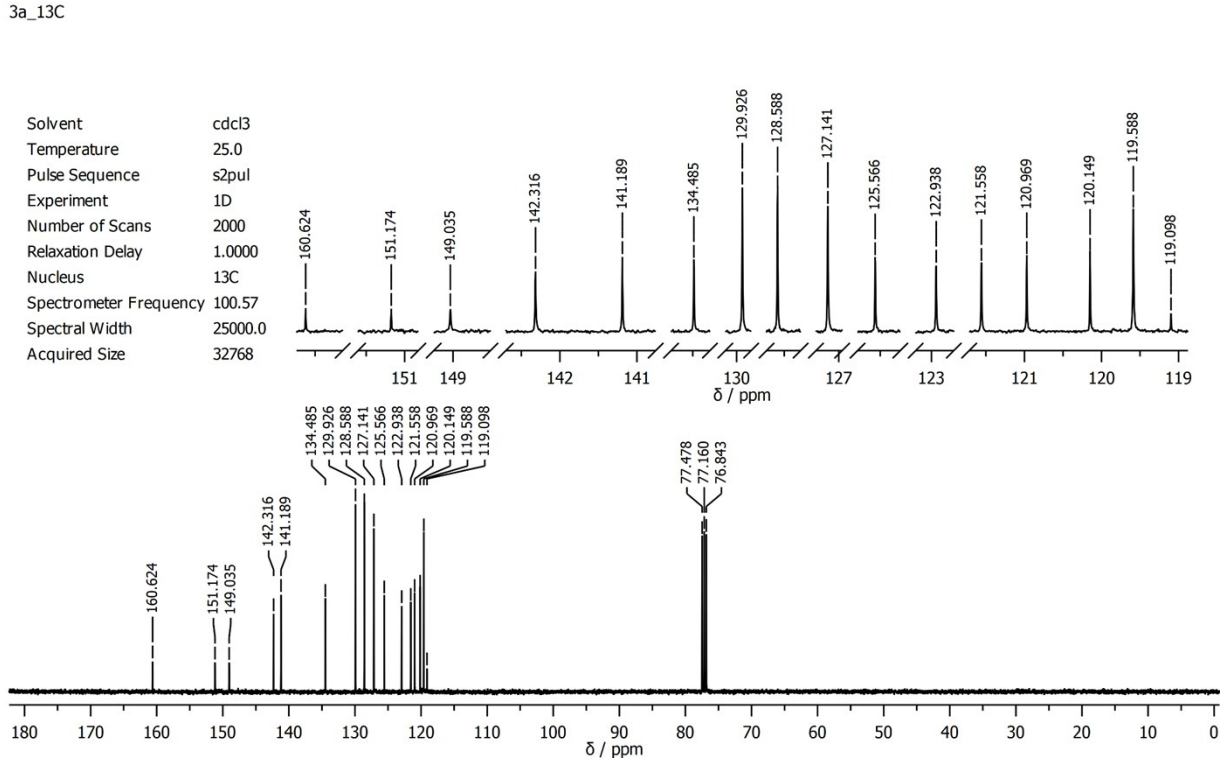

Figure S64. ^{13}C NMR spectrum of **3a** in $CDCl_3$

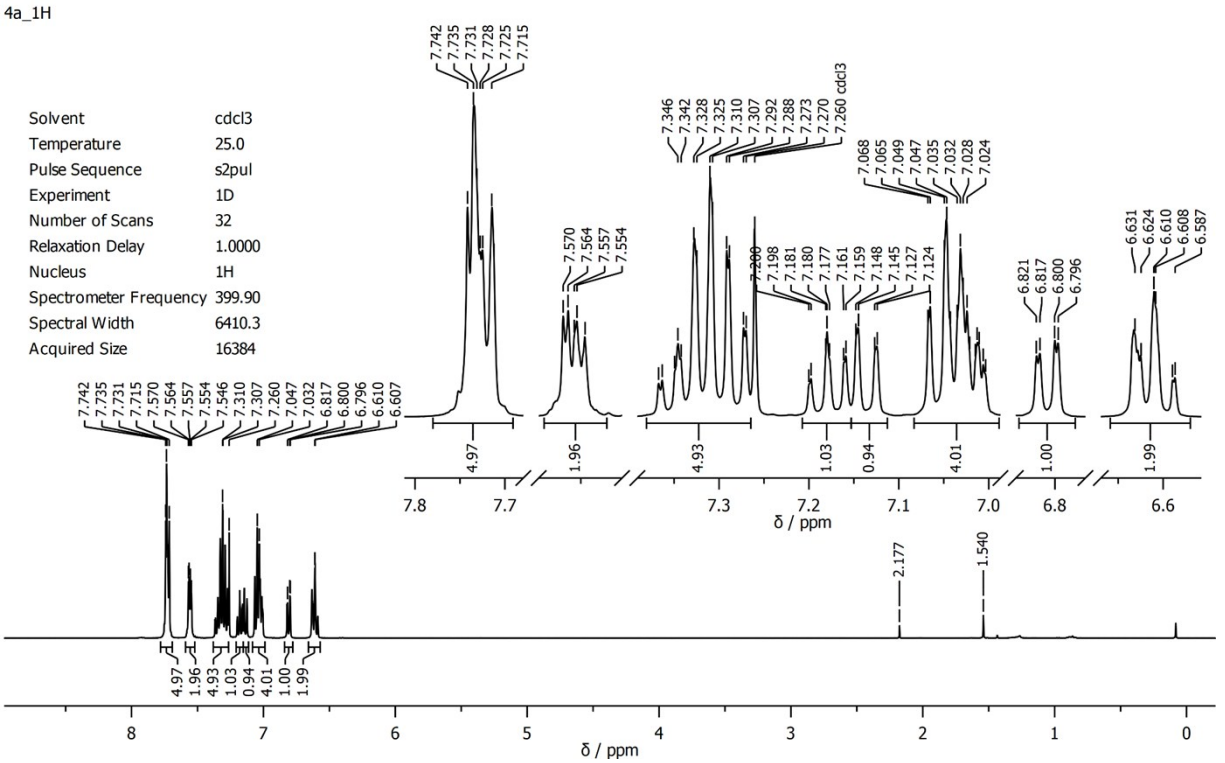

Figure S65. ^{1}H NMR spectrum of **4a** in $CDCl_3$

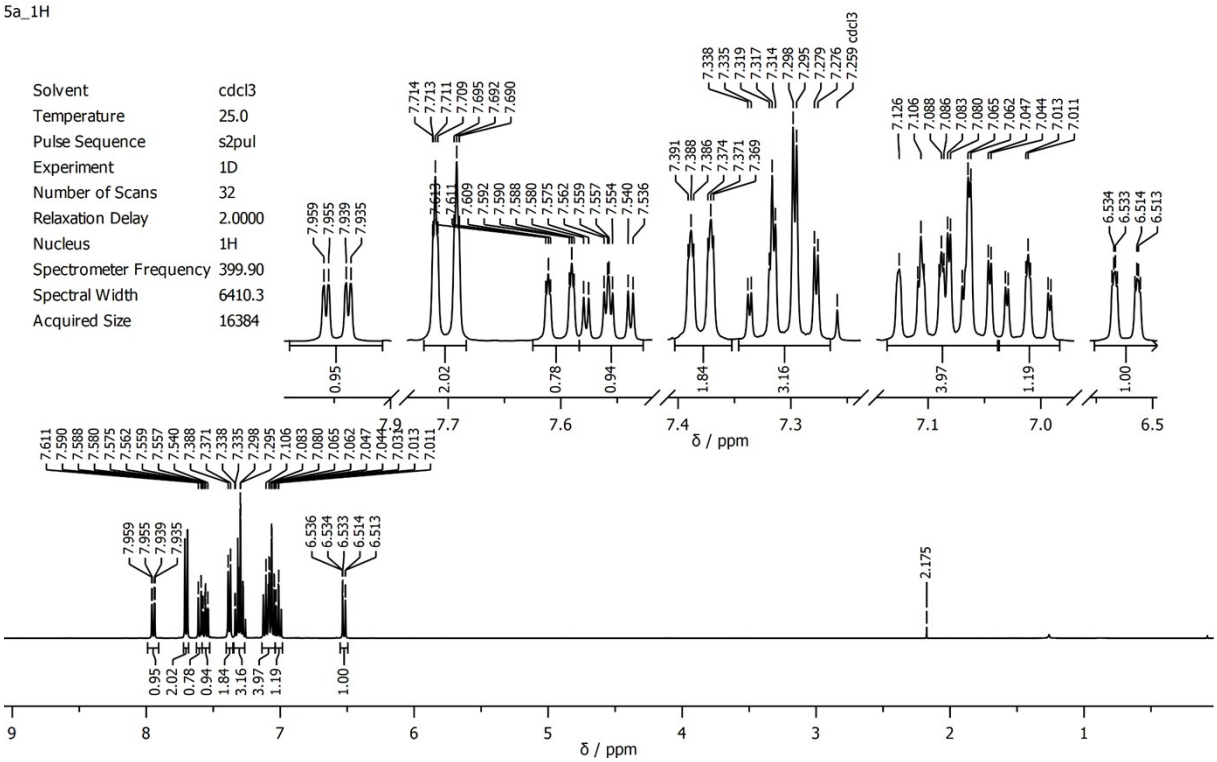

Figure S66. ^{1}H NMR spectrum of **5a** in $CDCl_3$

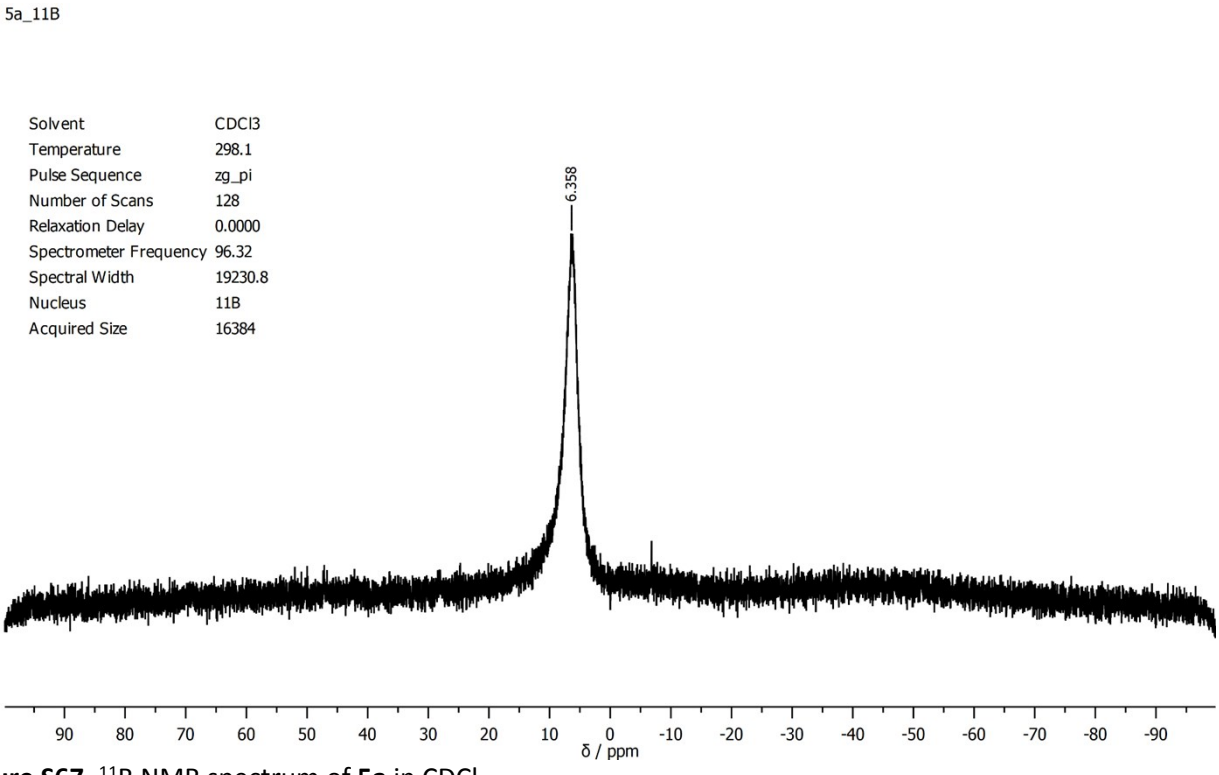

Figure S67. ^{11}B NMR spectrum of **5a** in $CDCl_3$

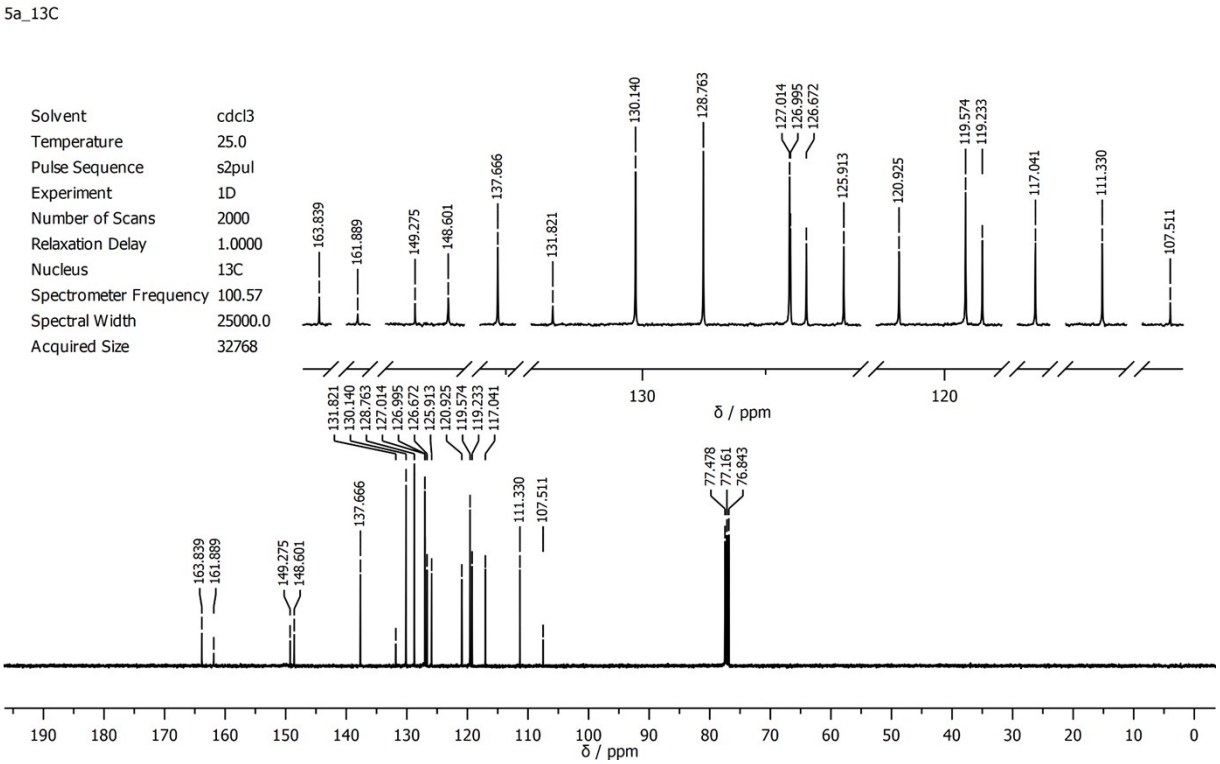

Figure S68. ^{13}C NMR spectrum of **5a** in $CDCl_3$

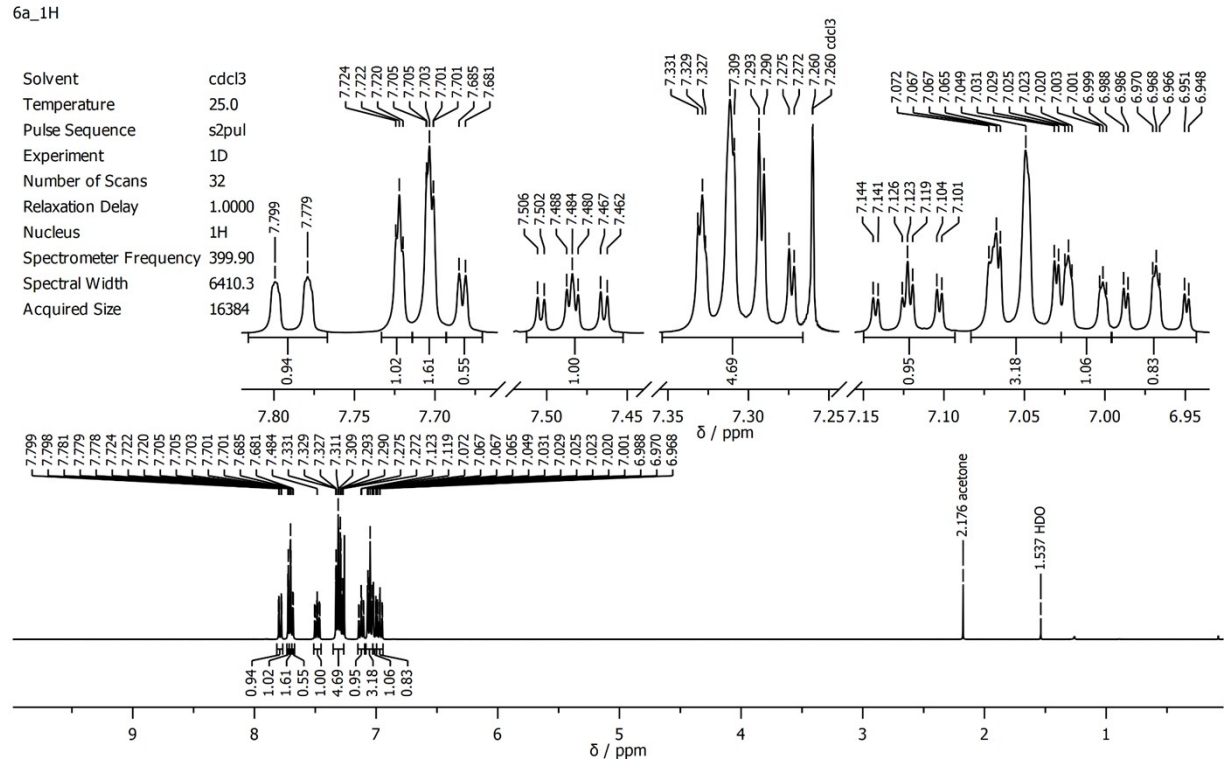

Figure S69. ^{1}H NMR spectrum of **6a** in $CDCl_3$

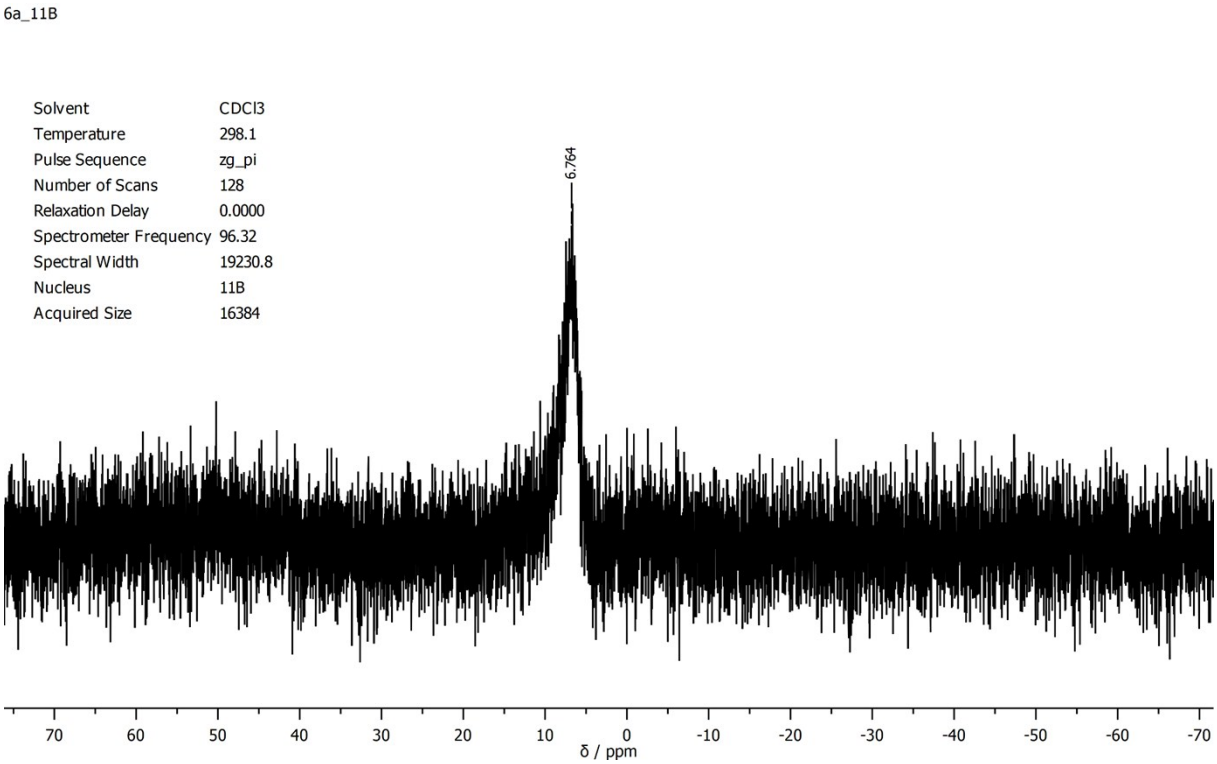

Figure S70. ^{11}B NMR spectrum of **6a** in $CDCl_3$

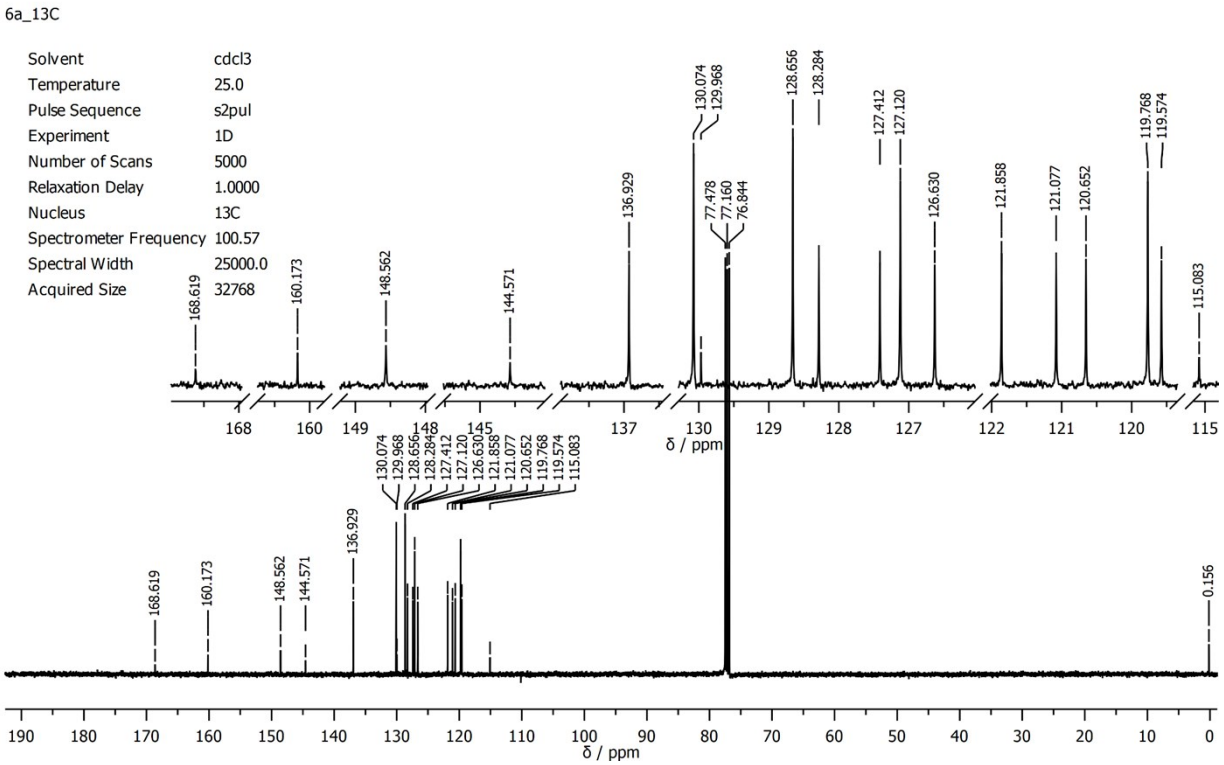

Figure S71. ^{13}C NMR spectrum of **6a** in $CDCl_3$

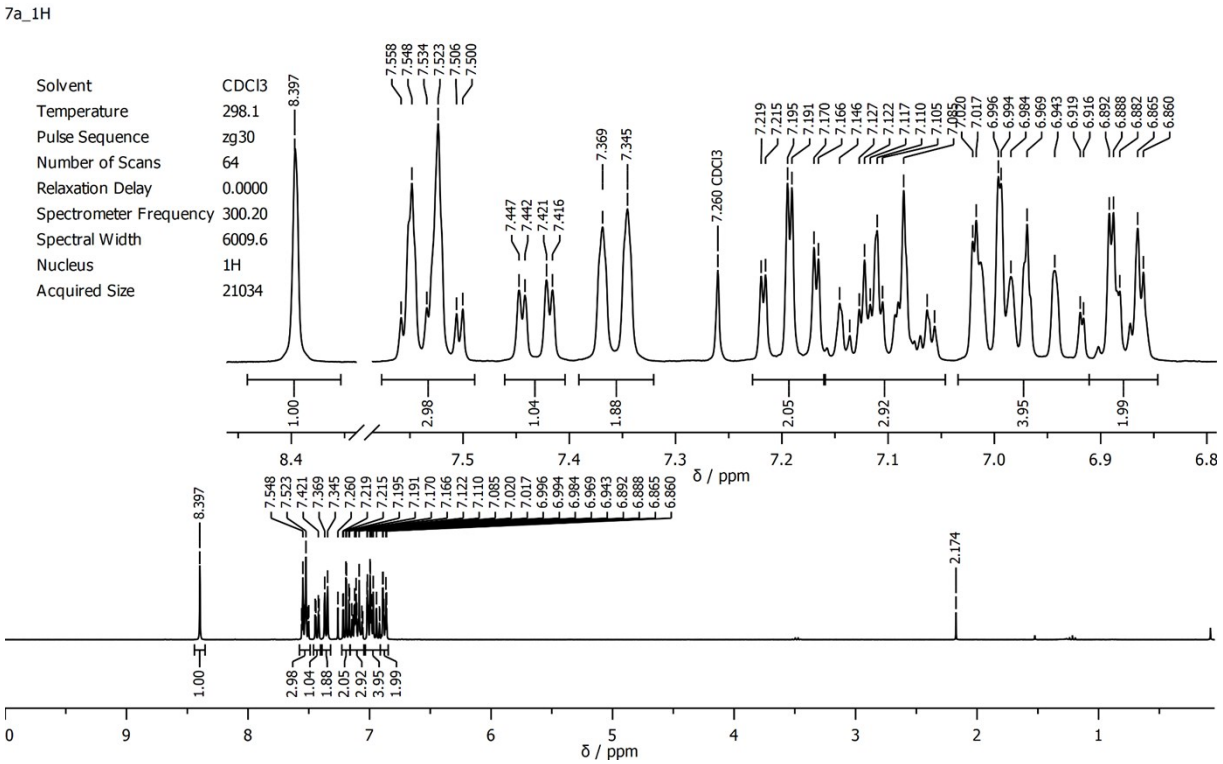

Figure S72. ^{1}H NMR spectrum of **7a** in $CDCl_3$

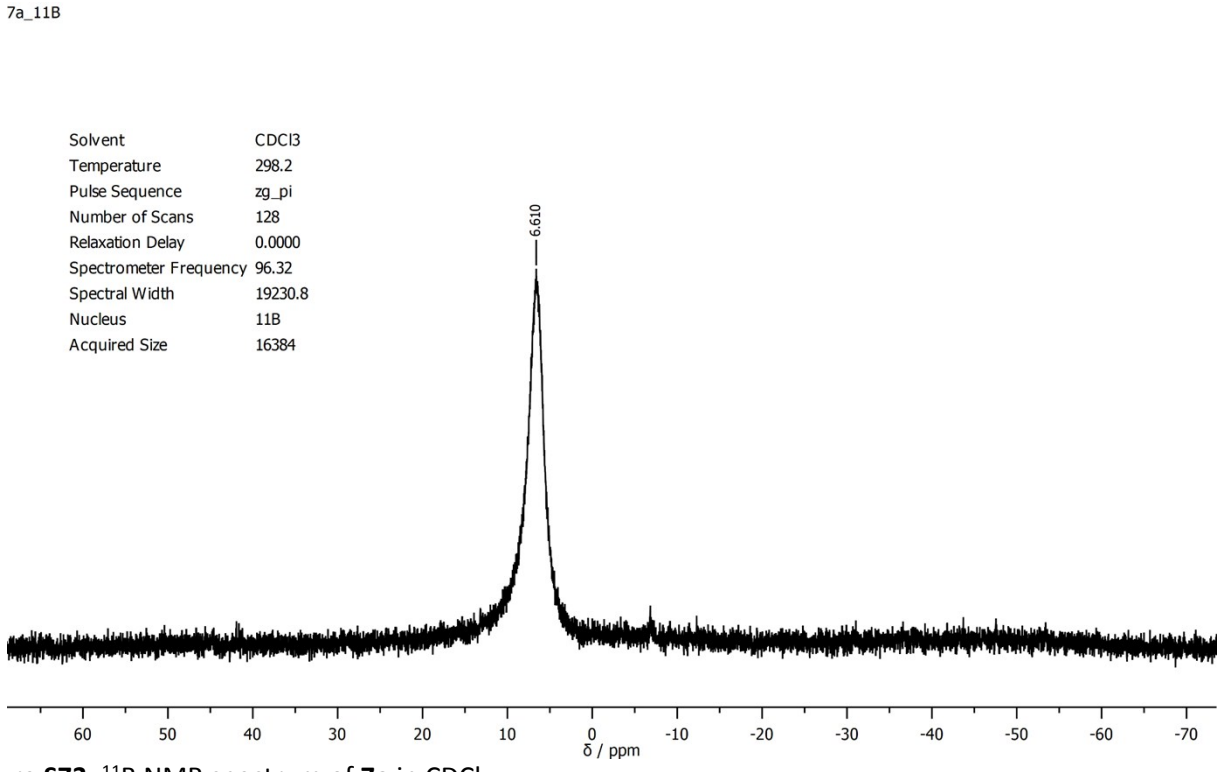

Figure S73. ^{11}B NMR spectrum of **7a** in $CDCl_3$

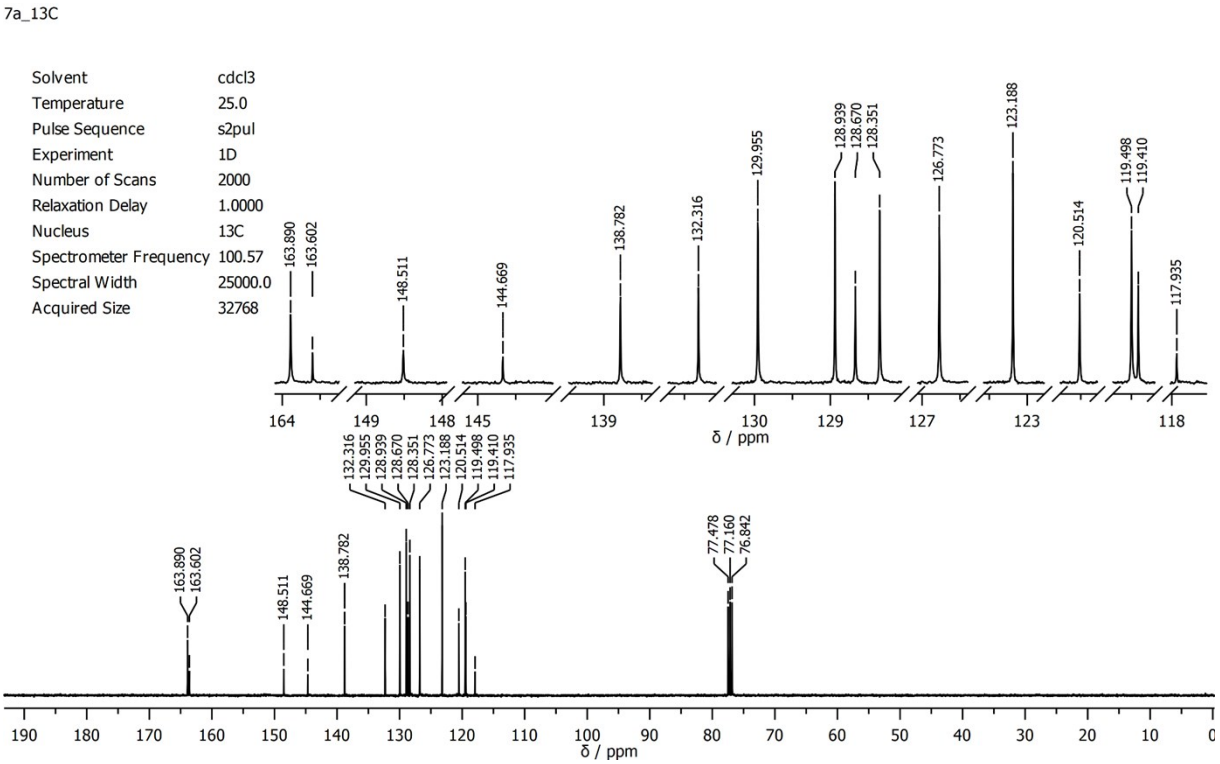

Figure S74. ^{13}C NMR spectrum of **7a** in $CDCl_3$

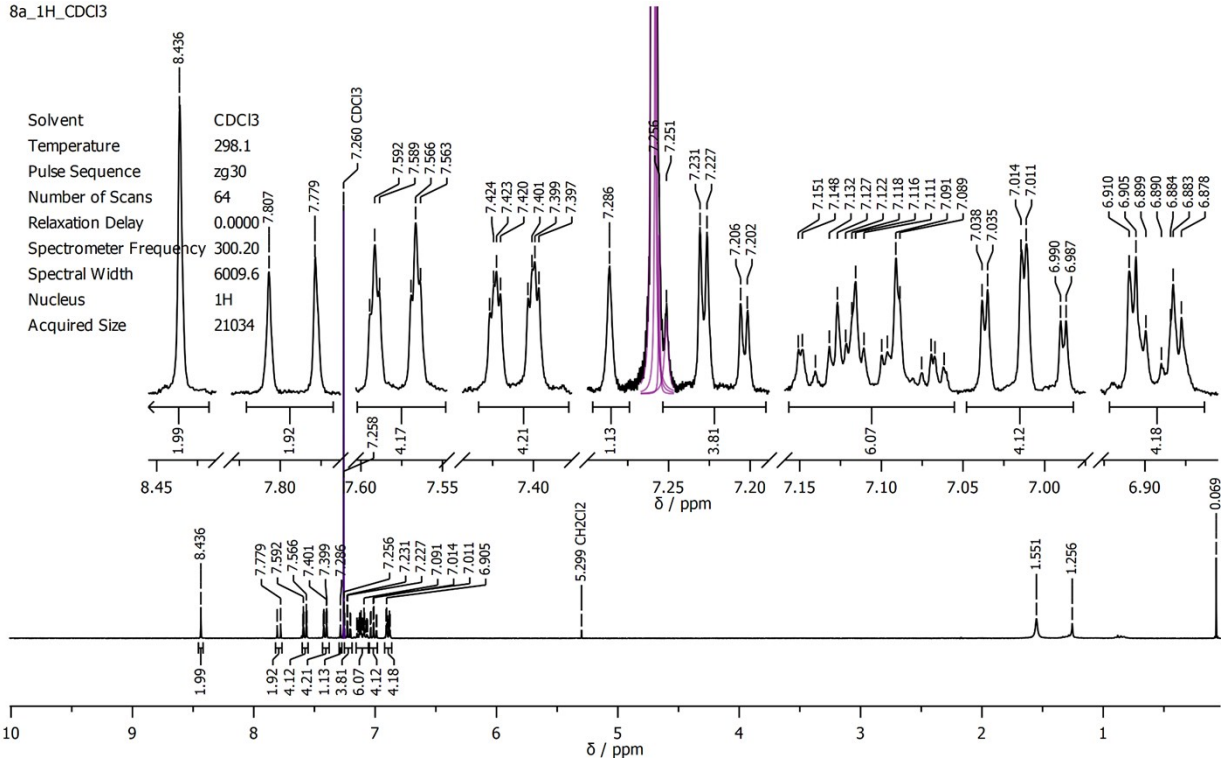

Figure S75. ^{1}H NMR spectrum of **8a** in $CDCl_3$

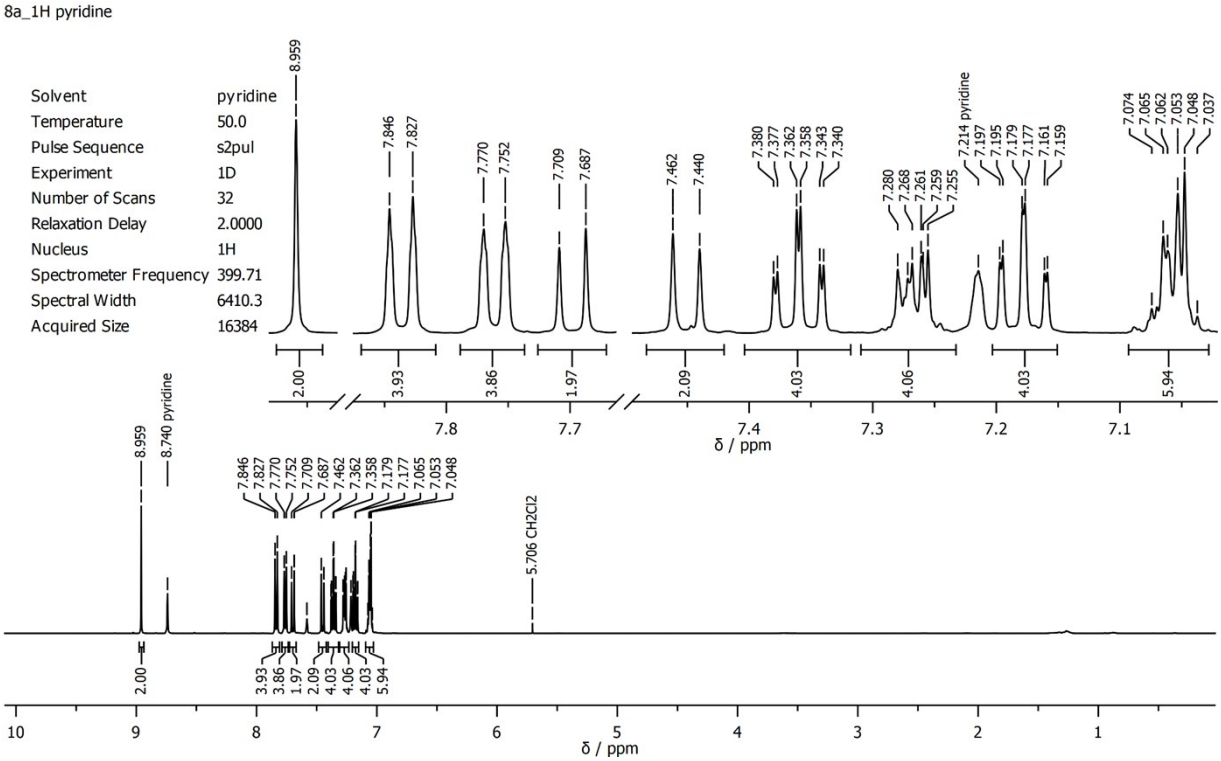

Figure S76. ^{1}H NMR spectrum of **8a** in pyridine-d_5

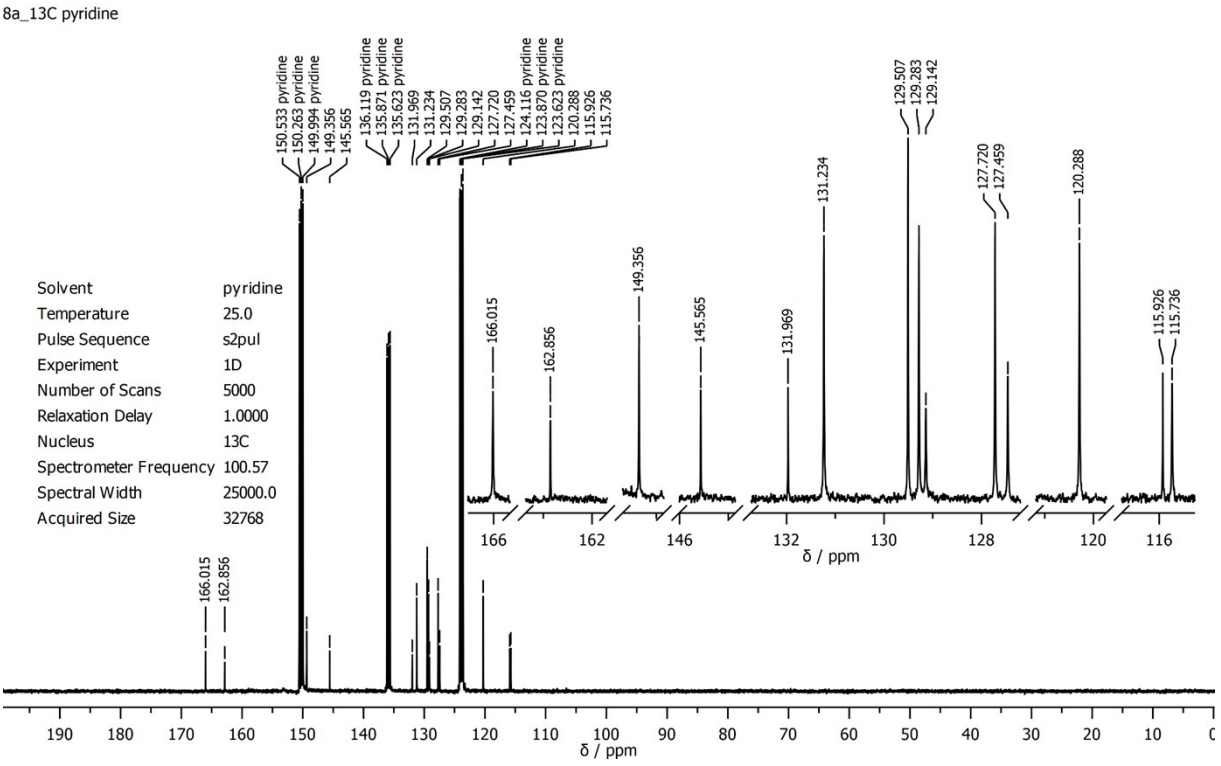

Figure S77. ^{13}C NMR spectrum of **8a** in pyridine-d_5

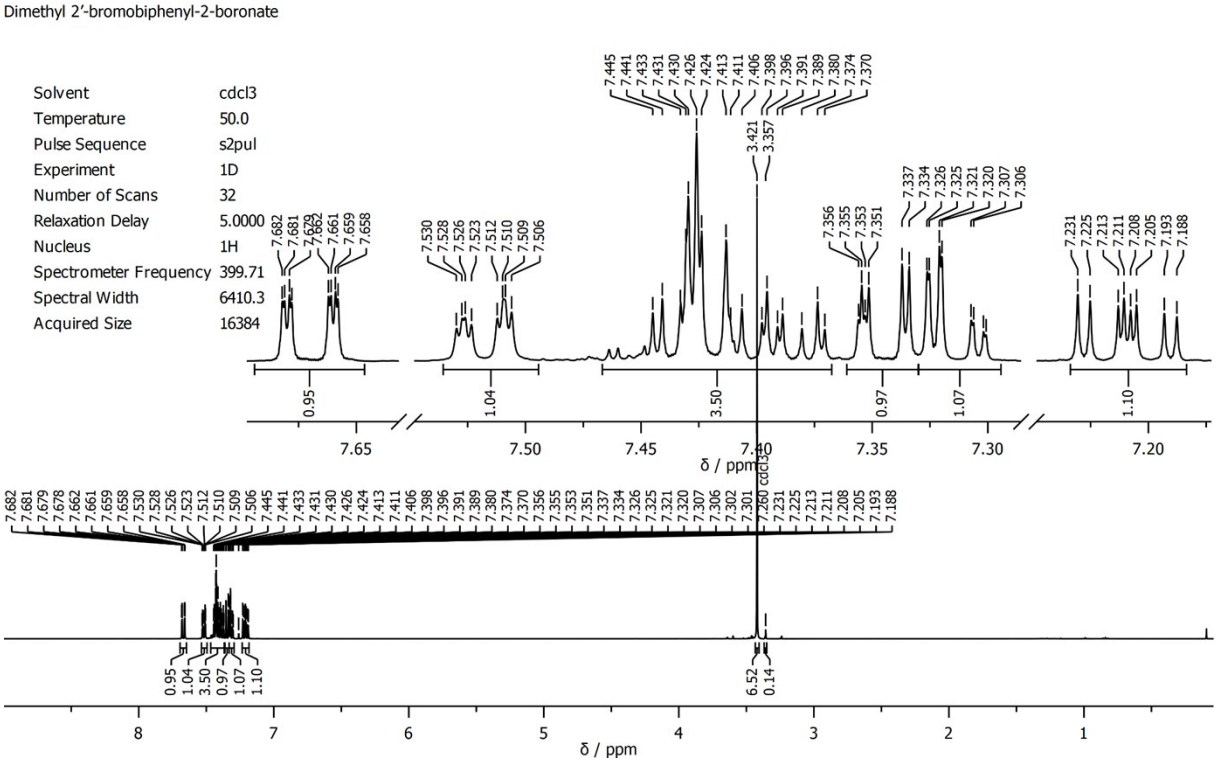

Figure S78. ^{1}H NMR spectrum of **11** in $CDCl_3$

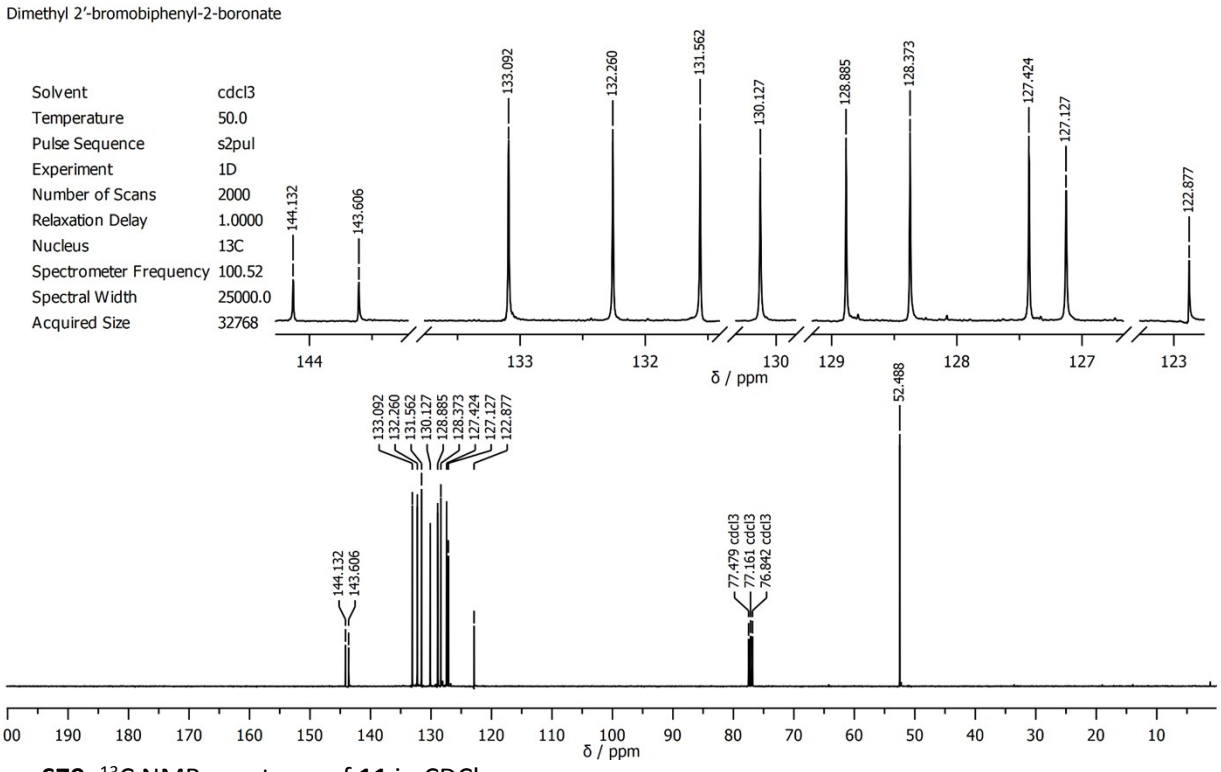

Figure S79. ^{13}C NMR spectrum of **11** in $CDCl_3$

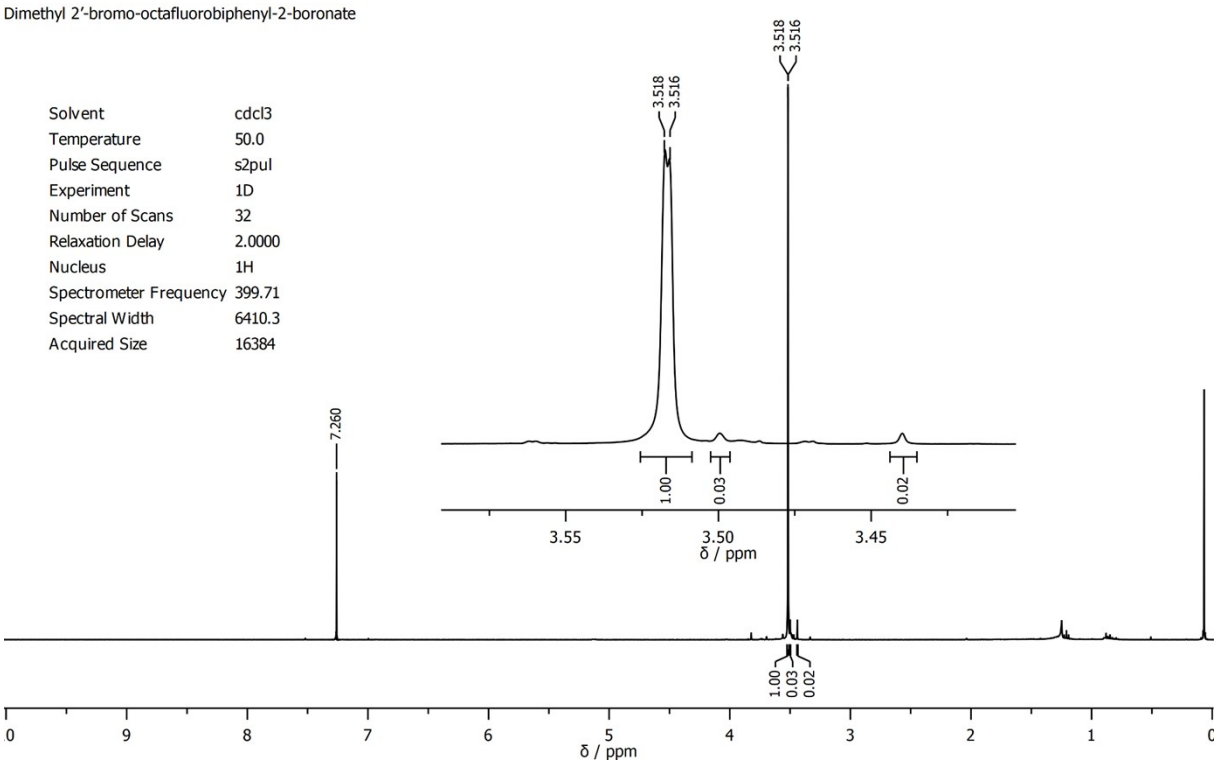

Figure S80. ^{1}H NMR spectrum of **12** in $CDCl_3$

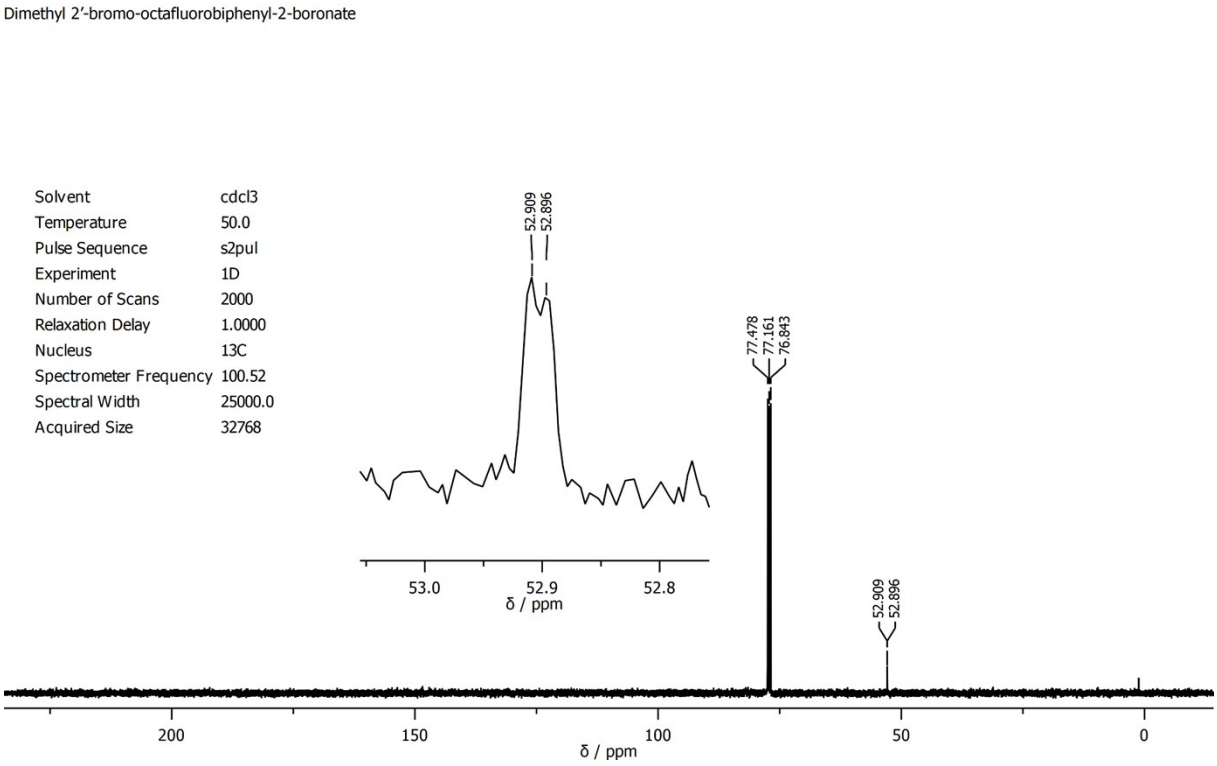

Figure S81. ^{13}C NMR spectrum of **12** in $CDCl_3$

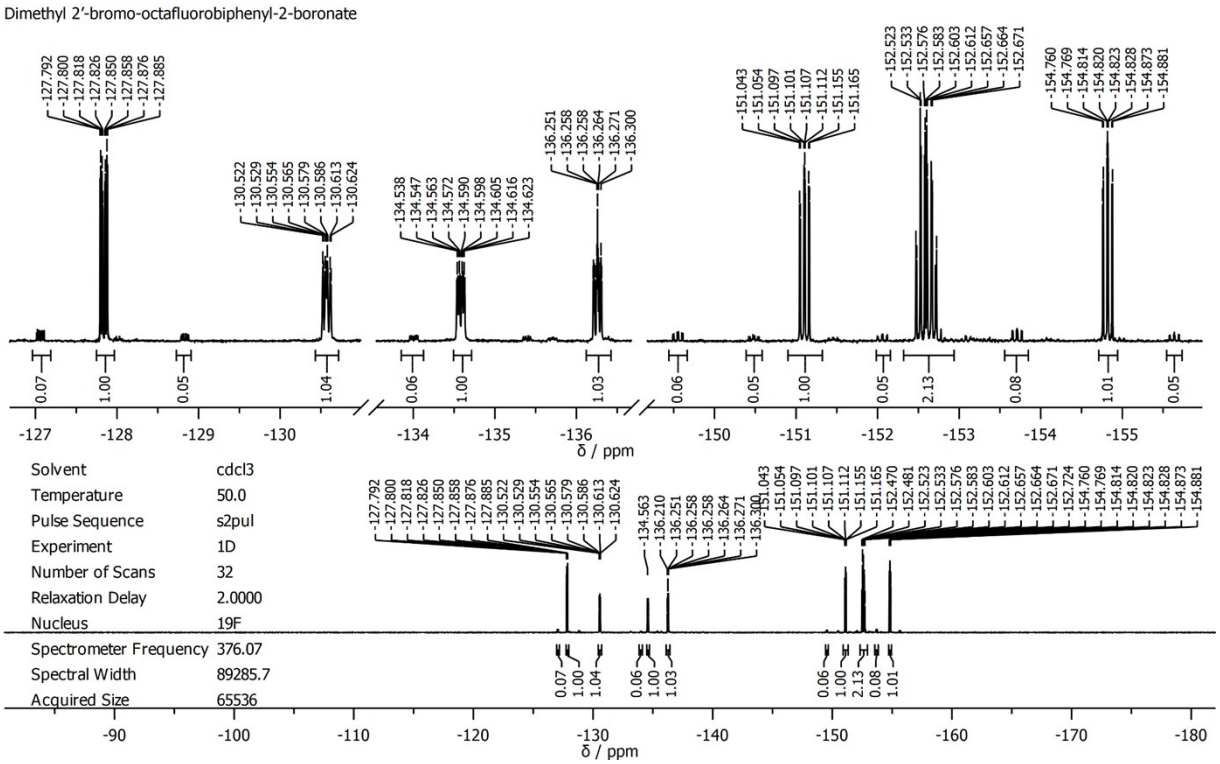

Figure S82. ^{19}F NMR spectrum of **12** in $CDCl_3$

10.References for Supporting Information

1 H. Höpfl, V. Barba, G. Vargas, N. Farfan, R. Santillan and D. Castillo, *Chem. Heterocycl. Compd.*, 1999, **35**, 912–927.

2 J. Ugolotti, S. Hellstrom, G. J. P. Britovsek, T. S. Jones, P. Hunt and A. J. P. White, *Dalton Trans.*, 2007, **0**, 1425–1432.

3 N. G. Kim, C. H. Shin, M. H. Lee and Y. Do, *J. Organomet. Chem.*, 2009, **694**, 1922–1928.

4 Z. Zhang, H. Zhang, C. Jiao, K. Ye, H. Zhang, J. Zhang and Y. Wang, *Inorg. Chem.*, 2015, **54**, 2652–2659.

5 D. Li, H. Zhang, C. Wang, S. Huang, J. Guo and Y. Wang, *J. Mater. Chem.*, 2012, **22**, 4319–4328.

6 G. Wesela-Bauman, M. Urban, S. Luliński, J. Serwatowski and K. Woźniak, *Org. Biomol. Chem.*, 2015, **13**, 3268–3279.

7 M. Urban, K. Durka, P. Jankowski, J. Serwatowski and S. Luliński, *J. Org. Chem.*, 2017, **82**, 8234–8241.